Universidad de Navarra

Facultad de Ciencias

Development of advanced genetic therapies for Primary Hyperoxaluria type I

Nerea Zabaleta Lasarte

Universidad de Navarra

Facultad de Ciencias

Development of advanced genetic therapies for Primary Hyperoxaluria type I

Memoria presentada por D./Dª Nerea Zabaleta Lasarte para aspirar al grado de Doctor por la Universidad de Navarra

El presente trabajo ha sido realizado bajo mi dirección en el Programa de Terapia Génica y Regulación de la Expresión Génica autorizo su presentación ante el Tribunal que lo ha de juzgar.

Pamplona, 19 de enero de 2018

Dr. Gloria González-Aseguinolaza

Dr. Juan R. Rodríguez Madoz

Este trabajo ha sido realizado gracias a las ayudas predoctorales de la Fundación para la Investigación Médica Aplicada y de la Asociación de Amigos (ADA) de la Universidad de Navarra.

ACKNOWLEDGEMENTS

En primer lugar me gustaría agradecer a la Universidad de Navarra que me haya brindado la oportunidad de realizar esta tesis doctoral y de formarme profesionalmente durante este periodo. Además, me gustaría agradecer al CIMA, particularmente al Programa de Terapia Génica y Regulación de la Expresión Génica, por dejarme participar en la investigación de alta calidad que se realiza en este centro.

Me gustaría dejar constancia de mi infinita gratitud hacia Gloria, que ha dirigido esta tesis con profesionalidad e ilusión. Gracias por confiar siempre en mí y dejar que durante estos casi 5 años que llevo en el laboratorio haya podido crecer todo lo que he podido. No se puede resumir en un párrafo todo lo que me has enseñado y el mundo que has abierto ante mí. Muchas gracias de corazón.

Gracias a Juanro, codirector de esta tesis, por enseñarme la ciencia más innovadora, por la ilusión y las ganas de hacer experimentos y probar nuevas terapias.

Mis compañeros de laboratorio seguramente sean las personas más importantes para el desarrollo de esta tesis, por hacer posible que se haya llevado a cabo tanto trabajo y que no haya perdido la salud por el camino. Gracias a David por ser tú, por estar siempre ahí, saber cómo me encuentro en cada momento y por ser el monkeyman. A Carla por ser un pilar para mí, siempre fuerte, segura e inteligente. A Miren por ayudarme en los momento de mayor locura y trabajo. Special mención a Cristina y a África por ser las personas que dan sentido y equilibrio al laboratorio, por sacar adelante muchísimo trabajo y por estar siempre, siempre ahí. A Irene por enseñarme todo lo que sé, por hacerme ver que la ciencia es paciencia y que siempre hay que mantener la calma y el ánimo. A Itzi, Diego y Luis por enseñarme el lado divertido de la tesis. A Mirja por sus rápidas y eficientes correcciones del inglés. Y a todas las personas que han pasado por el laboratorio 4.05, además del resto de compañeros del departamento que hacen que las transiciones por el pasillo sean más divertidas.

Quiero agradecer infinitamente al Dr. Eduardo Salido y a su equipo de la Universidad de La Laguna por todo el trabajo que han sacado adelante, pero sobre todo por los excelentes consejos y por toda la orientación que ha sido imprescindible para la realización de este trabajo.

Mencionar mi gratitud hacia el Dr. Ignacio Bilbao y la Dra. María Páramo por el excelente trabajo realizado durante las operaciones de los macacos.

I would like to thank to Dr. Federico Mingozzi (Genethon, Evry, France) and Dr. Jayanta Roy-Chowdurhy (Albert Einstein College of Medicine, NY, USA) for giving me the opportunity of being part of their laboratories, where I learnt a lot of science and where I made very good friends. Special thanks to Lina for teaching me how the good science is being done.

Además, me gustaría mencionar a todas las personas que me han apoyado durante estos años. Gracias a mis padres por haber hecho de mí lo que soy, por enseñarme a disfrutar del trabajo bien hecho, por enseñarme a ser responsable, por valorarme y por estar siempre ahí. Eskerrik asko Olaia, eztot hitzik deskribatzeko zuregatik sentitzen dotena. Nere Leitzeko eta Berako launei beti hor egoteagatik. En especial a Jaime, por hacer que mi vida durante esta tesis haya sido mucho mejor, por cuidarme, por apoyarme, por estar ahí y por todo lo que ya sabes.

Sin todos vosotros esta tesis no habría sido posible,

MUCHAS GRACIAS

A Gloria

A mis compañeros

A mis padres y mi hermana

A Jaime

INDEX

ABBREVIATIONS

AAT: α1-antitrypsin promoter

AAV: Adeno-associated virus

AAVR: AAV receptor

AAVS1: AAV safe harbor locus

AGT: alanine-glyoxylate aminotransferase

ALP: alkaline phosphatase

ALT: alanine-aminotransferase

AOA: aminooxyacetic acid

AST: aspartate-aminotransferase

CaOx: calcium oxalate

CHO: Chinese ovarian cancer cells

co: codon optimized

COD: oxalate dihydrate crystals

COM: oxalate monohydrate crystals

CPRT: chaperone-proteostasis regulator therapy

CRISPR/Cas9: clustered regularly interspaced short palindromic repeats/CRISPR associated protein 9

DSB: double-strand break

EAlb: albumin enhancer

EG: ethylene glycol

ERT: enzyme replacement therapy

ESRD: end-stage renal disease

FAA: fumarylacetoacetate

FAH: fumarylacetatoacetate hydrolase

FIX: factor IX

GAPDH: glyceraldehyde 3-phosphate dehydrogenase

GFR: glomerular filtration rate

GGT: gamma-glutamyl transferase

GO: glycolate oxidase

GRHPR: glyoxylate reductase/hydroxypyruvate reductase

gRNA: guide RNA

HA: hepatic artery

Hao1: hydroxyacid oxidase 1

HDAd: helper-dependent adenovirus

HDR: homology-directed repair

HEK293: human embryonic kidney 293 cells

HITI: homology-independent targeted integration

HOGA: 4-hydroxy-2-oxoglutarate aldolase

HP: L-hydroxyproline

HPD: hydroxyphenylpyruvate dioxygenase

HT1: hereditary tyrosinaemia type I

HYPDH: hydroxyproline dehydrogenase

IHC: immunohistochemistry

ILN: inguinal lymph nodes

ITR: inverted-terminal repeats

IV: intravenous

IVC: inferior vena cava

KO: knock out

LDH: lactate dehydrogenase

MAA: maleylacetoacetate

MCH: mean corpuscular hemoglobin

MCHC: MCH concentration

MCV: mean corpuscular volume

MLN: mesenteric lymph nodes

MTS: mitochondrial target signal

NC: nephrocalcinosis

NGS: next-generation sequencing

NHEJ: non-homologous end joining

NHP: non-human primates

NLS: nuclear localization signal

OFT: off-target

ONT: on-target

PAM: protospacer adjacent motif

PBMC: peripheral blood mononuclear cells

PBS: phosphate buffer saline

PH: primary hyperoxaluria

PLP: pyridoxal 5-phosphate

PTS: peroxisome target signal

RBC: red blood cells

RDW: red blood cell distribution width

RT: room temperature

RT-qPCR: real time-quantitative polymerase chain reaction

SaCas9: *Staphylococcus aureus* Cas9

SEAP: secreted human embryonic alkaline phosphatase

SEM: standard error of the mean

sgRNA: single-guide RNA

SH: secondary hyperoxaluria

SHV: suprahepativ vein

SpCas9: *Streptococcus pyogenes* Cas9

SPT: serine-pyruvate aminotransferase

SRT: substrate reduction therapy

TALEN: transcription activator-like effector nucleases

TBG: thyroxine-binding globulin

tracrRNA: trans-activating crRNA

VP: viral protein

WB: western blot

WBC: white blood cells

WT: wild type

ZFN: zinc-finger nuclease

ABSTRACT

Primary Hyperoxaluria type I (PH1) is an inherited inborn error of the glyoxylate metabolism in the liver. It is caused by mutations in the *AGXT* gene, a gene that codes the peroxisomal enzyme alanine-glyoxylate aminotransferase (AGT). As a result of AGT deficiency oxalate, which is an end-product of glyoxylate metabolism, is overproduced in the liver. In healthy individuals, oxalate is excreted into urine, but when it is produced at high concentration there is a tendency for calcium oxalate (CaOx) crystals to be generated and deposited in the renal parenchyma, where kidney stones can form. As a consequence, PH1 patients present with severe kidney damage and poor survival of kidneys, developing end-stage renal disease (ESRD) in most of the cases. The only curative treatment is liver transplantation, which is usually combined with kidney transplantation because of the loss of renal function. The main goal of this study was to develop new therapeutic alternatives for PH1 based on advanced genetic treatment.

In the initial part of this thesis we tried to improve PH1 gene therapy using adeno-associated viral (AAV) vectors. First, human *AGXT* was codon optimized in order to improve the expression levels of the protein. In this case, the optimization of the sequence of the *AGXT* gene resulted in no therapeutic advantage in comparison to the WT version of the gene. Second, we worked on the optimization of AAV gene delivery to the liver in non-human primates (NHP) changing the route of administration. It was demonstrated that the direct administration of AAV vectors into the hepatic blood flow resulted in a higher transduction of the liver in comparison to the systemic intravenous route.

In addition, a completely novel approach based on gene editing using the recently discovered clustered regularly interspaced short palindromic repeats/CRISPR associated protein 9 (CRISPR/Cas9) system was designed and characterized. This treatment was focused on a substrate reduction therapy (SRT) strategy, i.e. the reduction of glyoxylate production (the precursor of oxalate). Glycolate oxidase (GO) enzyme is a liver peroxisomal enzyme in charge of the production of glyoxylate. The inhibition of GO synthesis is known to reduce oxalate production. Therefore, a specific CRISPR/Cas9 system was designed to target and disrupt the *Hao1* gene (the gene that codes GO) in hepatocytes. Using this strategy we were able to efficiently reduce GO protein levels. Moreover, the treatment resulted in a significant reduction of oxalate production and of renal damage in PH1 mice challenge with oxalate precursors, in absence of toxicity.

In conclusion, several strategies to treat PH1 were developed and optimized during this project, which were able to reduce oxalate excretion in the urine of the PH1 mouse model.

RESUMEN

La Hiperoxaluria Primaria de tipo I (PH1 de las siglas en inglés) es una enfermedad hereditaria hepática causada por mutaciones en el gen *AGXT*, que codifica para la enzima peroxisomal alanina-glioxilato aminotransferasa (AGT). Debido a la deficiencia de AGT se sobreproduce oxalato en el hígado, un producto de desecho del metabolismo del glioxilato. En individuos sanos, el oxalato se excreta en orina, pero cuando se produce en concentraciones elevadas tiende a generar cristales de oxalato cálcico (CaOx) que sedimentan en el parénquima renal y forman piedras en el riñón. En consecuencia, los pacientes que padecen PH1 presentan un daño renal severo y baja supervivencia renal, desarrollando en la mayoría de los casos enfermedad renal terminal (ESRD de las siglas en inglés). El único tratamiento curativo es el trasplante hepático, que normalmente debe ser combinado con trasplante renal debido a la pérdida de función renal. El principal objetivo de este estudio era el desarrollo de nuevas alternativas terapéuticas para PH1 basadas en terapias genéticas avanzadas.

La primera parte de esta tesis está dirigida a la mejora de la terapia génica de PH1 mediante vectores AAV. En primer lugar, se optimizó la secuencia de codones del gen *AGXT* humano con el objetivo de incrementar los niveles de proteína. En este caso, la optimización de la secuencia de *AGXT* no confirió ventaja terapéutica en comparación con la versión WT. En segundo lugar, hemos tratado de mejorar los niveles de transducción del AAV en el hígado mediante la administración del vector por distintas vías en primates no humanos (NHPs). Se ha demostrado que la administración directa de los vectores AAV en el torrente sanguíneo hepático aumenta la transducción en comparación con la ruta intravenosa sistémica.

Además, se ha diseñado y caracterizado una aproximación complemente nueva basada en la edición génica mediante los sistemas CRISPR/Cas9 (clustered regularly interspaced short palindromic repeats/CRISPR associated protein 9). Este tratamiento estaba centrado en la estrategia de reducción de sustrato (SRT), es decir, en la reducción de la producción del glioxilato (el precursor del oxalato). La glicolato oxidasa (GO) es una enzima peroxisomal hepática encargada de la producción del glioxilato. Se sabe que la inhibición de la síntesis de GO es capaz de reducir la producción de oxalato. Por lo tanto, se ha diseñado un sistema CRISPR/Cas9 específico dirigido a la destrucción del gen *Hao1* (el gen que codifica GO) de los hepatocitos. Mediante esta terapia fuimos capaces de reducir eficientemente los niveles de proteína de GO. Además, el tratamiento redujo significativamente el nivel de oxalato producido y el daño renal en ratones PH1 estimulados con precursores de oxalato, en ausencia de toxicidad.

En conclusión, a lo largo de este proyecto se han desarrollado y optimizado varias estrategias para tratar PH1, que fueron eficaces para reducir la excreción de oxalato en la orina de los ratones PH1.

1. INTRODUCTION

Primary Hyperoxaluria type I (PH1) is an inherited autosomal recessive disorder affecting between 1-3 persons per million of population. It is caused by alterations in glyoxylate metabolism in the liver, which lead to oxalate accumulation in the kidneys.

1.1 Oxalate metabolism and hyperoxalurias

Oxalate (IUPAC name: calcium ethanodiate) is an end product of the metabolism, with unknown function in humans. It has two different sources: exogenous uptake in the diet and endogenous synthesis. It is excreted, mainly with urine (90-95%) (1) and secreted into the intestine in a lesser extent.

There are many foods that contain oxalate or its precursors. It is mainly present in fruits, vegetables (spinach) and nuts. The oxalate precursor L-hydroxyproline (HP) is generated during the degradation of collagen, and therefore the ingestion of collagen-containing meats will increase the synthesis of oxalate. Other precursor is glycolate, which is also abundant in vegetables. Oxalate is also produced during the degradation of ascorbic acid (vitamin C).

In the intestine, passive or paracellular and active or transcellular transport of oxalate have been described (1). The passive transport occurs due to the electrochemical gradient across the epithelium and it is conditioned by the junctions between cells (2). With respect to the transcellular transport, the involvement of the SLC26 transporter protein family is known; especially that of at least 4 proteins of this family, which are expressed in the intestine: SLC26A1 (sulfate anion transporter 1: SAT1), SLC26A2 (diastrophic dysplasia sulfate transporter: DTDST), SLC26A3 (donwregulated in adenoma: DRA) and SLC26A6 (putative anion transporter 1: PAT1). Little is known about the active transport of oxalate. In spite of some controversial results about the importance of the active absorption of oxalate (3,4), DRA has been identified as the main player in this process, being responsible for 41% of the absorption of oxalate (the remaining 59% are absorbed by passive mechanisms) (1). PAT1 is the only transporter directly associated to the secretion of oxalate in the intestine, as SLC26A6 KO mice presented high levels of oxalate in urine in several studies (5,6). The existence of an active transport involving several transporters implies that the transport of oxalate is regulated and can be modulated depending on different conditions.

As mentioned, oxalate is also synthesized in the human organism as a product of the glyoxylate metabolic pathway in the liver. This pathway is shuttled by different enzymes that act in different compartments of the cell: mitochondria, peroxisome and cytosol. Glyoxylate is produced in the mitochondria from HP in four steps and in the peroxisome from glycolate by the enzyme GO. When

glyoxylate is imported to the cytosol, some oxidases and dehydrogenases, such as LDH, are able to oxidize it to oxalate. However, in each cellular compartment enzymes can bypass the production of oxalate by the conversion of glyoxylate into other compounds. In the mitochondria and in the cytosol, the enzyme glyoxylate reductase/hydroxypyruvate reductase (GRHPR) transforms the glyoxylate into glycolate, which is then trasported into the peroxisome. Here the enzyme AGT produces glycine from glyoxylate (Figure 1) (7).

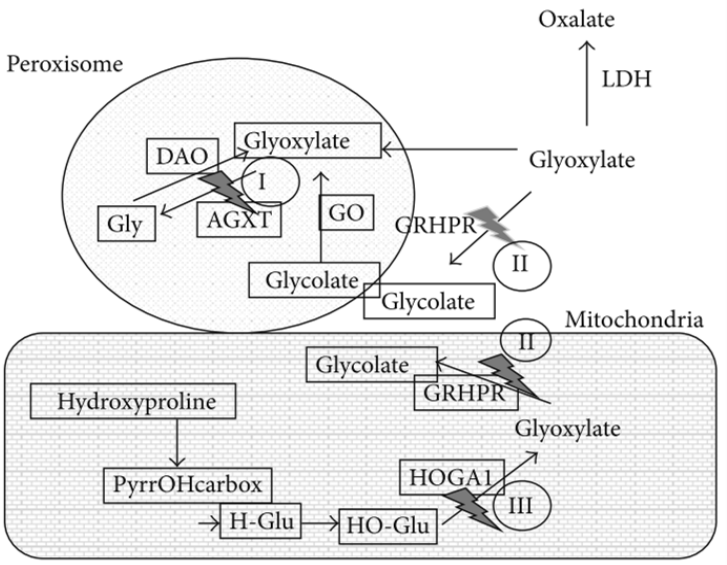

Figure 1. Simplified glyoxylate metabolism in the liver (7)**.** Synthesis of glyoxylate and oxalate from hydroxiproline and glycolate in the different compartments of the hepatocyte. Peroxisomal glyoxylate is detoxified by AGT, while mitochondrial and cytosolic glyoxylate is reduced to glycolate by GRHPR, thus preventing excessive oxidation to oxalate by LDH. The hydroxyproline metabolism results in the production of 4-hydroxy-2-oxoglutarate that is normally split into glyoxylate and pyruvate by HOGA1. The enzymes implicated in primary hyperoxalurias (types I, II and III) are alanine-glyoxylate aminotransferase (AGXT), glyoxylate reductase/hydroxypyruvate reductase (GRHPR) and 4-hydroxy-2-oxoglutarate aldolase 1 (HOGA1). PyrrOHcarbox=pyrroline-5-carboxylate; H-Glu= 4-hydroxy-glutamate; HO-Glu=4-hydroxy-2-oxoglutarate; GO=glycolate oxidase; DAO=D-amino acid oxidase; LDH=lactate dehydrogenase.

Oxalate produced in hepatocytes is secreted to the blood-stream and excreted in urine by glomerular filtration and active secretion and reabsorption. In fact, it is known that SLC26A6 functioning as Cl^-/oxalate exchanger is present in the epithelial cells of the proximal tubule (6). Furthermore, this transporter and others could be involved in the maintenance of constant oxalate levels in plasma by the regulation of oxalate secretion or reabsorption (8). However, under normal conditions the renal

excretion of oxalate is controlled by the glomerular filtration rate, and the secretion is activated when an oxalate overload occurs (9).

The alterations in oxalate metabolism are known as hyperoxalurias, characterized by an increase in oxalate levels, and classified as primary or secondary hyperoxalurias. **Primary hyperoxalurias (PH)** are autosomal recessive rare metabolic disorders caused by mutations in enzymes of the glyoxylate pathway. They are characterized by the increase in oxalate production and its excretion in urine. Three PH forms have been described, each affecting to different gene (Figure 1). PH type 1 (PH1, OMIM #259900) is caused by mutations in the *AGXT* gene, which causes deficiency in the enzyme AGT, PH type 2 (PH2, OMIM #260000) presents with mutations in the *GRHPR* gene and PH type 3 (PH3, OMIM #613616) with mutations in the *HOGA* gene. The malfunction of HOGA leads to the inhibition of GRHPR causing an increase in oxalate similar to that obtained in PH2. **Secondary hyperoxaluria (SH)** is a non-genetic disease in which the oxalate levels are higher due to high-oxalate uptake in the diet or abnormally high oxalate absorption in the intestine.

1.2 Primary Hyperoxaluria type I

PH1 is the most frequent (80%) and severe form of PH. As mentioned, PH1 is a metabolic disorder caused by autosomal recessive defects in the *AGXT* gene, which leads to the impaired function of the AGT enzyme in the liver. As a consequence, the liver overproduces oxalate, which sediments as CaOx crystals in renal parenchyma and causes kidney damage.

1.2.1 Epidemiology

PH1 is a rare disease with a prevalence of 1-3 patients per million of population (10–12) and an incidence of 1 per 120,000 births in European countries. However, it is thought that the prevalence is underestimated due to the heterogeneity of the disease (age at onset, symptoms, evolution) and the vague symptoms at onset (12). Even though PH1 cases have been reported all over the world (10,12–19), the prevalence of the disease is higher in some countries/regions where consanguineous marriage has been frequent, such as North Africa (Tunisia) (20) and the Canary Islands (17), where PH1 is the cause of up to 10% of the cases of end-stage renal disease (ESRD) (20).

1.2.2 Clinical manifestations

In PH1 patients the excretion of oxalate in urine is >0.5 mmol/1.73 m^2/24 hours (usually >1), which is higher than normal (<0.45) (21). This oxalate is eliminated in the urine, but due to the high amount accumulated in the kidney it leads to the formation of CaOx crystals (both

monohydrate/COM and dihydrate/COD crystals). In the medullary collection duct the crystals are attached to the surface of cells and lead to the blockage of the conduct; additionally, the progressive accumulation of crystals in the lumen leads to stone formation or urolithiasis. If the crystals adhere to the proximal nephron segments, they can be endocytosed or transcytosed to the renal interstitium causing the accumulation of CaOx crystal in the renal parenchyma or nephrocalcinosis. Some *in vitro* studies point towards the receptor CD44 and its ligand osteopontin together with hyaluronic acid as important players in the interaction between the COM crystals and renal tubular cells (only the proximal tubular cells and not distal cells) (22).

The nephrocalcinosis triggers inflammation into the renal parenchyma leading to formation of granulomas and progressive fibrosis (21). Finally, and especially in non-treated patients, the kidneys deteriorate progressively leading to ESRD. In some populations, it has been reported that the risk of developing ESRD at the age of 15 years is 50%, and this percentage increases up to 80% by the age of 30 (12,23). The mechanism by which CaOx crystals induce kidney damage remains unclear. Some *in vitro* studies reported an increased inflammatory response (mediated by prostaglandin E_2 secretion), oxidative stress (H_2O_2 production) and death of renal proximal tubular cell lines, but not renal collecting tubular cell lines (24,25). Recently, Brooks *et al*. published a paper in which the proteomics of the urine of PH1 patients was compared to that of healthy patients (26). This study indicated up-regulation of the MAPK pathway in ESRD patients, which is related to inflammation, oxidative stress and cell death. The NF-kB pathway was also found to be up-regulated in PH1 patients, indicating the activation of immune responses (chemokine and cytokine expression, adaptive immune response and compensatory responses to inhibit inflammation). Finally, they described many inflammation markers associated with the development of ESRD.

PH1 is the cause of about 1% of ESRD in children and teenagers in Europe and the USA (13,20). In advanced stages of the disease, when the renal function is strongly affected, the glomerular filtration rate (GFR) decreases to levels of less than 30-40 mL/min/1.73 m^2. The kidney is not able to control the levels of plasma oxalate (normal limits: 1-6 µmol/L (27)) and when it reaches supersaturation (>30 µmol/L) a systemic deposition of CaOx crystals occurs (23). The bones and the eye are especially affected by CaOx crystals, leading to fractures, bone pain, growth retardation, anemia, disturbed vision and brown retinal deposits (which can be easily diagnosed) (23,28,29). Less frequently arteries, myocardium, thyroid, skin, nerves, muscle, bowel and joints can be affected by systemic oxalosis. However, no evidence of liver damage has been reported.

In PH1, the correlation between genotype and phenotype is not always clear, since patients with the same mutations, even siblings, can present with completely different clinical manifestations. For

this reason, the clinical outcome is variable depending on the patient. However, some mutations are associated with better clinical outcome than others, for example mutations that cause AGT mistargeting that can be treated with vitamin B6, the cofactor of the enzyme.

1.2.3 Diagnosis

Median age of the manifestation of the first symptoms has been reported to be at 4 years and the median age for diagnosis is approximately 7.7 years (11,12,30). Five forms of presentation of PH1 at diagnosis have been described (30,31): (a) infantile oxalosis, with early appearance of the symptoms and rapid development of renal failure (26%); (b) nephrocalcinosis and recurrent stones that finally lead to ESRD in childhood or adolescence (30%); (c) occasional stone formation in adults, with late development of the symptoms (21%); (d) diagnosis after kidney transplantation, recurrence of stones and the deterioration of the new kidney (10%); and (e) diagnosis of asymptomatic patients because of the family history (13%). In a cohort of 155 patients (30) of European and Arab origin, the cumulative survival was similar to the general population (Figure 2A). However, when attempting to renal survival, the data are devastating, with a 50% of renal failure at the age of 20s (Figure 2B). Infantile oxalosis was found as the only subgroup of patients presenting a higher risk of dead.

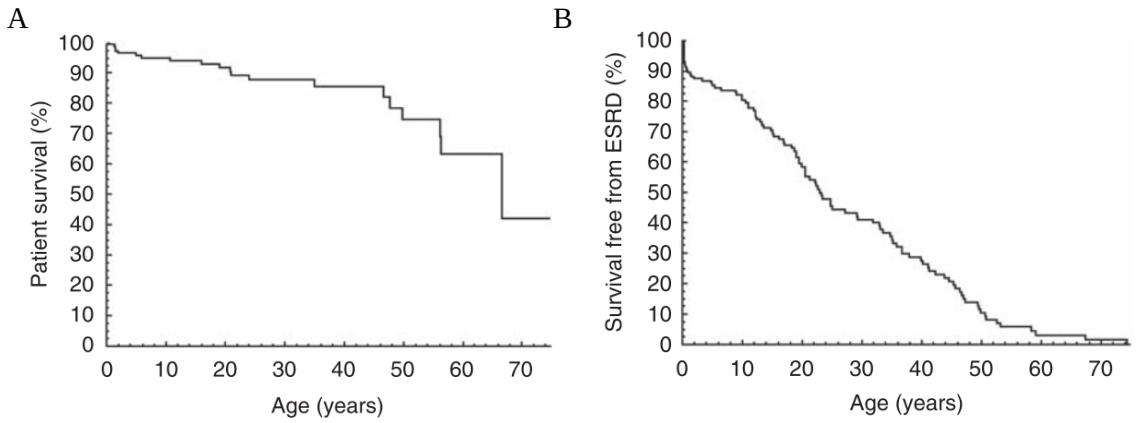

Figure 2. Progression and prognosis of PH1 in a cohort of 155 patients (30). A) Cumulative survival of PH1 patients. B) Cumulative survival free from ESRD in PH1 patients.

Usually, the patients presented renal damage at the time of diagnosis (12), except in the cases of family screening. Therefore, the initial symptoms are usually related to urolithiasis and nephrocalcinosis, such as hematuria, recurrent urinary tract infections or the passage of a stone (32). The main symptoms of urolithiasis are flank- or abdominal pain, nausea and vomiting, and more

than two red blood cell counts in urine microscopy (33). The nephrocalcinosis presents no symptoms and it is usually diagnosed by ultrasound imaging (33). It has been estimated that about 11-30% of the patients developed ESRD before the diagnosis, and in some studies and specific populations this percentage increases greatly (47% in the Netherlands (12)).

The common characteristic of all PH1 patients is the high oxalate excretion in urine, which is measured in 24-hour urine per body area. However, in young children the collection of 24-hour urine is not possible, and in these cases the collection of a single urine point and the calculation of oxalate/creatinine ratio is used as diagnostic measurement, although age-related tables have to be used to interpret the data (23,29). The presence of CaOx crystals in the urine can be analyzed as complementary result. Glycolate is another parameter that is elevated in the urine of two thirds of PH1 patients (21,29) and can be used to confirm the diagnosis. Plasma oxalate measurement is not very useful in the patients that preserve renal function, but this data is important in patients with ESRD to discard systemic oxalosis and to evaluate the efficacy of dialysis to eliminate oxalate from the plasma (23).

Imaging of the kidneys by ultrasounds is recommended to confirm urolithiasis or nephrocalcinosis. The analysis of the stones that were passed or removed by surgery revealed characteristic morphology and a composition of 95% of COM (28). Nephrocalcinosis is easily diagnosed in renal biopsies with abundant CaOx crystals (21), which is associated with a strong inflammatory response and the generation of foreign-type granulomas in the parenchyma (21).

However, the diagnostic methods described above are not conclusive and pathological observations can be the result of hyperoxalurias of different origin. The analysis of mutations in the *AGXT* gene by DNA sequencing could reveal the presence of a known mutation that causes AGT malfunction (34). The analysis is usually done in DNA extracted from blood samples. Initially, the screening of most commonly mutated exons can be done (exons 1, 4 and 7) resulting in disease confirmation in 50% of the cases (35); but it is strongly recommended to perform whole *AGXT* gene sequencing (28), since in 95% of the cases both mutated alleles can be identified (23). In the cases of screening for familial PH1, the mutation is known and the diagnosis is clear. Moreover, it is recommended to perform a screening of parents and siblings of PH1 patients and also prenatal screening of babies with documented PH1 siblings (samples from the chorionic villous biopsies) (28). However, in other cases the diagnosis by DNA sequencing can be difficult due to the high number of mutations described to date and the presence of non-pathogenic polymorphisms.

The gold standard for the diagnosis of the disease is the determination of AGT enzymatic activity in a liver biopsy taken by percutaneous needle biopsy (21), especially in the cases where the results of genetic testing were inconclusive. However, the technique is invasive and bears some risks, in particular considering that in PH1 the liver is healthy. Therefore, this diagnostic method is not mandatory in presence of a genetic diagnosis (28).

An interesting and important observation is that the incidence of the disease is underestimated; thus, the development of an efficient diagnostic guidance is crucial. Some guides have been developed and published (28) by an European consortium formed by experts in PH1 (OxalEurope, http://www.oxaleurope.org/) in order to help the physicians with the diagnosis.

Regarding the prevention, there is no way to anticipate the symptoms of the disease since they appear when there is already kidney damage. The only prevention possible would be the genetic screening in families with diagnosed cases.

1.2.4 Genetics and molecular alterations of AGT

The *AGXT* gene is located in the chromosome 2 in humans (specific location: 2p37.3) and consists of 11 exons and introns and has a size of approximately 10 Kb. It results in a cDNA of 1.7 Kb with an ORF of 1176 bp.

Little is known about the transcriptional regulation of the *AGXT* gene in humans. Sato *et al.* analyzed the 5' flanking region of the gene and detected the main transcription start site around -45 bp upstream from the translation start site (36). The deletion of fragments of variable length upstream of the translation start site revealed several regions with important regulatory functions. Binding sites were described for liver-specific transcription factors, such as a site for HNF4α. Interestingly, the region -2 to -325, which is part of exon 1, is the minimal sequence required to activate transcription and contains two TATA boxes. The region spanning from -325 to -439 contains a third TATA box, which contributed to an increased expression *in vitro*. The region -440 to -700 might contain enhancer elements and the region -701 to -1203 did not reveal any important regulatory elements.

Two main allelic variants have been described for *AGXT*: major and minor alleles. The minor allele is present in about 50% of PH1 patients, 20% of Caucasians and 2% in Japanese (37). Several changes are found in the minor allele: the modification c.32C>T causing a P11L change, an imperfect duplication of 74 bp in intron 1, some tandem repeats in intron 4 and c.1020A>G causing I340M substitution are the most important ones. These alterations in the gene cause a slight

mistargeting effect (5% of the AGT goes to mitochondria instead of localizing entirely into the peroxisome) (38), a reduction in the enzymatic activity of up to 50% (38), a decrease in thermodynamic and kinetic stability (39), a decrease in the dimerization ability *in vitro* (38) and a tendency to aggregation (38). Despite the minor allele is not pathogenic *per se*, it shows synergism with some mutation that lead to the development of the disease. A different minor allele variant was also found in 12% of black Africans, comprising a duplication in intron 1 and a 38 bp tandem repeat in exon 4 (40).

The translation of the *AGXT* gene results in AGT protein, which is a homodimeric enzyme composed of monomers of 43 KDa weight and 392 animo acids each. On one hand, the AGT enzyme is involved in the reaction in which alanine and glyoxylate are converted into glycine and pyruvate, and as a consequence, it is involved in the glyoxylate pathway (Figure 1). On the other hand, AGT is also known as serine-pyruvate aminotransferase (SPT) because it can also catalyze the reaction in which serine and pyruvate are transformed in hydroxypyruvate and alanine, therefore, acquiring an important role in the gluconeogenesis (41). Each subunit consists of an N-terminal coil (residues 1-21), which wraps over the surface of the other subunit and is essential to form active dimers (42); the large domain (residues 22-282), where the active site and the dimerization surface are located, and the C-terminal domain (residues 283-392) that contains the peroxisomal targeting region (43) (Figure 3). The quaternary structure was described by Zhang *et al*. (44). The N-terminal extension was found to be an irregular coil that wraps around the outside part of the other monomer, helixes 50-69 and 265-283, thus the large domain. The position of the polymorphism P11L found in the minor allele could explain the decrease in dimerization of the minor allele *in vitro*. The large domain presented a topology of alternating β-α-β structures and the C-terminal domain is a two-layer αβ structure with the α-helixes exposed at the protein surface and the four anti-parallel β-sheets interacting with loops in the large domain. The structures involved in the dimerization interface are the helices 223-231, 243–251 and 265–283, and the loop formed between the β-strands 202–206 and 218–222, all of them located in the large domain.

In order to be functional, AGT needs the binding of the cofactor pyridoxal 5'-phosphate (PLP) (Figure 3). The vitamin B6 vitamers are pyridoxine (PN), pyridoxamine (PM), pyridoxal (PL) and its 5'-phosphate form; they are essential, and thus they have to be taken up with the diet (45). Moreover, the structure of AGT was found to be similar to other PLP-dependent enzymes (44). This cofactor is covalently bound to K209 forming a Schiff base while S158 and D183 form H-bonds and are implicated in the orientation of the cofactor in the pocket of the dimerization interface. The residues H83, G82, Y260 and T263 were found to form another three H-bonds with PLP (44).

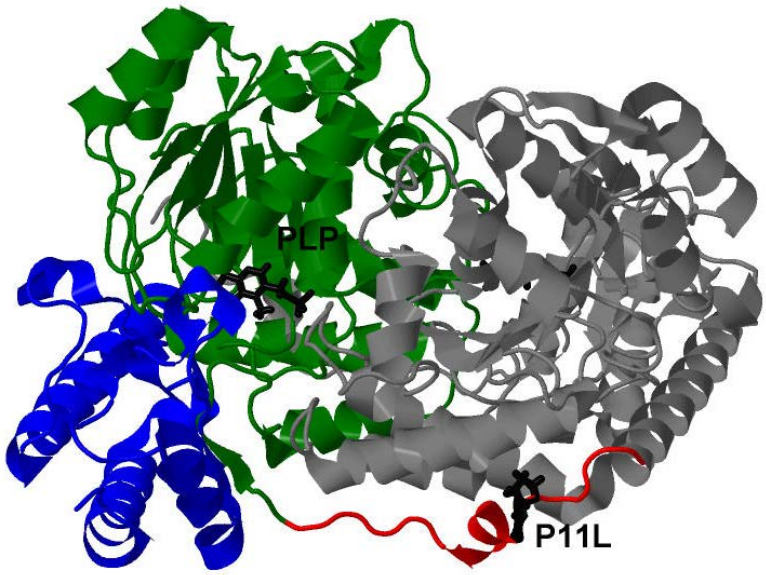

Figure 3. Quaternary structure of AGT homodimer. The three domains of one of subunits are highlighted: N-terminal coil in red, the large domain in green and the C-terminal domain in blue. PLP cofactor and the residue 11 are marked in black.

AGT is a peroxisomal enzyme in humans, but the analogs of AGT in other mammals are located in the mitochondria and/or in the peroxisome (46). The compartmentalization of AGT is believed to have evolved in relation to the diet, as it has been shown that it is located in the mitochondria mainly in carnivorous species, in the peroxisome in herbivorous ones and in both in the case of omnivores. In humans, the presence of the AGT in the peroxisome can be explained by the herbivore diet of our great ape ancestors (47). As explained, glycolate and HP are the precursors of oxalate, which are present in certain diets. Glycolate is mainly located in plants and it is metabolized to glyoxylate in the peroxisome. Therefore, the AGT activity of the peroxisome acquires an important role in species that mainly feed on plants. In contrast, HP is synthesized during the degradation of collagen, which is especially high in meat. HP is metabolized to glyoxylate in the mitochondria, explaining the need of AGT activity in the mitochondria of carnivorous animals (21,48). Moreover, carnivorous animals have a high-protein diet and the gluconeogenesis is necessary to obtain glucose, which makes the SPT activity important in the mitochondria (46), where other gluconeogenic enzymes are located. Moreover, in rats, where both peroxisomal and mitochondrial forms coexist, the administration of hormones that alter the glucose metabolism (glucagon and/or insulin) triggered a specific increase in the synthesis of the mitochondrial form of AGT (49).

In addition, some studies suggest that the high frequency of the minor allele, which codes a partially defective protein and is more prone to cause disease, is a consequence of a high meat uptake in some populations (50). The frequency of the minor allele in different populations was analyzed and related to the type of diet. In the Eastern countries, such as China and India, a low frequency of the minor allele is observed (2.3%-6.9%), while in Africa it is 8.9-10.9% and in Europe 14.6-27.9%. It is known that the diet tends to be mainly vegetarian in countries like China and India, while more meat is consumed in Western countries. The most evident case is the one of the Saami population, with a 27.9% of minor allelic frequency and a well-known meat-diet history. The rationale is that the minor allele results in 5% of the AGT mistargeting to the mitochondria (where it remains catalytically active (51)), and where HP is metabolized in high amount in high-meat diets.

The signals involved in the selective transport of AGT have been studied in different species: the mitochondrial target sequence (MTS) is located in the N-terminal region while the peroxisomal target sequence is found in the C-terminal region. In animals that express both forms of the protein, two different transcripts are produced, with two different transcription and translation start sites (46). The larger form encodes for the mitochondrial enzyme, while the MTS is not transcribed in the shorter one. The human AGT has been described to be imported by the PTS1 pathway via the peroxisomal targeting sequence KLL located at the end of the protein (52) and an ancillary PTS1A sequence located in the C-terminal domain between V324 and I345 (53). These two signals are close to each other in the quaternary structure of the protein and Pex5p is the protein in charge of the transport of AGT to the peroxisome (54).

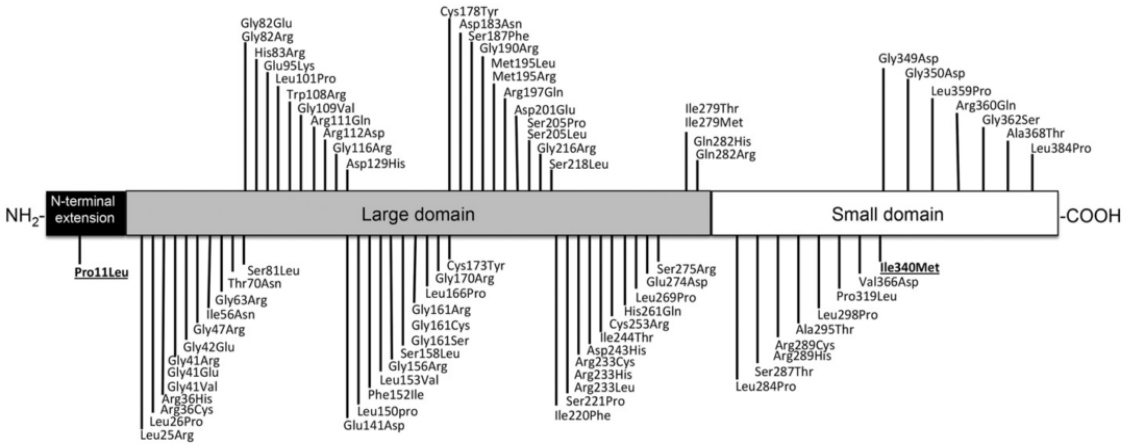

Figure 4. Schematic representation of the location of some mutations in the AGT enzyme (37)**.**

A total of 146 mutations have been identified in the *AGXT* gene, with all the exons involved (36,55) (Figure 4). Most of them (75%) are point mutations: 73 missense mutations, 19 nonsense and 18

single-nucleotide changes affecting splice sites. The rest correspond to major or minor deletions or insertions and 31 have been described to date. As can be seen in Figure 4, no pathogenic substitutions have been found in the short N-terminal extension, most of them occur along the large domain without hot-spots and some in the C-terminal domain (37). Despite of the heterogeneity in the location and type of the mutations, they can be classified depending on the effect exerted on the protein. The presence of insertions, deletions or alterations in splicing can easily lead to the expression of a truncated protein that is unstable and rapidly degraded (37). However, more detailed studies are needed to understand the effect of the single amino acid substitutions found in PH1 patients and many molecular and cellular analyses have been carried out to elucidate the molecular effect of each described mutation on the AGT synthesis, location and activity. The expression of each AGT variant in mammalian cells is considered the closest to the real scenario found in patients (17,38,51). Another approach is the expression and characterization of AGT activity and structure in *E.coli* (56,57). In addition, yeast and cell-free methods have been used to evaluate the activity, stability and assembly of the protein; however, this is considered a fast but semi-quantitative method (58). Opicci *et al.* reviewed all the publications in which the characteristics of AGT variants were analyzed (37). In this paper they classified the mutations depending on their molecular or cellular effect. However, a simplified classification differentiates four main molecular alterations of the AGT protein associated with several mutations that will be discussed in more detail (Table 1) (21).

Table 1. Summary of the main molecular mechanisms implicated in AGT malfunction and their mechanisms, the most common mutations and the affected allele associated with the molecular phenotype.

Molecular alteration	Mutation	Allele	Mechanism
Mitochondrial mistargeting	G170R	Minor	Unmasking of mitochondrial targeting signal
	F152I	Minor	
Protein aggregation	G41R	Major and Minor	Destabilization of the dimerization or protein folding
	I244T	Minor	
Catalytic defects	G82E	Major and minor	Inhibition of the binding of the cofactor
Synthesis defects	c.33dupC	Major and minor	Expression of truncated protein

1.2.4.1 Mitochondrial mistargeting

One of the most frequent mutations found in PH1 patients is G170R (about a third of PH1 alleles (59)), which is pathogenic only on the background of the minor allele and produces the mistargeting of AGT to the mitochondria (38,60). The variant G170R is usually associated with a normal catalytic activity and immunoreactivity (61).

The description of the quaternary structure of AGT allowed generating a hypothesis of the molecular mechanism implicated in this mistargeting (44). The N-terminal coil of AGT has a sequence (MASHKLLVT**PP**KALLKPLSI) with some similarities to MTS sequences, such as the absence of acidic residues, a good distribution of basic, neutral and hydrophobic and hydroxyl amino acids (48). However, the structure is not an α-helix due to the P10 and P11 residues that break the helix (Figure 3). As explained before, the minor allele presents a P11L change that results in 5% of the protein being mistargeted to the mitochondria. This is because of the change in the structure of the coil. Moreover, the experimental introduction of a P10L mutation in the minor allele completely changed the localization of AGT from the peroxisome to the mitochondria (62). However, this effect is exacerbated by the mutation G170R, a residue that is located on the surface that interacts with the N-terminal coil, therefore further destabilizing the interaction. Two related mechanisms have been proposed to explain this phenomenon: First, it was suggested that the concomitant presence of P11L and G170R could weaken the interaction between the N-terminal coil (MTS signal) and the other subunit, therefore releasing the coil and allowing the interaction with TOM20 (a protein implicated in the mitochondrial transport). Another explanation is that the presence of these alterations in the protein could decrease the dimerization kinetics, prolonging the time between the protein synthesis and its dimerization, and as a consequence, the time when the N-terminal coil is free to bind to TOM20. The diagram proposed by Zhang *et al.* shows the formation of various dimerization intermediate stages (Figure 5): in intermediate B the N-terminal coil would be important during the dimerization process while in intermediate C it would be important for the stability of the dimer (44). Evidence found by Motley *et al.* shows that in cells defective for the transport system PTS1 AGT remains in the cytosol. This suggests that the second hypothesis could be the correct one, since once the dimers are formed the protein would not be transported to the mitochondria (52).

The mutation F152I has been described to cause similar molecular alterations, with no significantly reduced catalytic activity, but making the protein more prone to the ‘apo’ form (in which the enzyme is not bound to the cofactor, and thus is less stable) and decreased dimerization stability, thereby promoting the transport to the mitochondria (63).

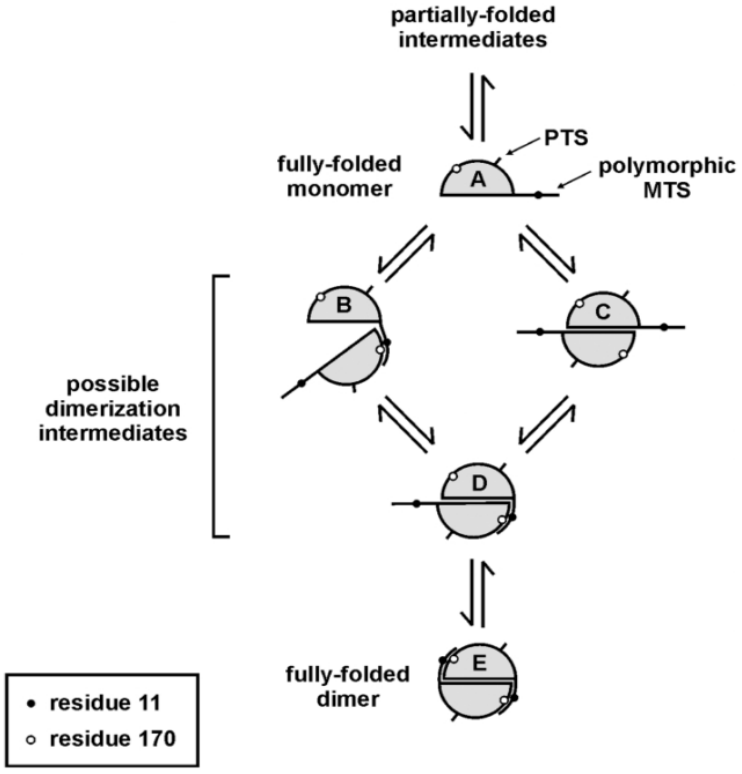

Figure 5. Description of the possible dimerization pathway of AGT (44)**.** The black circle indicates the location of proline 11 (P11L in the minor allele) and the white circle that of glycine 170 (mutated to R in PH1). A=monomeric form; B and C=possible first dimerization intermediate; D=second dimerization intermediate; E=full-folded AGT dimer**.**

1.2.4.2 Protein aggregation

In PH1 two mutations have been associated with this aggregation phenotype in the minor allele: G41R (64) and I244T (17). Interestingly the mutation G41R has been described as a pathogenic mutation in the major allele (65). This residue is located in the dimerization surface in the helix 34-42, and it participates in a direct van-der-Waals interaction between G41-G42 from a monomer with the same amino acids of the other (44). In this scenario, the change G41R adds a long charged side-chain that destabilizes the dimerization, which leads to monomer degradation and/or aggregation. The analysis of liver biopsies of three patients with the G41R mutation showed a lower AGT immunoreactivity by gold-labeling in electron microscopy compared to controls without mutation. In addition, the protein was mainly located in intra-peroxisomal electron-dense amorphous cores, suggesting an intra-peroxisomal aggregation of the monomers (64). The mutation I244T is also frequent in PH1 patients, since it has been reported in 9% of PH1 alleles (66) but its frequency is

increased in certain regions such as the Canary Islands (Spain) up to 91.6% (17), most likely due to a founder effect. The I244T variant also synergizes with the minor allele, producing an enzymatically inactive protein aggregated inside the cells, together with chaperones such as Hsp90 (17). These findings implicated a possible conformational effect of the mutation in residue 244, which is involved in the interaction between helices 243-251 and 223-231. However, no increased degradation of the protein was found in relation to this mutation (17).

1.2.4.3 Catalytic defects

Mutations affecting the amino acids implicated in the structure of the active site or in the PLP binding (G41R, S81L, G82E, H83R, F152I, S158L and D183N) (39,63,67,68) result in altering the catalytic efficiency of AGT or its binding to the cofactor. As an example, in presence of the mutation G82E, both in the major and the minor allele, AGT is properly synthesized, folded and located in the peroxisome, it is immunoreactive but completely inactive (68). At structural level, G82 is located in the pocket where PLP is bound and the carboxylate side chain of the glutamate in this position maps to the site where PLP should be, therefore inhibiting the binding of the cofactor and the activity of the protein (44).

1.2.4.4 Synthesis defects

Some mutations causing PH1 are associated with the presence of a small insertion or deletion in the coding region leading to synthetic defects due to a frameshift and the introduction of an early STOP codon. c.33dupC is the most common among this type of mutations, constituting 13% of the PH1 alleles (21). In fact, other mutations associated with this nucleotide have been found, such as c.33dupC, c.33delC and c.32_33delCC, suggesting a possible hot-spot for mutations. Some nucleotide mutations have been described to cause alterations in splicing, as is the case of the mutations c.424-2A>G and c.776+1G>A, found in splice acceptors of intron 3 and intron 7, respectively (35). The splice change in intron 3 triggered a loss of 12 nucleotides at the beginning of exon 4 and the one in intron 7 an addition of 24 nucleotides at the end of exon 7 (35). However, some amino acid changes can also lead to the destabilization of the protein and its fast degradation, for example the substitution S205P results in a very unstable variant that is almost undetectable in liver extracts of patients (69).

The genotype-phenotype relation is not always clear in PH1, since - as explained - the phenotype can vary completely even between siblings (discordant families). However, some concordance has been observed in the case of patients with mutation G170R, for which a better outcome of the

disease has been described (30), especially in cases where the renal function is preserved at the time of diagnosis.

1.2.5 Current treatments for PH1

Nowadays, the only curative treatment for PH1 is liver transplantation. Moreover, it is recommended to perform kidney transplantation before the development of systemic oxalosis in ESRD. Kidney transplantation alone is not an appropriate therapeutic approach since the liver will continue to overproduce oxalate, which will again damage the new kidney. Thus combined liver-kidney replacement is strongly recommended, either simultaneously or successively. However, the transplantation carries high risks and especially in PH1 patients, since the high plasma oxalate causes a rapid deterioration of the allograft. Nevertheless, this problem seems to have been solved during this century due to a better management of the oxalate levels (70).

Today some other palliative treatments are applied in the clinic:

1.2.5.1 High fluid intake

The concentration of oxalate in urine is critical for the formation of CaOx crystals (31). An increase in the urine volume dilutes oxalate, and therefore a high fluid intake is prescribed in PH1 patients (3 L/m^2 of body surface distributed during 24 hours) (28). The use of a gastrostomy tube is needed in infants and young children to assure a high fluid supply. Special care has to be taken in cases of fluid losses (diarrhea, vomiting and fever), and even during normal activities, such as physical exercise.

1.2.5.2 Diet

In the case of PH1 a dietary change is not required, since the majority of the oxalate is endogenously produced (28). However, oxalate-rich foods and excessive ascorbic acid (Vitamin C) intake should be avoided (23). Calcium restriction is counter-productive since it binds to dietary oxalate in the intestine and avoids its absorption (29).

1.2.5.3 Alkalization of urine and other inhibitors of CaOx formation

Alkaline citrate is used to reduce CaOx saturation. The first reason is that citrate forms soluble complexes with calcium, thus inhibiting its interaction with oxalate. In addition, it is converted to bicarbonate in the liver and excreted in urine, where it triggers an increase in the pH. Urine alkalization stimulates the secretion of citrate and also its binding to calcium (71). In PH1 the

standard treatment includes 0.1-0.15 g/kg of potassium citrate divided into 3-4 doses per day. It has been shown that this treatment decreases stone formation and nephrocalcinosis and stabilizes the renal function (72). However, sodium citrate should be used in cases of high levels of potassium in plasma (28). Orthophosphate (20-60 mg/kg/day) has the same effect and has been reported to trigger a benefit comparable to potassium citrate (73).

1.2.5.4 Management for urolithiasis

Surgical intervention for removal of stones is not recommended in PH1 patients, since the surgery would increase the inflammation and contribute to the development of ESRD. Therefore, an endoscopic procedure is the most adequate method to remove multiple stones in PH1 (28).

1.2.5.5 Dialysis

Renal replacement has to be performed in PH1 patients that develop ESRD. An aggressive dialysis treatment is required to decrease the plasma oxalate levels, and hemodialysis and peritoneal dialysis are recommended (28). The plasma oxalate levels are reduced up to 60% during hemodialysis, but bounce back to 80% of the pre-dialysis level within 24 hours and to 95% within 48 hours (31). The liver of PH1 patients produce a mean of 4-7 mmol/1.73 m^2/24 h of oxalate, while the dialysis is only able to remove 1-4 mmol/1.73 m^2/24 h, therefore not completely preventing the accumulation of the metabolite (21). As a consequence, hemodialysis has to be applied 5-6 times a week for 3-5 hours/session and it is combined with nightly peritoneal dialysis (23). Considering the low efficacy, dialysis is only used while waiting for transplantation and is not recommended if preventive transplantation is feasible (28).

1.2.5.6 Pyridoxine hydrochloride (pyridoxal 5'-phosphate, PLP)

The elevation of the concentration of PLP in the cytoplasm increases the binding speed of this cofactor to the monomeric form of AGT and acts as a prosthetic group. In addition, PLP can act as a chaperone for AGT since it triggers a better transport to the peroxisome (74). The treatment with pyridoxine hydrochloride (5-20 mg/kg/day) is known to be effective only in some PH1 patients, depending on the molecular alterations, but it should be tested in every patient (28). Clear evidences suggest that this treatment is effective in patients carrying the mutations G170R and F152I (75,76), where the defective folding of the enzyme leads to the mistargeting of the AGT to the mitochondria. The increased concentration of the cofactor leads to an improved protein folding and its correct transport to the peroxisome. Other mutations that destabilize the structure of the protein (such as the mutation I244T in the minor allele) could also respond to the treatment (56,77).

1.2.6 Development of novel therapies

Many novel approaches are being tested preclinically in several PH1 models. Martin-Higueras *et al.* recently reviewed some of these approaches (Figure 6) (78).

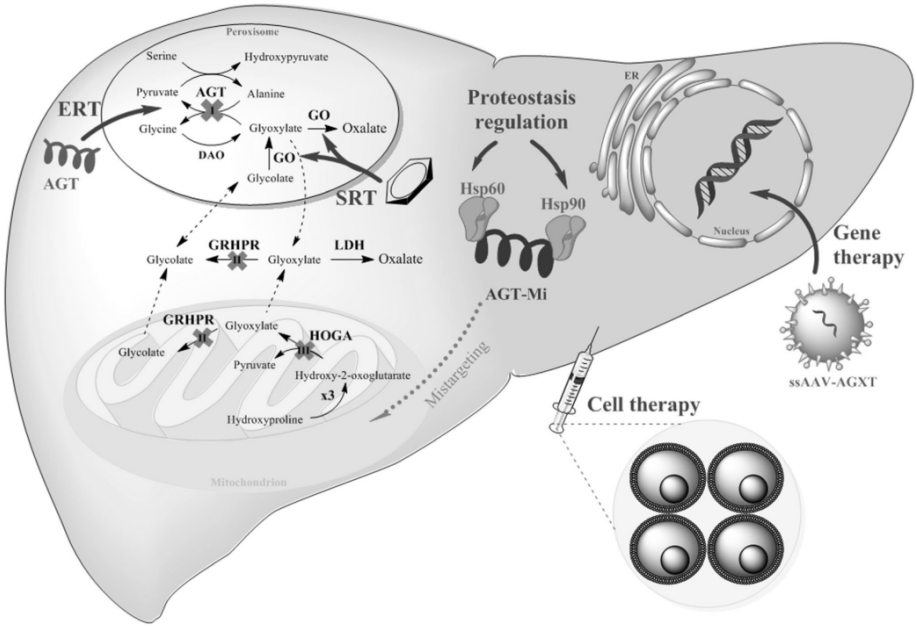

Figure 6. New therapeutic strategies that are currently being developed for the treatment of PH1 (78)**.** Enzyme replacement therapy (ERT) using intravenously delivered modified AGT recombinant protein; substrate reduction therapy (SRT) inhibiting glycolate oxidase (GO) enzyme; regulation of the proteostasis of AGT to allow complete and correct folding of the protein; cell therapy using hepatocytes with correct AGT expression, and gene therapy using recombinant single-strand AAV vectors carrying the correct *AGXT* gene (ssAAV-AGXT).

As in many other diseases, the development of new molecular therapies for PH1 requires a good knowledge of the mechanisms involved in the stabilization and progression of the disease. In PH1 is important to note that AGT-deficient hepatocytes conserve all other metabolic functions and are not damaged due to oxalate overproduction. For this reason, the hepatocytes that express a functional AGT do not have a selective advantage. Therefore, if only a low percentage of hepatocytes was corrected, the rest would continue producing the toxic metabolite causing renal damage. Researchers should be aware of this characteristic to develop and optimize new therapeutic strategies to reach a high percentage of hepatocytes. The exact percentage of hepatocytes that needs to be corrected to achieve a therapeutic reduction in oxalate remains unclear. Some approximations

suggest that a correction of 40% could be enough, although it is based on gene therapy experiments in mice and could be different in humans (79,80).

1.2.6.1 Enzyme replacement therapy (ERT)

ERT is based on the administration of the missing enzyme to the patients intravenously, modified or not, to reach the target organ and restore its activity. This strategy has been used in hemophilia, a disease characterized by the deficiency in a coagulation factor, and in lysosomal storage diseases (LSD). The approach has been applied successfully in these diseases because the coagulation factors act in the blood and the lysosomal enzymes can enter the lysosome directly by endocytosis. However, in the case of AGT the enzyme needs to overcome several barriers, such as specific liver targeting, the escape from the lysosome to the cytoplasm, and the re-transportation to the peroxisomes. Different strategies have been considered in order to increase the transport of AGT to the hepatic peroxisomes. For example, the addition of a cell-penetrating peptide (CPT) like trans-activator of transcription (TAT), poly-arginine or chemically attached galactose residues could target the enzyme specifically to the liver. Hemaglutinin tags have been added to facilitate the endosomal escape. The posterior transport to the peroxisome has to be also feasible after the modifications (81). However, this approach has not been tested so far in the clinic.

1.2.6.2 Substrate reduction therapy (SRT)

The rational of SRTs is to reduce the production of the toxic metabolite or its precursor. In the case of PH1 the inhibition of glyoxylate synthesis from glycolate has been suggested as efficient SRT, since glycolate is metabolized from HP in the mitochondria and then transported to the peroxisome, where it is converted into glyoxylate (82,83) (Figure 1). As described, the glyoxylate is synthesized from glycolate by the enzyme GO, and the inhibition of this enzyme is expected to decrease glyoxylate synthesis. GO is a peroxisomal, FMN-dependent α-hydroxyacid oxidase (84) that is encoded by the gene *HAO1* in humans (*Hao1* in mice) that catalyzes the oxidation of glycolate to glyoxylate (the precursor of oxalate) (85). In 2016, Martin-Higueras *et al.* generated a *Hao1*$^{-/-}$ mouse that developed non-pathogenic glycolic aciduria as only phenotypic change (78). Glycolate was accumulated in absence of GO activity, but being a small and highly soluble molecule it was easily eliminated through urine. Moreover, they generated a double KO *Hao1*$^{-/-}$/*Agxt*$^{-/-}$ mouse, which presented no hyperoxaluria but glycolic aciduria. Therefore, they concluded that the inhibition of GO led to decreased oxalate synthesis without any pathological phenotype, thus proving to be a safe and efficient target. Several strategies are being developed to inhibit the expression or activity of GO. Several authors have inhibited *in vivo* the expression of GO by means

of *HAO1*-specific siRNAs directed to the liver using siRNAs in lipid nanoparticles (86) or by binding to N-acetylgalactosamine (87). An efficient *Hao1* mRNA and GO protein reduction was achieved in mice, rats and NHPs. Moreover, two pharmaceutical companies are running Phase I clinical trials in PH1 patients using these strategies to target *HAO1* expression: Dicerna (Dicerna Pharmaceuticals 2016, NCT02795325) and Alnylam (Alnylam Pharmaceuticals 2016, NCT02706886). In fact, preliminary results from the Alnylam trial were presented during the annual meeting of the American Society of Nephrology in 2017 (https://www.asn-online.org/education/kidneyweek/2017/program-abstract.aspx?controlId=2827611). Furthermore, the use of small molecules to inhibit the activity of GO could be also an interesting approach (88). In a recently published paper, a high-throughput study was performed to identify new small molecules with capacity to inhibit GO activity and three promising hits were obtained (89).

However, the safety of this approach is still controversial since contradictory results have been reported in the literature. GO deficiency has been described as a benign rare metabolic disorder. Proof of it is a case reported in 2014, of a child with the mutation c.914-1G>C. This mutation affects a splice acceptor in intron 5 of the *HAO1* gene, which leads to a 53 amino acid deletion and the loss of protein function (90). No associated pathological phenotype was observed, except for a glycolic aciduria. However, recently another case was reported, where the patient showed hyperoxaluria and glycemic aciduria in presence of a mutation in the *HAO1* gene and normal AGT activity and immunoreactivity (91). A similar phenomenon was described in a study of Li *et al.*, where the treatment of WT mice with a siRNA for *Hao1* led to an increase in urinary oxalate (83). The authors suggested that a possible reabsorption and metabolism of glycolate into oxalate in a GO independent manner could occur in the kidneys of mice, and also humans.

Other possible targets for SRT in PH1 still remain unexplored. Some evidence suggested that the inhibition of the expression of hydroxyproline dehydrogenase, or HYPDH, the enzyme that catalyzes HP in the mitochondria (Figure 1), decreases the oxalate production in the PH1 mouse model (83). It has been shown that HP contributes to 65% of the glycolate synthesized in humans (83) and, as in the case of GO, a rare autosomal recessive disorder of HYPDH deficiency (Hydroxyprolinemia) has been described, which is non-pathological (92). Another possibility could be the inhibition of LDH, which is involved in the transformation of glyoxylate into oxalate. Finally, the reduction of glyoxylate could come from the increase of its degradation instead of a decreased synthesis. For example, an increased GRHPR activity would lead also to decreased glyoxylate levels.

The combination of complementary strategies could be the most beneficial to reduce oxalate to non-damaging levels.

1.2.6.3 Chaperone-proteostasis regulator therapy (CPRT)

The term “proteostasis” refers to the intracellular homeostasis of the proteins and comprises protein expression and regulation, folding and stability, interaction with chaperones, degradation and intracellular trafficking. In the case of AGT, proteostasis has special importance since most of the mutations leading to PH1 affect protein folding, stability, dimerization and subcellular localization. Moreover, AGT is a big protein with a complex structure and it has been described that some of its partially folded states associate with chaperones such as HSP90, HSC70 or GroEL (a bacterial chaperone) *in vitro* (17,56,93). As explained, the treatment with pyridoxine leads to the stabilization of unfolded AGT and to its proper intracellular targeting because of the chaperone effect of the cofactor. Therefore, two CPRT approaches could be applied. On one hand, the intracellular HSP70 chaperone machinery could be activated; however, the main problem of this approach is that the HSP machinery is very complex and safe and efficient targets have to yet be described. On the other hand, pharmacological and chemical chaperones could be designed to stabilize unfolded or partially folded AGT forms. Normally, these types of compounds are structurally similar to known protein ligands or inhibitors and favor a compact state of the proteins. It is thought that this novel therapy could be applied successfully in PH1 but its usefulness is limited by the high concentration of chaperone needed inside the cells, which complicates the administration to the patient (21). Opicci *et al*. investigated the role of the AGT inhibitor aminooxyacetic acid (AOA) as chaperone (94). They concluded that the *in vitro* treatment with AOA increased the detoxification of glyoxylate in cells expressing the G41R, G170R and I244T variants. The improvement is associated with an increase of thermal stability, the proper localization of G170R and I244T in the peroxisome variants and an increased enzymatic activity of the G41R variant. As AOA is an inhibitory molecule they designed and tested AOA analogues with reduced inhibitory activity, obtaining a hit molecule that only decreased 30% of the activity of WT AGT and conserved all the beneficial effects over the mutant AGT variants.

1.2.6.4 Oxalate degradation

The oxalate is an end product of the metabolism and cannot be further metabolized in humans. However, a bacterium from the gut microbiota called *Oxalobacter formigenes* has the potential to degrade oxalate: It produces an oxalate-formate membrane transporter, oxalyl-CoA decarboxylase, and formyl-CoA transferase – all off which are involved in oxalate processing. The colonization of

this bacterium could lead to the metabolism of the oxalate taken up in the diet. As known, oxalate is transported through the intestine by passive and active transport, implicating a possible elimination of oxalate through this pathway. Moreover, it has been shown in the PH1 mouse model that the colonization with *Oxalobacter formigenes* activated the secretion of oxalate into the intestine and led to a reduction in urine oxalate (95). Four Clinical trials have been performed to date where PH1 patients orally received a preparation of *Oxalobacter formigenes*. The treatment was demonstrated to be safe and a beneficial effect was observed in the first Phase I trial (96). However, in further Phase I/II and Phase II/III trials the main endpoint of the studies was not fulfilled, namely the reduction of oxalate levels in urine (97–99). It was hypothesized that some parameters, such as the stratification of patients based on baseline renal functionality, could have biased the results. Nevertheless, in the last two studies a correction in plasma oxalate levels was observed (98,99). Further studies should be carried out in order to increase the efficacy of this treatment, which could easily be combined with other treatments.

1.2.6.5 Gene and cell therapies

PH1 can be cured with liver transplantation, which means that the reconstitution of correct function of AGT enzyme in the liver would lead to the improvement of the disease. This can be achieved by gene and cell therapy approaches, which aim at altering or substituting the diseased cells. These strategies are currently being developed and applied to PH1. Cell therapy for PH1 consists of the transplantation of WT or patient-derived-corrected hepatocytes to substitute the AGT-deficient cells. This was the approach performed by Jiang *et al.*, in which a correction of oxalate levels in *Agxt*$^{-/-}$ mice transplanted with WT hepatocytes was observed (100).

Several viral vectors have been tested for gene therapy of PH1 in the *Agxt*$^{-/-}$ mice: First generation adenovirus (101), third generation adenovirus or helper-dependent adenovirus (HDAd) (79) and AAV (80). In all the cases, the treatment demonstrated to be safe and to efficiently express AGT protein and reduce urine oxalate levels. However, a deep analysis of each treatment needs to be done in order to select the most adequate vector and strategy to treat PH1 patients. Further explanation of some of these methods is given in the “Gene therapy” section.

In this context, gene or genome editing strategies are being developed and could be applied to treat human diseases in two ways: *ex vivo* editing to correct patient cells and their subsequent transplant to patients, and *in vivo* editing using gene therapy tools. These approaches are also explained in ‘Genome editing’ section.

1.2.7 PH1 models

Several models have been established for the study of molecular mechanisms of PH1 and the application of new treatments.

1.2.7.1 Cell models

The most frequently used cell culture model is based on Chinese hamster ovarian cells (CHO). These cells do not express the enzymes involved in the glyoxylate pathway, such as GO, AGT and GRHPR. Behnam *et al.* generated CHO lines stably expressing these genes individually or in combination (102). The CHO cell line expressing GO only was sensitive to glycolate, which caused cell death, and this toxicity was corrected co-expressing AGT or GRHPR. This model has been widely used to characterize the two polymorphic variants and the mutants of AGT (77) as well as to study different therapeutic approaches, such as a high-throughput screening of GO inhibitor molecules (89).

The generation of patient-derived induced pluripotent stem cells (iPSCs) has brought the opportunity to study many diseases in the genetic context of each patient. In the particular case of PH1, iPSCs have been generated from fibroblasts of a patient carrying the I244T mutation (103). The differentiation of these pluripotent cells to hepatocytes could allow the study of molecular mechanisms of the disease and the testing of various treatments *in vitro*. Furthermore, the correction of the iPSCs and the subsequent transplantation of iPSC-derived hepatocytes could be used as a cell therapy for PH1 patients.

1.2.7.2 Animal models

A mouse model generated by Salido *et al.* in 2006 has been used in most of the *in vivo* experiments published to date (101). To generate this model, mouse embryonic stem cells were subjected to a recombination process that substituted the genomic region comprising exon 4 to 8 of murine *Agxt* by a neomycin resistance cassette. The model was established on a mixed background (129Sv x C57BL/6) and subsequently backcrossed with C57BL/6 to obtain a pure C57BL/6 background. Several differences between *Agxt*$^{-/-}$ mice and their WT littermates were observed, in particular the oxalate excretion in 24-hour urines. It was higher in males than in females, which was probably due to the hormonal regulation of GO that leads to an increased glyoxylate load in males (101). All KO mice were positive for COM crystals in urine sediments. Male animals of a mixed background (129Sv x C57BL/6) developed CaOx stones in the bladder, while pure C57BL/6 animals and 129Sv x C57BL/6 females did not. This was an interesting fact, taking into account that no gender- or

background-related difference in ionic composition of the urines was observed. However, in other studies higher calcium levels in the urines of male mice were reported, independent of the genotype (6). As for kidney damage, mild nephrocalcinosis together with isolated CaOx deposits was observed in some of the mixed background mice. The almost absent kidney damage, observed even in the presence of high oxalate concentration in urine, could be explained by the high GFR in these mice, which makes them less prone to generate CaOx deposits. When C57BL/6 PH1 animals were challenged with the precursor of oxalate ethylene glycol (EG), which was added to drinking water (0.7% concentrated) during 3 weeks, the mice presented with elevated oxaluria and plasma oxalate when compared to WT littermates at the end of the challenge. Moreover, all KO animals had decreased creatinine clearance and nephrocalcinosis ranging from mild to severe.

1.3 Gene Therapy

According to the NIH, gene therapy is an experimental technique that uses genetic material to treat or prevent disease (https://ghr.nlm.nih.gov/primer/therapy/genetherapy). Four strategies are being used: (a) replacement of the mutated gene by introducing a healthy copy of the gene; (b) inactivation of a mutated gene that is not functioning properly or of another gene directly involved in the disease, (c) introduction of a new gene that will help to fight the disease, and (d) edition of the genome of the diseased cells.

The wide application of gene therapy can be deducted from its description. After many years of research defining strategies to treat a whole variety of diseases, the preferential investigation lines have been stablished. Taking into account the clinical trials performed to date, the most common application of gene therapy is cancer treatment (64.6% of the trials), followed by the treatment of monogenic disorders (10.5%) (Figure 7A). The vectors more often used in gene therapy clinical trials are adenovirus and retrovirus (Figure 8A). However, the comparison between the statistical analyses performed in 2012 and 2017 referring to gene therapy clinical trials shows the increase in frequency of trials for monogenic disorders and the use of AAV vectors (Figures 7 and 8).

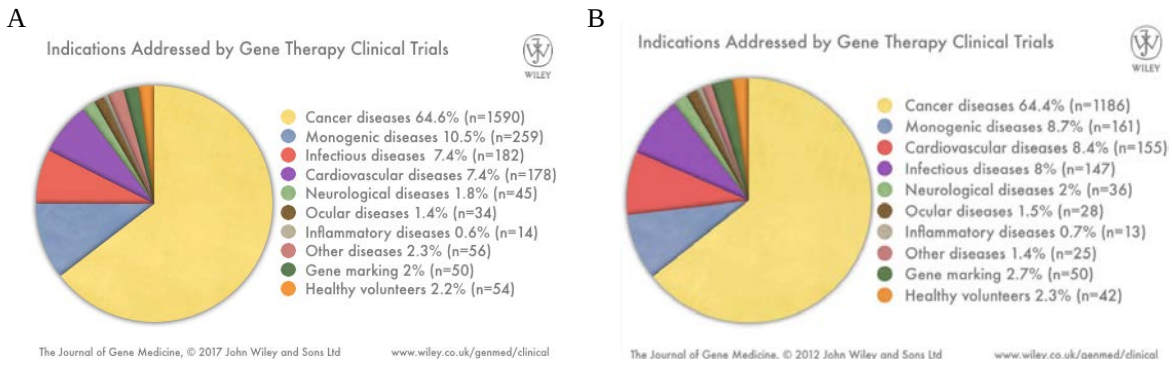

Figure 7. Indications for the treatment with gene therapy in all the clinical trials performed until 2017 (A) and 2012 (B). Data obtained from The Journal of Gene Medicine (www.wiley.co.uk/genmed/clinical) and (104).

E*x vivo* gene therapy is based on the isolation of cells from a patient or a healthy donor, the *ex vivo* expansion and genetic modification of these cells, and the administration of the modified cells to the patient to treat a disease. It has been mainly applied to hematological disorders and to cancer immunotherapies. The gene transfer to hematopoietic stem cells (HSC) has been used in several pre-clinical and clinical studies aimed at curing diseases such as severe combined immunodeficiencies (SCID), Wiskott-Aldrich syndrome (WAS), β-thalasemia and Fanconi's anemia (105,106). The development of chimeric antigen receptor (CAR) T-cells has emerged as an efficient therapeutic approach to treat several type of cancers (107).

The *in vivo* applications of gene therapy have been widely studied, mainly for the treatment of monogenic disorders. The best example is the treatment of hemophilia B using AAV vectors to express the deficient coagulation Factor IX (108).

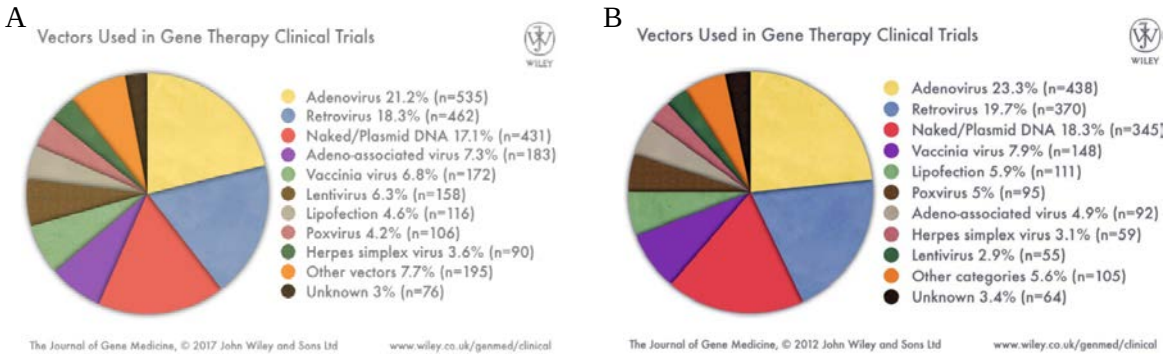

Figure 8. Vectors used in gene therapy clinical trials performed until 2017 (A) and 2012 (B). Data obtained from The Journal of Gene Medicine (www.wiley.co.uk/genmed/clinical) and (104).

1.3.1 AAV vectors

1.3.1.1 AAV biology

AAV is a helper-dependent parvovirus from the Parvoviridae family, which requires the coinfection of another virus (adenovirus or herpes simplex virus) to complete its replication cycle. AAVs are not pathogenic in human, which explains their relatively recent discovery as a contaminant in a simian adenovirus preparation (109). They are small viruses (18-25 nm of diameter) with a single stranded DNA (ssDNA) of 4.7 Kb. Many different serotypes, which are similar in structure and genome, have been isolated from organs of humans and primates (110). Each particle is composed of an icosahedric capsid formed of three proteins called viral protein 1, 2 and 3 (VP1, VP2 and VP3). A single copy of the viral genome of either polarity is found inside the capsid. The genome consists of two inverted terminal repeats (ITR) that form hairpins in the extremes of the genome and contain the only *cis* regulatory elements in the virus: origin of replication, terminal resolution site as well as packaging and integration signals. Furthermore, the genome contains two genes, one involved in virus replication (Rep) and other responsible for the synthesis of the capsid proteins (Cap), and three promoter sites, which allow the generation of seven different transcripts by alternative splicing (Figure 9). The first two promoters, called P5 and P19, are involved in the synthesis of the four Rep proteins (111). The two major Rep proteins, Rep78 and Rep68, are involved in the viral genome excision, rescue, replication and integration; while the two minor proteins, Rep52 and Rep40, are essential for the accumulation and packaging of replicated ssDNA genomes. The P40 promoter is implicated in the transcription of the Cap gene, which gives the viral proteins VP1, VP2 and VP3 by splicing. They assemble at a ratio of 1:1:10 to form the capsid (112). Recently a new ORF was found inside the Cap gene that generated the assembly activating protein 2 (AAP2), which is thought to interact with the proteins of the capsid and acts as an assembly scaffold (113,114).

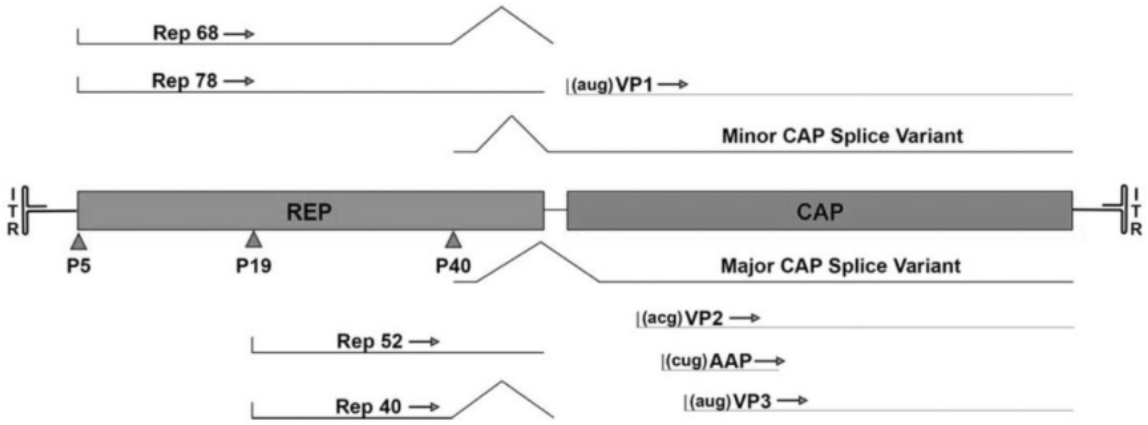

Figure 9. Structure of WT AAV genome and transcriptional variants (111)**.** ITR=inverted terminal repeats; REP=genes involved in replication; CAP=genes involved in the generation of the capsid. P5, P19 and P40 are the three promoters that have been described.

1.3.1.2 AAV as gene therapy vector

In order to generate a recombinant AAV vector the viral genes, Rep and Cap, are eliminated and substituted by the therapeutic expression cassette of interest. The ITR sequences are the only viral genomic sequences required to package the DNA into the capsid.

The production of recombinant AAV vectors requires provision of the genes deleted from the genome (Rep and Cap), and are supplied in *trans* together with the necessary genes from the helper-virus. Today, the two most common procedures for AAV vector production are based on transfection of mammalian cells (such as HEK293 cells) and baculovirus infection of insect cells (Baculovirus-SF9 cells system) (112).

Normally, the ITRs from the AAV serotype 2 are employed together with a variety of serotype capsid depending on the gene therapy strategy. All serotypes have been tested in several pre-clinical models (Figure 10). In the clinic, AAV2, AAVrh10 and AAV9 have been used for the brain; AAV2, AAV4 and AAV8 for the eye; AAV1, AAV2 and AAV9 for the muscle, and AAV2, AAV5 and AAV8 for the liver (Figure 10) (115,116). Some of the serotypes have shown special characteristics, such as the ability to cross the blood-brain-barrier as in the case of AAV9 (117).

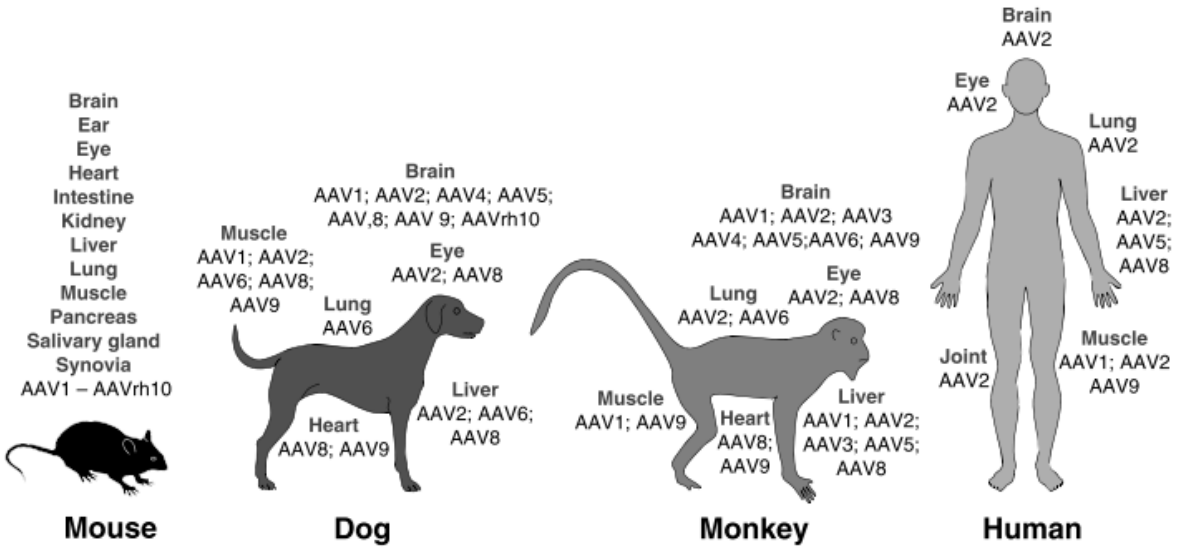

Figure 10. Summary of the AAV serotypes tested in various animal models and in humans to target different organs (115)**.**

The recombinant virus is believed to follow the same infection process as the WT virus, except for the transcription of the transgene instead of the viral genes. The receptors and co-receptors that mediate the entrance of the vector into the cell have been identified for almost all the serotypes of AAV. Glycans are used as attachment receptors and a broad range of cell surface receptors to mediate the uptake. It is believed that the tissue-specific tropism is determined by the binding specificity of the vector to the glycan and the entry receptor (111). Recently a 'universal' receptor necessary for the infection of all the serotypes has been described (118), it was called AAV receptor (AAVR).

The intracellular trafficking pathway of the vector remains unclear and it may be serotype-dependent. However, a model has been established in which the vector enters by the endosomal pathway, is able to escape from the endosome and enters the nucleus. Once in the nucleus, the DNA is released from the capsid, the complementary DNA strand is synthesized and transcription is started. The viral genomes remain stable in the nucleus forming concatamers, which are the result of the joining of many genomic molecules (ITR-ITR binding), which result in the formation of a circular and stable structure that remains episomal. Despite concatamer formation, a low percentage of AAV genomes integrate into the host genome. In fact, it is known that WT AAVs are able to integrate in the chromosome 19 in a locus called AAVS1 (119), which is considered a safe harbor locus for integration. The specificity of integration is mediated by the protein Rep78 (120); thus the integration of recombinant AAVs would not be specific since the Rep gene is eliminated from the genome. There is some concern about the potential occurrence of insertional mutagenesis in AAV

gene therapy. For example, Nault *et al.* analyzed samples derived from human hepatocellular carcinomas (HCC) and they found insertions of WT AAV2 genome fragments (121). In contrast, Gil-Farina *et al.* analyzed the integration profile of a recombinant AAV5 vector in the livers of patients and non-human primates (NHPs) treated with a gene therapy vector for acute intermittent porphiria (AIP), showing that the integration was random. Furthermore, they did not observe integration in HCC driver genes (122,123).

AAV is considered a low immunogenic virus, due to the absence of inflammation during the first hours post-infection and the low cellular immune response generated by the capsid. However, the humoral immune response against the capsid is high, producing elevated titers of binding and neutralizing antibodies. As a consequence, the administration of AAV vectors is dramatically affected in patients with pre-existing antibodies as the vector is neutralized and hence not able to transduce the target tissue. Although all pre-clinical data obtained from animal models suggested that AAV vectors do not elicit T cell responses, the first trial using an AAV2 to treat hemophilia B indicated otherwise: Upon delivery of an AAV2 expressing the human Factor IX (FIX) to the liver, the patients developed a response against the capsid, which led to the elimination of infected hepatocytes (measured as transient transaminitis) and the loss of transgene expression (124).

1.3.1.3 AAV-based gene therapy directed to the liver

The liver is the central metabolic organ of the body and many compounds and drugs are metabolized here by the hepatocytes. In addition, the production of many secreted proteins is carried out by this organ. More than 400 rare monogenic disorders with hepatic origin have been described and most of them could potentially be cured by liver transplantation (125). This fact leads to think that gene therapy aimed at restoring the function of the affected gene can also serve to cure the disease.

Another characteristic that makes the liver preferred target for gene therapy is its anatomy: It is a central organ, which receives blood from two different circulatory systems (systemic and portal), which filters approximately 1 L of blood per minute and which contains 10-15% of the total blood volume (126). This fact increases the probability of accumulating a systemically administered gene therapy vector. Another characteristic that favors the infection of the liver with gene therapy vectors is the existence of a fenestrated endothelium that facilitates the entrance of the virus into the hepatic parenchyma as well as its interaction with hepatocytes. Finally, as the AAV genomes form stable concatamers in the nucleus of the cells, a long-term expression is achieved in cells with low division rate, like hepatocytes that have a division rate of 1-2 divisions/year. However, AAV

genomes are rapidly lost in actively dividing cells, such as neonatal liver, which have limited the use of these vectors to adult livers.

The number of preclinical studies and clinical trials using AAV vectors to cure a wide range of rare monogenic hepatic disorders is rising with time (126). However, to date only a single study has characterized the use of AAV-based therapy for PH1 (80). This study was performed in the PH1 mouse model described above (1.2.7.2 section) and the vectors used were AAV5 and AAV8, which have known tropism for the liver. The expression cassette consisted of the hepatospecific promoter of the α1-antitrypsin gene (AAT) fused to the albumin enhancer (EAlbAAT), the human *AGXT* cDNA sequence followed by the woodchuck hepatitis virus posttranscriptional regulatory element (WPRE – an element that triggers increased transgene expression (127)) and the polyadenylation signal of the bovine growth hormone. The administration of these vectors resulted in the expression of AGT in the peroxisomes of the hepatocytes. The oxalate levels decreased in animals treated with both AAV8 ($5x10^{12}$ vg/kg) and AAV5 ($5x10^{12}$ vg/kg and $1.5x10^{13}$ vg/kg). In males but not in females the lowest dose of AAV5 ($5x10^{11}$ vg/kg) also corrected the oxalate metabolism, suggesting that in females the percentage of transduced hepatocytes was insufficient at this dose. The nephrocalcinosis observed after an EG challenge was also significantly reduced in the animals treated with AAV8.

As mentioned, the main impediment to treating PH1 with gene therapy is the necessity to correct a certain percentage of hepatocytes in order to decrease oxalate levels to normal values. To date, the greatest success obtained in the AAV-based liver gene therapy field has been in hemophilia B, where long-term therapeutic expression of the transgene could be achieved using an AAV8 expressing FIX (128). Furthermore, it was shown that the expression of only 5% of normal FIX levels in serum translated to therapeutic effect, converting the disease into mild hemophilia. Moreover, the transduction of a low percentage of hepatocytes was sufficient for expression of therapeutic FIX levels. However, the scenario found in PH1 is completely different and its AAV-based therapy has to be optimized to guarantee the correction of a high percentage of hepatocytes.

1.3.1.4 Strategies to optimize AAV-based gene therapy

- ***Optimization of the recombinant AAV genome***

Several strategies to improve the transduction of AAV vectors have involved changes at the recombinant genome level.

- Changes in ITR sequences: Some strategies to improve gene therapy include the modification of the ITRs as well as the combination of ITRs and capsids from different serotypes. ITR regions are versatile and can support changes that affect the packaging capacity minimally (129). Some studies propose the elimination of specific sequences from the ITRs, thereby decreasing the packaging capacity but increasing the transgene expression (130).
- Self-complementary AAV vectors (scAAV): In order to initiate the transcription of the transgene, the ssDNA genome of AAVs needs to be converted into double stranded DNA. This can be achieved by two different mechanisms: *de novo* synthesis of the complementary strand by the cellular polymerase or by complementary binding of the positive and negative strand. In scAAV genomes the replication termination signal in one of the ITRs is eliminated, which instead of stopping in the second ITR after replicating the first strand, leads to synthesis of the complementary sequence of the newly synthesized strand, generating a double stranded genome. scAAVs trigger faster and higher expression of the transgene (131,132); however, this strategy implies the reduction of the cloning capacity to 2.5 Kb.
- Promoter and enhancer sequences: Another strategy to increase the expression of the transgene is the use of different promoters and enhancers. In some cases, more potent promoters are needed, even if there is some leakage in non-targeted organs. In other cases, the promoter should be strictly specific to the target organ.
- Codon optimization of the transgene: The degeneration of the genetic code allows changing the DNA sequence of a gene without changing the protein sequence. Codon optimization has been used to enhance the expression of the transgene because of a higher affinity of the tRNA for certain codons (133). Many gene therapy strategies have included codon optimization of the transgene, which allowed a higher transgene expression (128,132,134).
- *Cis* activating elements: Some elements that enhance transcription of the transgene can be added to the cassette, such as the WPRE (127) or an intron (134).

- ***Change or optimization of the capsid***

As mentioned, different serotypes can be used to increase the transduction of a specific target organ (115,116). Moreover, several strategies led to the generation of new capsids: evolution of capsids by selective pressure (135), engineering of capsids that are able to escape the immune system (135), modification of single amino acids, combination of various serotypes (136) and reconstruction of ancestral capsids (137). Some of the capsid discovered using these strategies proved to increase the transduction of the liver.

- ***Changes in the administration procedures***

Various different administration routes have been investigated to increase the transduction of the target organ or tissue. For example, in order to improve liver transduction, direct administration into the hepatic bloodstream was assessed. Previous studies performed by our group in rodents have shown that the use of administration routes allowing direct access to the liver of AAV vectors increased the transduction of hepatocytes and mitigate gender-dependent differences (138). Mimuro *et al.* tested a combination of saline flushing and direct AAV8 injection into the portal vein in *Macaca fascicularis*, or cynomolgus monkeys, as a strategy for avoiding the effect of existing neutralizing antibodies (139). However, no studies on the effect of the administration route on transduction of AAV vectors are available in clinically relevant animal models like non-human primates (NHP). In these animals previous studies analyzed the impact of the administration route on liver transduction mediated by HDAd. In these studies the vector was injected via portal vein or peripheral vein with simultaneous occlusion of the hepatic blood outflow by placing a balloon catheter in the inferior vena cava (IVC) (140–143). The fenestrated endothelium of the liver favors the entrance of vector delivered intravenously and when the intrahepatic pressure increases, fenestrae become larger. This facilitates the penetration of the liver parenchyma by the vector in a way similar to what has been described for hydrodynamic injection in mice (144,145). In comparison with systemic administration, higher and longer-term transgene expression was achieved using these procedures. Oka *et al.* administered an HDAd-expressing LDL receptor (LDLR) to LDLR-deficient macaques via the hepatic artery while occluding the IVC (146). This resulted in an improvement of the LDLR expression levels and had a better therapeutic effect (measured as cholesterol reduction in blood) than when using IV administration. However, balloon occlusion of the IVC caused a 50% decrease of blood pressure with detrimental consequences.

A recent paper published by Greig *et al.* tested the impact of the infusion time in *Macaca fascicularis* and they found a trend of proportional correlation between infusion time and transgene expression (147). However, the variability within groups was high.

1.3.2 Genome editing

The genome or gene editing is a genetic engineering technique used to modify the DNA of a cell in a specific and precise way. To date it has been applied for the generation of several *in vitro* and *in vivo* models of disease and also as a therapeutic tool in many genetic diseases. Some gene editing strategies make use of engineered nucleases that specifically target the DNA and produce double-strand breaks (DSBs) while others are based on the insertion of a sequence by homologous recombination without causing any damage to the DNA. The last strategy has been used for decades to generate genetically modified animal models.

Regarding the gene editing processes using site specific nucleases, various biological tools have been adapted for investigational or therapeutic purposes. Three major platforms are used to target specific DNA sequences: ZFN (zinc finger nucleases), TALEN (transcription activator-like effector nucleases) and the CRISPR/Cas9 system (clustered regularly interspaced short palindromic repeats/CRISPR associated protein 9).

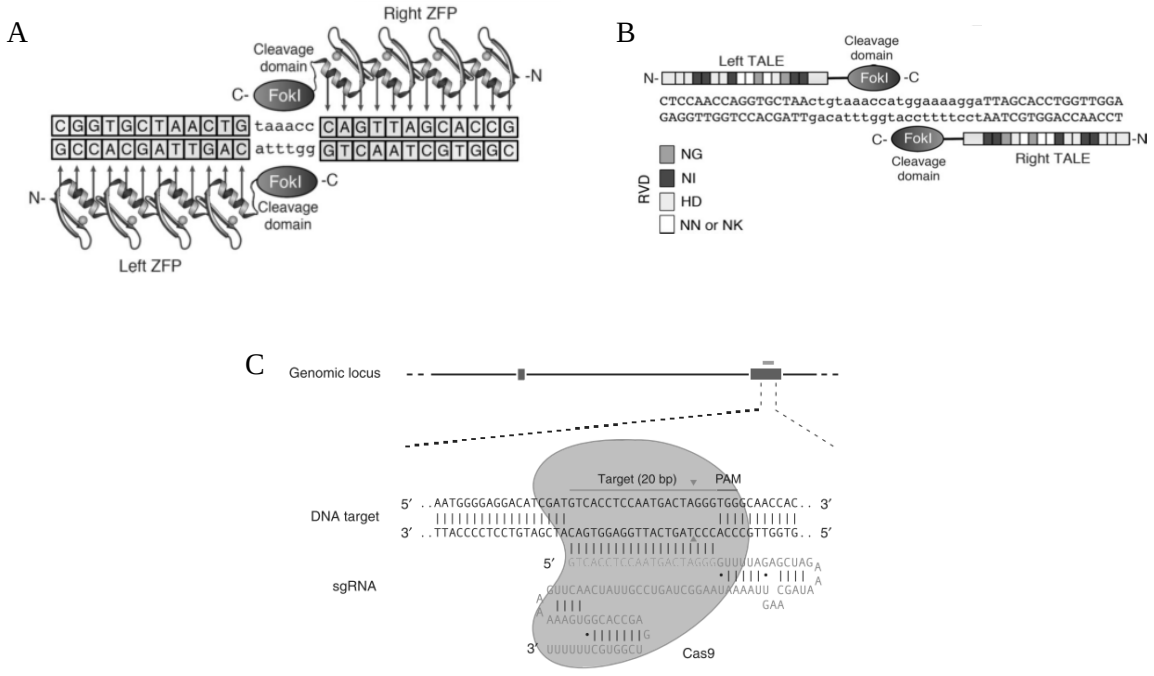

Figure 11. Schematic representation of the mechanism of action of several DNA-specific nucleases used in eukaryotes. A) Each domain of ZFN is engineered to recognize a specific trinucleotide (148). B) TALE nucleases recognize each nucleotide depending on the repeat-variable diresidues (RVD) (148). C) CRISPR/Cas9 system consists of the Cas9 nuclease and a single guide RNA (sgRNA) that is complementary to the target DNA (149).

ZFN derived from zinc finger DNA-binding domains (DBDs), which are the most frequent DBDs generated in eukaryotes. Each domain recognizes a triplet of nucleotides and the artificial engineering of the domain allows the recognition of several sequences. Thus, zinc finger DBD arrays have been built using a linker sequence, which allowed targeting of longer sequences. Moreover, the addition of a FokI nuclease led to the generation of ZFN that generate DSBs in the genome (Figure 11A) (148).

TALE domains derived from DNA binding proteins present in the plant pathogenic bacteria genus *Xanthomonas*. These DBDs are composed of 33-35 amino acid repeat domains that bind to a single nucleotide. The specificity of the binding is derived from two hypervariable amino acids called repeat-variable diresidues (RVD). The arrangement of nucleotide-specific domains is engineered to target any sequence in the genomic DNA, but the sequence must start with a T to promote the binding of the protein. These TALE sequences have been fussed to FokI nucleases that generate DSBs in the targeted region (Figure 11B) (148).

CRISPR/Cas9 is a system derived from bacteria consisting of a nuclease (Cas9) that is guided by a RNA to the specific target site in the genome. The alignment of the guide RNA (gRNA) with the target DNA sequence leads to DSBs generated by the Cas9 nuclease (Figures 11C and 12) (149).

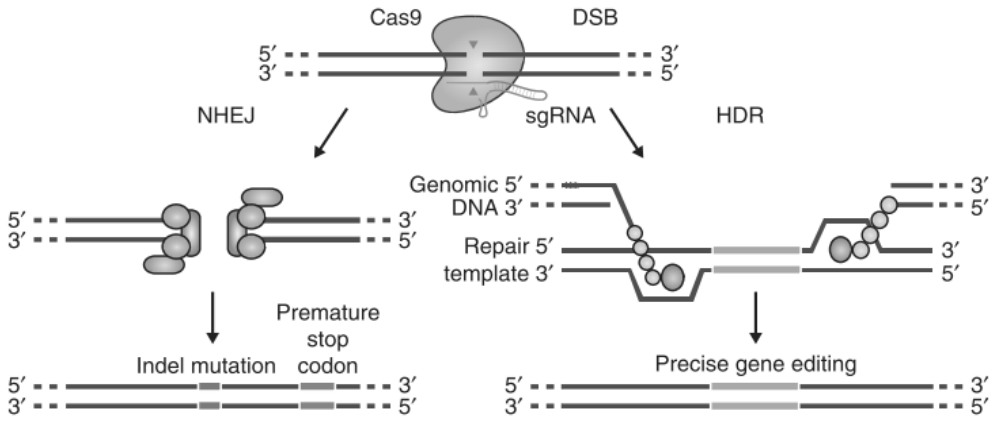

Figure 12. Cellular repair mechanisms after the generation of a DSB (149)**.** The generation of a DSB (in this case using CRISPR/Cas9 system) triggers the activation of the cellular repair mechanisms, namely non-homologous end joining (NHEJ) and homology-directed repair (HDR). Indels (insertions and deletions) are generated by NHEJ, which introduces errors in the coding sequence. The DNA is specifically repaired by HDR whenever a DNA template is present.

The generation of DSBs in the genomic DNA promotes the activation of cellular mechanisms involved in the repair of the DNA damage. There are two main DSB repair pathways: non-

homologous end joining (NHEJ) and homology-directed repair (HDR) (Figure 12). NHEJ is an error-prone mechanism to repair DNAs with a DSB (Figure 13). In the canonical pathway (150), the heterodimer Ku (Ku70/Ku80) binds immediately to the ends left by the introduction of a DSB. Then Artemis, which has various nucleolytic activities, is recruited into the DNA-PK complex and is activated by DNA-PK autophosphorilation. Subsequently, another complex containing XRCC4 (involved in the stabilization of the free DNA ends) and DNA ligase IV (ligation of free ends) is recruited (151) (Figure 13). Alternative pathways have been described, which depend on the DSB characteristics (152). Overall, insertions and/or deletions (indels) are generated in the damaged DNA during NHEJ DNA repair. Genome editing strategies have taken advantage of this mechanism to introduce errors in specific regions, particularly in coding regions, to inhibit the expression of a certain gene, e.g. when generating KOs. HDR on the other hand, is a mechanism that leads to specific repair of the DSB in presence of a template, which contains sequences homologous to those present in the flanking region of the DSB. It is a complex mechanisms in which proteins such as RAD and BRCA1 are involved (150). The HDR mechanism has been used to integrate sequences in the genomic DNA or to correct point mutations (Figure 12).

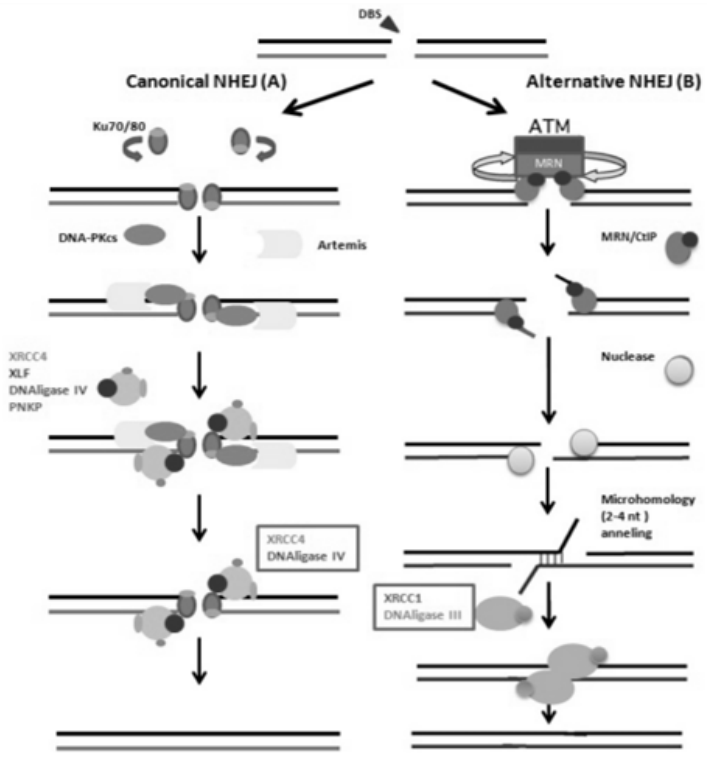

Figure 13. Schematic representation of canonical and non-canonical (or alternative) NHEJ pathways (151)**.** The canonical pathway includes proteins such as Ku70/80, DNA-PK and Artemis, and the broken

DNA ends are joined by DNA ligase IV. In the non-canonical pathway, DNA ligase III is the enzyme that repairs the break.

1.3.2.1 CRISPR/Cas systems in bacteria

CRISPR/Cas9 systems are present in many bacteria and archaea and they are the 'adaptive immune system' of these microorganisms. CRISPR loci were first sequenced by Mojica *et al.* in the archaea *Haloferax mediterranei* (153). The genomic structure of CRISPR had not been observed previously (Figure 14A) (154): It is made up of repeated palindromic fragments of 24-47 bp, which are separated by spacers of 26-72 bp. The number of repeated sequences varies between species. The spacers are not usually repeated and most of them match with sequences that can be found in phages or in plasmids. Upstream of the CRISPR loci a sequence called leader was found, which can span up to 550 bp. The CRISPR associated genes (Cas genes) are located in the same genomic region, upstream of the leader. In the 5' extreme of the CRISPR loci another fragment is transcribed, the so-called trans-activating crRNA (tracrRNA) (154).

When a bacterium is infected by a phage or receives a plasmid, Cas proteins fragment the foreign DNA into small pieces, which are then introduced in the CRISPR loci between the leader and the first palindromic repeat. The CRISPR locus is transcribed and other Cas proteins are involved in the delivery of RNA fragments containing a palindromic repeat and a spacer, which is called crispr RNA (crRNA). Once produced the crRNA binds to tracrRNA and to the Cas nuclease. This complex is able to recognize a phage or plasmid DNA fragment that is complementary to the spacer and it generates a DSB in the fragment. Therefore, the bacterium becomes resistant to certain phages or plasmids (Figure 14B) (154).

The only limitation in using these systems for targeting is the need of a consensus sequence located 5' or 3' of the targeted regions. This sequence is called 'protospacer adjacent motif' or 'PAM' and varies in sequence and location depending on the Cas nuclease.

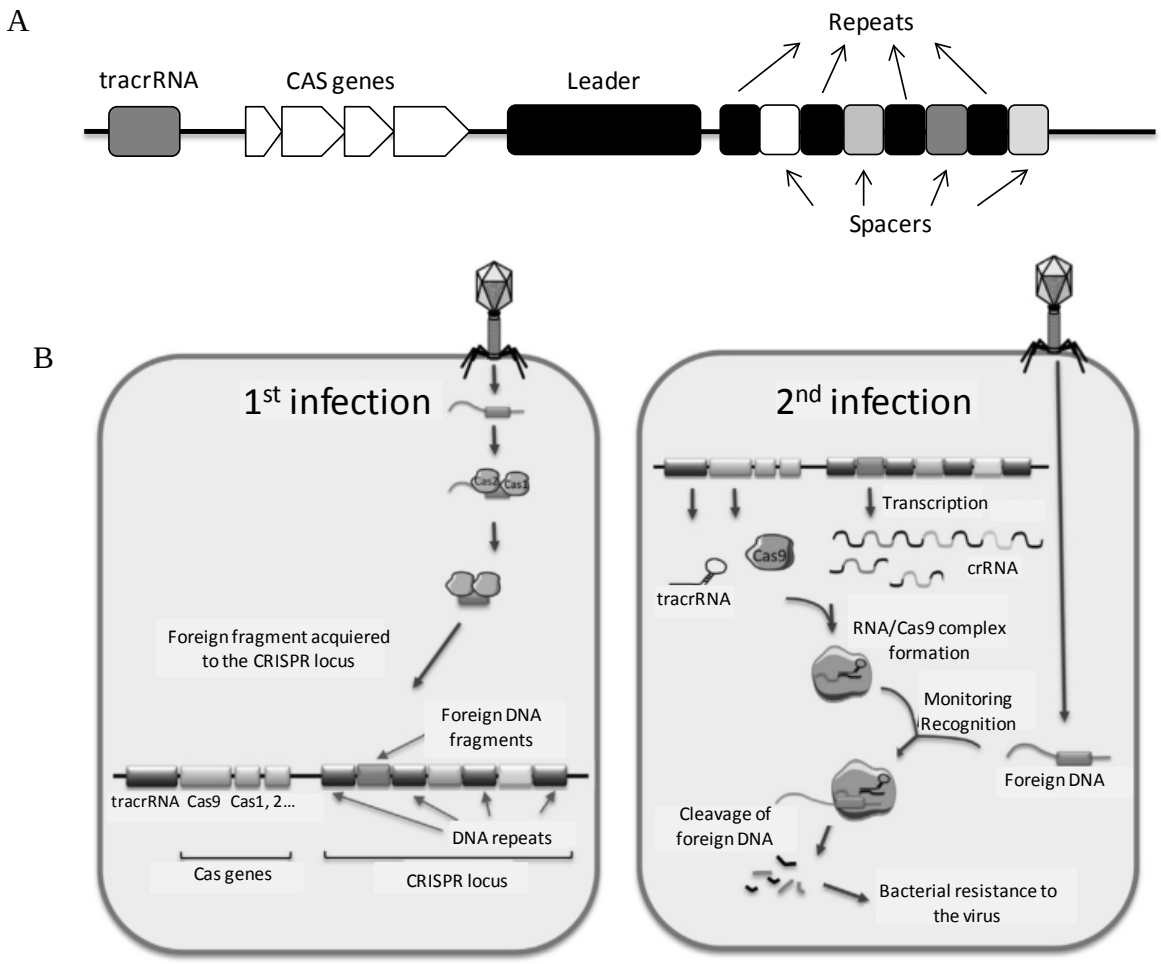

Figure 14. CRISPR/Cas9 system. A) Structure of the genomic loci that encode the complete CRISPR/Cas9 system in bacteria. B) Function of CRISPR/Cas9 system in bacteria (155). During the first infection with a phage, the foreign DNA is fragmented by Cas enzymes and incorporated into the CRISPR locus between the leader and the first palindromic repeat. Upon secondary infection, Cas9 is bound to the tracrRNA and the crRNA and this complex is able to introduce DSBs in the foreign DNA, leading to its destruction and to resistance against the infection. tracrRNA=trans-activating crRNA; crRNA=crispr RNA.

1.3.2.2 CRISPR/Cas systems adapted for eukaryotic genome editing

So far many types of CRISPR/Cas systems have been described in bacteria, however, only a few have been adapted for their use in eukaryotic cells. Most of the publications in which CRISPR/Cas systems are applied in eukaryotic cells or organisms use the Class 2 CRISPR/Cas system, mainly the type II (156). The Cas for this kind of CRISPR is called Cas9 and the most popular one is derived from *Streptococcus pyogenes* (SpCas9) (149). SpCas9 has been used for both *in vitro* and *in vivo* applications. In addition, many sequence changes have been explored to increase the

specificity and the efficiency of targeting, such as introducing nicks instead of generating DSBs, and the fusion of crRNA and tracRNA to form a single guide RNA (sgRNA).

The PAM sequence needed by SpCas9 to generate a DSB is NGG, which has to be located after the 3' end of the gRNA-targeted region. The main problem of SpCas9 is its large size (4.1Kb), which has hampered its cloning and expression in AAV vectors. Recently Cas9 from *Staphylococcus aureus* (SaCas9) was discovered. SaCas9 has a comparable efficiency to that of SpCas9 and the advantage of a smaller size, which allowed its cloning into recombinant AAV genomes (157).

- ***In vivo applications of a CRISPR/Cas9 system directed to the liver***

The liver is an ideal organ for the experimental application of CRISPR/Cas9-based therapies because of the following reasons: the targeting and the expression of the Cas9 nuclease and the gRNA can be done using viral gene delivery vectors; also, many preclinical models of monogenic liver diseases are available and well characterized. Thus, AAV vectors would be the perfect delivery platform to perform *in vivo* proof-of-concept studies with the objective of exploring the efficacy of CRISPR/Cas9 system to treat certain disease. However, since SpCas9 was employed in the first works, it was administered using adenoviral vectors or hydrodynamic injection of plasmids into the tail-vein due to its size.

Initially, NHEJ-based gene disruption and knocking out was tested in genes such as *Cebpα*, *Pten* and *Psck9* (158–160). Overall, the generation of indels was observed in a high percentage of the targeted genomic region in hepatocytes, as well as the reduction of the targeted protein levels and the effects of this reduction (steatosis in the liver of the mice with Pten inhibition and alterations in cholesterol metabolism in animals with Psck9 inhibition). Adenoviruses were used as carries of the CRISPR/Cas9 system in all this studies. Interestingly, the adenoviral recombinant genome and Cas9 expression were almost lost by day 90 after vector administration, while the genomic modification was maintained, even after a partial hepatectomy (158).

The efficiency of gene disruption and long-term KO generation using CRISPR/Cas9 system was high in these studies and it was also used as SRT for hereditary Tyrosinaemia type I (HT1) (161). In HT1 fumarylacetatoacetate hydrolase, or FAH, is mutated. It is an enzyme implicated in the tyrosine metabolism. The substrate of FAH, fumarylacetoacetate (FAA), and its precursor maleylacetoacetate (MAA) are accumulated in the hepatocytes of patients causing hepatotoxicity. Overturf *et al.* transplanted WT hepatocytes into the *Fah*$^{-/-}$ mouse model and they observed the repopulation of the liver with the transplanted hepatocytes (162). This means that the hepatocytes expressing a functional FAH enzyme have a selective advantage over the uncorrected hepatocytes,

which facilitates the treatment by gene therapy and potentially gene editing. NTBC (2-(2-nitro-4-trifluoromethylbenzoyl)-1,3cyclohexanedione) is the drug used for the treatment of HT1, because it blocks the enzyme hydroxyphenylpyruvate dioxigenase (HPD), which is located upstream of the mutated FAH enzyme in the tyrosine metabolism pathway. The inhibition of HPD allows reducing the hepatotoxic metabolite that is accumulated in HT1. Pankowicz *et al.* knocked out the *Hpd* gene in the $Fah^{-/-}$ mouse model using hydrodynamic injection of a plasmid encoding SpCas9 and the specific gRNAs to delete an exon of the *Hpd* gene (161). The selective advantage of the corrected hepatocytes in HT1 gave rise to the almost complete repopulation of the liver with the engineered cells.

To date, less experience has been acquired with the knock in (KI) strategy mediated by the HDR mechanism. Yin *et al.* corrected the point mutation in the *Fah* locus in the $Fah^{-/-}$ mouse model applying hydrodynamic injection of a plasmid expressing SpCas9 and the gRNA directed to the region where the point mutation is located, together with an ssDNA oligo as donor template with the correct sequence of the gene (163). The elimination of NTBC triggered the expansion of the corrected cells, which repopulated the liver, and the correction of the disease phenotype. A similar study was subsequently published by the same group, in which the delivery method was different: the mRNA of SpCas9 was formulated in lipid nanoparticles and delivered intravenously together with an AAV8 containing the donor DNA and expressing the gRNA (164).

In April 2015, Ran *et al.* published the discovery and characterization of SaCas9 (3.1Kb), which is smaller than SpCas9. It was cloned into an AAV vector and tested *in vivo* targeting the *Pcsk9* gene (157). In the case of SaCas9, the PAM is NNGRRT and is located 5' of the gRNA-targeted sequence. However, this sequence is less abundant in the genome and thus may generate restrictions for some targets. Nevertheless, the *Pcsk9* KO efficacy was similar to that observed using the SpCas9.

The discovery of SaCas9 gave rise to other HDR-based strategies. An example is the work published by Yang *et al.*, where they used a dual AAV vector strategy to treat a urea cycle disorder caused by ornithine transcarbamylase (OTC) deficiency (165). They corrected the point mutation that is present in the *Oct* locus in the spf^{ash} mouse model for this disorder. One of the AAVs expressed SaCas9 while the other carried the donor template with the correct sequence and also expressed the gRNA targeting the region of the mutation. Interestingly, this approach was applied in newborn as well as in adult mice and the maximum HDR observed was 20.1% and 2.1% respectively. This data confirmed that newborns are more prone to HDR than adults, in which NHEJ was more prevalent. Another important fact reported in this publication is that when the

AAV vector expressing SaCas9 was administered to newborns, it was diluted with time and led to undetectable SaCas9 expression by 8 weeks after the treatment.

The main concern about gene editing is the possible off-target DSB generation in sequences that are similar to the target sequence. Some considerations have to be given to this issue in order to eliminate its negative consequences: such as finding equilibrium between the efficacy and predicted off-targeting effect of the gRNA. Furthermore, the Cas9 can be sequence modified in order to be less prone to off-target modifications. This is the strategy used by Ran *et al.*, who modified SpCas9 to generate nicks in the DNA instead of DSB and used two gRNAs to generate the DSB in the specific DNA sequence (157). Despite the development of strategies to reduce the probability of off-targeting effects, its analysis and characterization remains essential. Many methods have been developed to address this problem (166) but the most conservative approach would be the whole genome sequencing analysis in order to detect every possible off-targets.

In conclusion, it has been demonstrated that the *in vivo* applications of CRISPR/Cas9-based therapies for liver are feasible and efficient. However, the therapeutic strategy has to be carefully chosen for each disease, and there may be many monogenic diseases that cannot be cured using these approaches.

2. HYPOTHESIS AND OBJECTIVES

2.1 Hypothesis

Since PH1 is a genetic disease that can be cured by liver transplantation, gene therapy or gene editing strategies targeting the liver might offer promising therapeutic strategies for patients suffering this devastating disease.

Gene therapy has been successfully used for the treatment of PH1 in mice, but as explained, a high percentage of hepatocytes needs to be corrected to decrease oxalate production and to achieve therapeutic efficacy. Therefore, this approach requires optimization. Moreover, an important part of the preclinical development of gene therapy for PH1 is the analysis of efficacy and toxicity in relevant animal models, such as NHP. Thus, new PH1 models should be stablished for this purpose. Furthermore, SRT by inhibiting GO using siRNAs has been described to provide beneficial effects in a PH1 preclinical model. We hypothesize that CRISPR/Cas9-based long-term GO inhibition may improve SRT therapy and may serve as lifelong treatment for these patients (Figure 15).

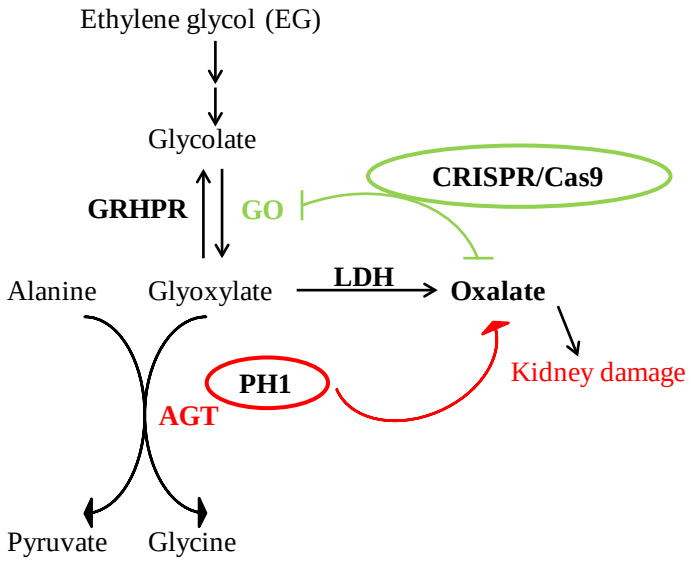

Figure 15. Therapeutic strategy to treat PH1 with CRISPR/Cas9-based SRT. Scheme of glyoxylate pathway indicating the cause of PH1 (in red) and the strategy based on the inhibition of GO using the CRISPR/Cas9 system (in green) to reduce oxalate levels. GRHPR=glycolate reductase/hydroxyproline reductase. GO=glycolate oxidase. LDH=lactate dehydrogenase. AGT=alanine-glyoxylate aminotransferase. PH1=primary hyperoxaluria type I.

2.2 Objectives

Since PH1 is a fatal disease lacking proper therapeutic alternatives, the main goal of this work is to contribute to the development of new therapies. Our approaches include the improvement of AAV-mediated gene therapy strategies and the evaluation of CRISPR/Cas9-mediated *in vivo* gene editing as an SRT strategy for PH1.

Specific goals:

1. Optimization of AAV-mediated gene therapy for PH1.
    a. Generation of new *in vivo* diet-induced hyperoxaluria models in WT mice and non-human primates (NHP).
    b. Improvement of the AGXT expression cassette by codon optimization of human *AGXT* cDNA.
    c. Increasing of AAV-mediated liver transduction efficiency by using liver directed administration routes.
2. Evaluation of CRISPR/Cas9-mediated SRTs for PH1
    a. Design and characterization of CRISPR/Cas9 systems targeting GO.
    b. Evaluation of therapeutic effect and safety of newly designed CRISPR/Cas9 systems.

3. MATERIALS AND METHODS

3.1 Primers for cloning, qualitative and quantitative PCR

The names, sequences and applications of all the primers used in this thesis are shown in Table 2.

Table 2. Description of the primers used: name and sequence of each primer are shown, and the method for which they were used.

Primer name	Sequence	Application
mHao1 gRNA1 Fw	5' CACCGTCCGTGGATAGAGCTTCCATC 3'	gRNA cloning
mHao1 gRNA1 Rv	5' AAACGATGGAAGCTCTATCCACGGAC 3'	
mHao1 gRNA 2 Fw	5' CACCGTCAACTTCTGTTTTAGGACA 3'	
mHao1 gRNA 2 Rv	5' AAACTGTCCTAAAACAGAAGTTGAC 3'	
U6 promoter	5' ACTATCATATGCTTACCGTAAC 3'	Sequencing of gRNA
mHao1.int1.F2	5' CCAAAGCCTATAAGGGGATG 3'	PCR of exon 2 of *Hao1* gene for SURVEYOR and sequencing
mHao1.int2.R1	5' CATCCTAGGAAGGGTGTTCG 3'	
mHao1.int1.F1	5' CACCATGTCAGGCTCAGAAGGC 3'	Primers to sequence exon 2
mHao1.ex2.R1	5' GTCCACGTGAGCCATGCACTG 3'	
SaCas9 Fw	5' AAGCCATCCCTCTGGAAGAT 3'	Vector titration, quantification of viral genome copies and SaCas9 mRNA expression
Sa Cas9 Rv	5' TGCCCTTCTTGCTGTTTTCT 3'	
mGAPDH Fw	5' TGCACCACCAACTGCTTA 3'	qPCR
mGAPDH Rv	5' GGATGCAGGGATGATGTTC 3'	
m-β-actin gDNA Fw	5' GACACTGGCACAGCCAACTTT 3'	
m-β-actin gDNA Rv	5' GTGTCTACACCGCGGGAATG 3'	
m-β-actin cDNA Fw	5' ACGGCCAGGTCATCACTATTG 3'	
m-β-actin cDNA Rv	5' CAAGAAGGAAGGCTGGAAAAGA 3'	
coAgxt Fw	5' TACACTGGACAGACAGGGCAT 3'	
coAgxt Rv	5' CCTT GTCGCTGAAGCTGAT 3'	
wtAgxt Fw	5' GCATCGACATCCTGTACTCG 3'	
wtAgxt Rv	5' CTGAAGGAGATGAGCGAGGT 3'	
mHao1 Fw	5' ACCCCTTTTCCTTCATTGCT 3'	
mHao1 Rv	5' TTGCCCAAACACATTTTCAA 3'	
hGAPDH Fw	5' GGTCGGAGTCAACGGATTT 3'	
hGAPDH Rv	5' CCAGCATCGCCCACTTGA 3'	
hSEAP Fw	5' CCTGTTTGCTCCTCCGAT 3'	
hSEAP Rv	5' GGGTTCTCCTCCTCAACT 3'	

3.2 Antibodies

All antibodies and their characteristics are listed in Table 3.

Table 3. Description of the antibodies used for WB and IHC.

Target	Origin	Type	Label	Method	Supplier	Cat#	Dilution
α-GO	Rabbit	Polyclonal	N/A	WB	Self		1:2,500
α-GAPDH	Mouse	Monoclonal	N/A	WB	Sigma-Aldrich	G8795	1:5,000
α-AGT	Rabbit	Monoclonal	N/A	WB	Abcam	ab178699	1:2,000
α-mouse IgG	Sheep	Polyclonal	HRP	WB	GE-Healthcare	NA931V	1:5,000
α-rabbit IgG	Sheep	Polyclonal	HRP	WB	GE-Healthcare	NA934V	1:2,500

3.3 Animal models: Manipulation and procedures

3.3.1 Non-human primates (NHP)

Eight young-adult male cynomolgus monkeys (*Macaca fascicularis*) obtained from R.C. Hartelust (Tilburg, Holland) were used to test new routes of administration of AAV vectors. All animals weighed between 4 and 6 kg at the start of the experiment and were housed in standard facilities with controlled temperature and humidity, 12-hour light cycles, and with *ad libitum* access to water and food. The animals were tested for neutralizing antibodies against AAV5 virus before receiving the vector. All experiments were performed in compliance with the regulations of the ethics committee for animal experimentation of the University of Navarra and were approved by the Government of Navarra (protocol number 167-14).

Vector administration: Two new routes of administration were used and compared to the intravenous (IV) administration route. The monkeys were divided into three groups, each receiving a dose of $3x10^{13}$ viral genomes per kilogram (vg/kg) of the vector AAV5-AAT-SEAP (see "AAV vectors" section) using different routes. The first group (n=2) received the vector intravenously (IV group) in the saphenous vein diluted in a volume of 4 mL/kg. The other two groups received the vector through the suprahepatic veins (SHV group) and the hepatic artery (HA group) respectively, in a total volume of 20 mL.

Extraction of samples: The first days after vector administration heparinized blood samples were collected in order to analyze acute hematological toxicity. Furthermore, serum samples were obtained during the experiment (basal and days 1, 3, 7, 14, 21, 28 and then every two weeks until the end of the experiment) for the analysis of biochemical serum parameters, viral shedding and transgene expression. All blood samples were extracted by inguinal vein puncture and aspiration. Nasal secretion, saliva, urine and feces samples were also collected (as before up to week 6) in order to analyze viral shedding in different body fluids. The secretions were collected with a sterile cotton-tipped swab and diluted in water to be processed as described below.

L-hydroxyproline inductions: An amount of L-hydroxyproline (HP, Applichem A3742) equivalent to 1% of the weight of the animal was mixed with yogurt and was administrated orally to the animals. Each animal received 1 dose per day during 3 days.

Euthanasia and necropsy: Animals were sacrificed by an injection of the drug T61 (Intervet). Animals were anesthetized prior to being sacrificed (Imalgene 1000, Ketamine 100 mg/kg). During the necropsy, frozen and 4% paraformaldehyde (PFA) fixed samples from different organs were obtained. The liver of each animal was dissected and samples of 8 regions were taken. Depending on its size, each region was further subdivided into 1-5 subregions in order to obtain 30 samples per animal for the analysis of the spatial distribution of vector genomes within the liver. Other organs were also collected for vector biodistribution studies. All tissue samples were frozen immediately and stored in liquid nitrogen until further processing.

3.3.2 Mice

Two animal strains were used: a PH1 mouse model (C57BL/6.Agxt^{tm1Ull}) obtained from Dr. Salido's laboratory (University of La Laguna, Tenerife, Spain) and WT C57B6/J animals purchase from Jackson Laboratories. The mice were maintained in specific pathogen free condition and with *ad libitum* access to food and water, with 12-hour light cycles. All the experimental procedures were approved by the Ethical Committee for Animal Testing of University of Navarra.

Vector administration: The animals received the vectors intravenously diluted in Dulbecco's phosphate buffer saline or PBS (Thermo Fisher Scientific) in a final volume of 150 µL/mouse under general anesthesia (Imalgene 500, Ketamine mixed with Rompun 2% Bayer). The dose of the vector differed between studies.

Extraction and processing of samples: Blood samples were obtained before the euthanasia from the suborbital venous plexus. Serum was obtained by allowing the blood to clot for at least 20 min at room temperature (RT) incubation, followed by centrifugation for 15 minutes at 3,000 rpm. The serum was stored at -20ºC until its analysis. Metabolic cages (Tekniplast) were employed for 24-hour urine collection. The urines were collected in 50 µL of 5N HCl for their acidification and oxalate conservation. Both, urine volume and water intake were monitored while the animals were inside the metabolic cages.

L-hydroxyproline administration: For L-hydroxyproline (HP, Applichem A3742) diet preparation powdered mouse-food was mixed with a solution of HP in drinking water. Food with different HP

percentages was prepared by weight relationship. Before the administration the food was irradiated for sterilization. The food was changed every day during the challenge.

Ethylene-glycol challenge: The ethylene-glycol (EG) (Sigma Aldrich, # 324558) gavage was performed by oral administration using an oral cannula. Each mouse received 15.5 mg of EG diluted in sterile water. For a longer induction, animals received EG diluted in drinking water (0.5% EG in water) and the challenge lasted for 7 days.

Euthanasia and necropsy: All the animals were sacrificed by cervical dislocation under general anesthesia. During the necropsy liver, spleen, kidneys, lungs, heart and brain were extracted from the animals. All the samples were frozen in liquid nitrogen. Liver and kidney samples were also fixed in 4% PFA for histological examination.

3.4 gRNA design and cloning

Benchling software was used to design the guide RNAs (gRNA) targeting the exonic sequences of mouse *Hao1* gene (www.benchling.com). The target sequences consisted of 21-nt followed by 5'-NNGRRT-3' PAM sequence, which is required for *Staphylococcus aureus* Cas9 (SaCas9) to generate a DSBs. Two gRNAs were selected based on their predicted on-target and off-target score, targeting the exon 2 of the gene (Table 4).

Table 4. Characteristics of the gRNAs designed using Benchling software.

Name	*Hao1*-g1	*Hao1*-g2
Taget gene	Mouse *Hao1* gene	
Region	Exon 2	
DSB position	6075	6139
Direction	Antisense	Sense
Sequence	5' TCCGTGGATAGAGCTTCCATC 3'	5' GTCAACTTCTGTTTTAGGACA 3'
On-target score	51.8*	45.1*
Off-target score	87.8**	65.5**

* Score calculated using the algorithm published by Doench *et al.* (187).
** Algorithm published by Hsu *et al.* (188).

They were cloned in pX602-AAV-TBG::NLS-SaCas9-NLS-HA-OLLAS-bGHpA;U6::BsaI-sgRNA plasmid (Addgene plasmid # 61593) (Figure 16) (157). The cloning was performed following the manufacturer's instructions. Briefly, two oligonucleotides were designed for each gRNA (Table 2), which were complementary except for the 5' extreme that was designed to overhang when the oligonucleotides were hybridized together. The vector was digested using BsaI enzyme, which

generated overhanging ends that were compatible with the ends left after the hybridization of the gRNA. The plasmid contained the SaCas9 gene expressed under the thyroxine-binding globulin (TBG) promoter, tagged with HA and OLLAS tags and flanked by nuclear localization signals (NLS). In addition, the plasmid had a U6 promoter for the sgRNA expression (gRNA and the tracrRNA fusion) and a cloning site where gRNAs were cloned using BsaI restriction enzyme. The expression cassette was flanked by the inverted terminal repeats (ITRs) that are necessary for the packaging of the DNA in AAV capsids.

Three vectors were generated for gRNA expression: one containing no gRNA as control of SaCas9 expression effect in absence of a guide (pAAV-SaCas9), and the other two expressed the two gRNAs (pAAV-SaCas9-*Hao1*-g1 and pAAV-SaCas9-*Hao1*-g2).

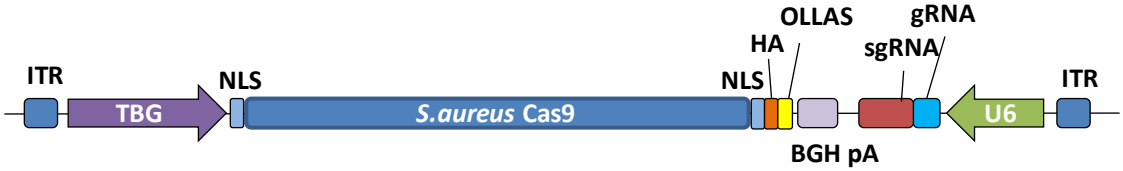

Figure 16. Cassette of the plasmid used for gRNA cloning. ITR: inverted terminal repeats. TBG: thyroxine-globulin binding promoter. NLS: nuclear localization signal. *S.aureus* Cas9: *Staphylococcus aureus* Cas9. BGH pA: Bovine growth hormone polyadenilation sequence. sgRNA: single guide RNA. U6: U6 promoter.

3.5 AAV vectors

Serotype 5 recombinant AAV (AAV5) vectors were used in the NHP study. The expression cassette of the AAV5 contained the coding sequence of the human secreted embryonic alkaline phosphatase (SEAP) gene under the control of the liver-specific promoter of the human α1-antitrypsin (AAT) gene (AAV5-AAT-SEAP). SEAP is a secreted protein, which is normally only expressed in embryos. Hence it can be used as a reporter protein and its expression can be measured in serum samples.

Figure 17. Recombinant AAV genome used for codon optimization studies. The construct contained AAT promoter with the albumin enhancer (EAlb), codon optimized or WT AGXT cDNA and the polyadenylation signal of the bovine growth hormone (BGH pA). The cassette was flanked by the ITRs of the AAV.

Different AAV serotypes were used for the studies in mice: for PH1 gene therapy serotype 5 AAV vectors were generated, while recombinant serotype 8 AAV (AAV8) vectors were produced for the gene editing approach. The AAV5 vectors carried constructs that expressed different versions of the *AGXT* gene (the human WT AGXT or the human codon optimized AGXT – coAGXT - sequence) under the control of a hepatospecific (AAT) promoter (Figure 17).

For the gene editing approach different construct were made as explained in the "gRNA design and cloning" section. These sequences were packaged in AAV8 capsids.

3.6 Generation of AAV particles

3.6.1 AAV production

HEK293T cells were used as packaging cells. The constructs containing the recombinant AAV genomes were transfected together with the helper plasmid pDP8.ape (Plasmid Factory, # PF478) that provides the genes required for the replication and encapsidation. The transfection was carried out using poly-ethylene imine (PEI, Sigma-Aldrich, # 408727). Cells were incubated for 72 hours and during this time the viral particles were assembled inside the packaging cells. Cells were collected in lysis buffer (50 mM Tris, 150 mM NaCl, 2 mM $MgCl_2$, 0.1% Triton X-100) and various freeze-thaw cycles were performed to release the viral particles. Cell debris was eliminated by centrifugation. The supernatant of the cells was collected and incubated in 8% poly-ethylene glycol (PEG-8000, Sigma-Aldrich, # P5416) for 48-72 hours to precipitate the particles. The supernatant was centrifuged and the pellet resuspended in lysis buffer. Cell lysate and precipitated supernantant were mixed and treated with 0.1mg/plate of DNaseI (Roche, # 10104159001) and RNaseA (Roche, # 10109169001) for 1 hour at 37ºC.

3.6.2 AAV purification

The viral particles were purified by ultracentrifugation in iodioxanol (OPTIPREP, Atom, # 415468) gradient. Different iodioxanol concentrations were prepared and added to an ultracentrifuge tube (Beckman, # 344326) as shown in Figure 18. Some of the solutions contained phenol red to facilitate the localization of the vector band. After sealing, the tubes were centrifuged at 69,000 rpm for 2.5 hours at 16ºC. The viral particles were packed in the 40% iodioxanol solution (between the two red solutions). An 18-19G gauge needle was employed to collect the virus, which was purified and concentrated using Amicon 100K columns (MERK Millipore, # UFC910008).

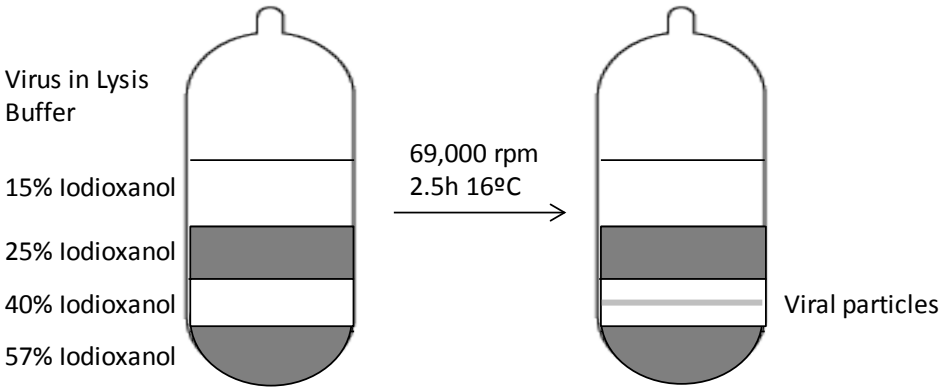

Figure 18. Iodioxanol gradient used for the purification of complete AAV particles. The grey bands indicate the solutions to which phenol red was added to facilitate the visualization of the band.

3.6.3 AAV titration

The titer of the vector was calculated by qPCR. Viral DNA was extracted using the High Pure Viral DNA Kit (Roche, # 11858874001) following the manufacturer's instructions. qPCR with sequence specific primers was performed and titers were calculated using a standard curve of the plasmid employed for the production.

3.7 Tissue processing

3.7.1 Isolation of genomic DNA

Total DNA was extracted from frozen tissues with the NucleoSpin® Tissue kit (Macherey-Nagel) following the manufacturer's instructions. Nanodrop 1000 machine (Thermo Fisher Scientific) was used to quantify the total DNA amount obtained from tissues.

3.7.2 Isolation of total RNA and retrotranscription

Total RNA was obtained using TRI Reagent® (Sigma-Aldrich, # A15T9424) following the protocol of the manufacturer. Subsequently, after quantification, 1 µg of RNA was treated with TURBO DNA-free kit (Thermo Fisher Scientific) to eliminate the contaminant DNA. Then, the RNA was retrotranscribed using a mix containing RNase OUT recombinant ribonuclease inhibitor (Invitrogen, # 10777019), M-MLV reverse transcriptase and its buffer (Invitrogen, # 28025013), dNTP mix (Applied Biosystems) and random primers (Thermo Fisher Scientific). The reaction consisted of 1 hour incubation at 37ºC followed by 1 minute at 95ºC to inactivate the enzymes.

3.7.3 Isolation of total protein and quantification

RIPA Buffer (0.75M NaCl, 5% of Tris 1M pH 8, 0.1% SDS, 1% Triton X-100, 0.5% sodium deoxycholate diluted in water) was supplemented before each use with 1 mM sodium orthovanadate, 1 mM PMSF, 1 mM sodium pyrophosphate and protease inhibitor cocktail. Tissue pieces were homogenized in RIPA buffer by mechanical disruption and ultracentrifuged at 45,000 rpm for 30 minutes at 4ºC. The protein concentration of the supernatant was calculated using the Pierce BCA Protein Assay Kit (Thermo Fisher Scientific).

3.8 Measurement of biochemistry parameters in serum

Biochemical serum profiles were analyzed both in NHP and in mice. In NHP primate alanine-aminotransferase (ALT), aspartate-aminotransferase (AST), gamma-glutamyl transferase (GGT), alkaline phosphatase (ALP), bilirubin, total serum proteins, urea and creatinine were measured after vector administration up to day 7. Reference values used to determine alterations in these parameters are shown in Table 5. At further serum extraction points, ALT and AST were measured to monitor liver damage and ALP to monitor transgene expression. All measurements were carried out in an autoanalyzer (COBAS, Roche).

Table 5. Summary of biochemical parameters measured in NHP, the abbreviation used, units and the normal reference range.

Parameter	Abbreviation	Units	Normal range
Albumin	Alb	g/dL	3.8-4.8
Total proteins	TP	g/dL	6.4-8.6
Bilirubin	Bil	mg/dL	0.2-0.4
Urea	Urea	mg/dL	8.8-37.4
Creatinine	Crea	mg/dL	0.5-1.1
Gamma-glutamyl tranferase	GGT	U/L	92.6-155-8
Alanine aminotrasferase	ALT	U/L	0-138
Aspartate aminotrasferase	AST	U/L	9.0-68.0

In mice, hepatic function was evaluated in the serum of treated animals extracted on the day of the sacrifice. ALT and bilirubin were measured for this purpose. Serum urea and creatinine were also measured to explore kidney function after EG challenge. Creatinine levels were calculated in all urines to normalize oxalate concentration. All measurements were carried out in a COBAS machine with serums diluted 1:5 and urines diluted 1:10 in PBS.

3.9 Hematological profile

The hematological parameters were measured in heparinized blood using the Hemavet 1700 (Drew Scientific) machine. Table 6 shows the ranges considered normal for each parameter.

Table 6. Summary of hematological parameters measured in NHP, the abbreviation used, units and the normal reference range.

Parameter	Abbreviation	Units	Normal range
White blood cells	WBC	K/uL	8.1-21.3
Neutrophils	NE#	K/uL	1.3-8.1
Lymphocytes	LY#	K/uL	3.5-8.3
Monocytes	MO#	K/uL	0.2-0.8
Eosinophils	EO#	K/uL	0.02-0.5
Basophils	BA#	K/uL	0-0.1
Red blood cells	RBC	M/uL	3.9-7.1
Hemoglobin	HB	g/dL	11.6-14.5
Hematocrit	HCT	%	38-48
Mean corpuscular volume	MCV	fL	56-69
Mean corpuscular hemoglobin	MCH	Pg	17.5-21.1
Mean corpuscular hemoglobin concentration	MCHC	g/dL	29.1-31.1
Red cell distribution width	RDW	%	12.8-14.6
Platelets	PLT	K/uL	300-512
Mean platelet volume	MPV	fL	NA

3.10 Assessment of total and neutralizing antibodies against AAV5

Levels of anti-AAV5 total antibodies in monkey serum were measured by an anti-AAV5 specific ELISA. 96-well flat-bottom plates (MaxiSorpR, Thermo Fisher Scientific) were coated with 100 ng of AAV5 capsids. Serial dilutions of monkey sera in PBS-Tween 20 (Sigma-Aldrich, P3563) were incubated with capsid in order to establish the antibody titer. As negative control PBS-Tween 20 was used. Subsequently, specific antibodies were detected with Protein A bound to horseradish peroxidase or HRP (Sigma-Aldrich). TMB reagent (BD, # 555214) was used to develop the ELISA. The titer was established as the lowest dilution resulting in an absorbance value higher than 5-times the absorbance corresponding to the negative control.

To detect neutralizing antibody (Nab) levels HEK293T cells were seeded in black 96-well culture plates (Costar) at a density of $5x10^4$ cells/well in 100 µl DMEM with 10% FBS and antibiotics (1% penicillin/streptomycin, Gibco). Cells were incubated overnight at 37°C. The day after, the following mix was prepared: an AAV5 expressing firefly luciferase under a cytomegalovirus

promoter (AAV5-CMV-luc) incubated with heat-inactivated serum sample at a total volume of 100 µl of DMEM 2% FBS supplemented with antibiotics. The multiplicity of infection (MOI) was $1x10^4$ viral genome copies per cell. Serial dilutions of each serum sample were prepared in duplicate. The mix was kept for 2 hours at 37ºC before being added to cells. Medium of the HEK293T cells was removed by aspiration, the mix was added to the cells and the plate incubated for 20 hours at 37°C. As a positive control, cells without any plasma addition were analyzed, while as a negative control not infected cells were used. The cells were washed with PBS and a PBS solution containing luciferine was added to the cells. Light emission from each well was captured using a PhotonIMAGER™ (Biospace LAB, France) and quantified in photons/cm^2/seg by drawing 96 squares grid over the plate. The anti-AAV NAb titer (EC50) was calculated with the use of LabKey Software. Plasma samples were considered to have neutralizing activity if the lowest plasma dilution inhibited vector transduction by at least 50%, as described before.

3.11 IFN-γ ELISPOT assay

These analyses were carried out in Dr. Mingozzi's laboratory (GENETHON, Evry, France). The cellular immune response in peripheral blood mononuclear cell (PBMC) samples was analyzed using monkey IFN-γ ELISpot PLUS kits (Mabtech), according to the manufacturer's instructions. PBMC samples were thawed during 10 minutes at 37ºC and placed in serum-free AIM V® medium (Life technologies). Benzonase nuclease was added to avoid cell aggregation before centrifuging at 300 rpm during 10 minutes. Cells were counted and $2x10^5$ cells per well were plated in commercial anti-IFN-γ antibody pre-coated plates over different stimuli. As negative control serum-free medium was used. As positive controls Concanavalin-A and anti-monkeyCD3 antibody were added. As specific stimulus an AAV5 peptide library was created, which consisted of 15-mers overlapping by 10 amino acids and covering the whole capsid protein sequence. The library was arranged in two different pools and added to the cells at a final concentration of 2 µg/peptide/well. Cells were incubated ON at 37ºC, with ambient O_2 and 5% CO_2. On the second day, the cells were removed and wells washed 4 times with 200µL of PBS. Biotin-conjugated secondary antibody (10 µg/mL) was diluted 1:1000 in PBS-1% BSA and added to each well. It was incubated for 2 hours at RT. After washing with PBS, 10 ng/mL of Streptavidin-ALP diluted in PBS-1% BSA was added to the wells and incubated for 1 hour at RT. The substrate was added to wash wells and incubated for 10-20 minutes at RT. The reaction was stopped using tap water, the plate washed and dried ON. The spots were quantified using a CTL analyzer.

3.12 Viral shedding

Body fluids (urine, feces, nasal secretion and saliva) were collected on days 0, 1, 3, 7, 14, 21, 28 and 42 for the analysis of the elimination of the virus. The secretions were collected with a swab and diluted in water. Total DNA was extracted with the NucleoSpin® Tissue kit (Macherey-Nagel) and quantitative PCR (qPCR) was performed using specific primers for SEAP gene (Table 2).

3.13 Measurement of SEAP activity in serum samples

SEAP activity was determined using the SEAP Reporter Gene Assay kit (Sigma-Aldrich, # 11779842001) according to the manufacturer's protocol. In short, serum samples containing SEAP were heated at 65ºC for 30 minutes in order to eliminate the endogenous alkaline phosphatase activity. A chemoluminescence substrate (CSPD) was added and dephosphorylated by placental alkaline phosphatase activity. Chemoluminescence was measured and related to a standard curve provided by the manufacturer.

3.14 Determination of indel generation in targeted DNA sequence

3.14.1 Surveyor assay

Surveyor assay kit (IDT Technologies 706020) was used for the analysis of indel generation after CRISPR/Cas9 treatment. Total genomis DNA was extracted and the targeted site was amplified using the Platinum taq (Thermo Fisher Scientific 11304011) enzyme and the primers named mHao1.int1.F2 and mHao1.int2.R1 (Table 2). The following PCR protocol was applied: 1 cycle of 2 minutes at 94ºC and 30 cycles of 15 seconds at 94ºC, 15 seconds at 58ºC and 45 seconds at 68ºC. The PCR protocol was followed by one cycle of heating and a constant temperature decrease (as specified in the manufacture's protocol) in order to rehybridize the PCR product. During the rehybridization heteroduplexes were formed between unmodified WT sequences and indel-containing modified sequences. Rehybridized samples were treated with Surveyor nuclease, which had endonuclease activity in the mismatches. Finally, the products were separated by electrophoresis in a 2% agarose gel and the band profile was analyzed (Figure 19).

Figure 19. Principle of Surveyor assay (149)**.**

3.14.2 TIDE analysis

The TIDE online tool (https://tide-calculator.nki.nl/) was used for the estimation of indel percentage in the targeted site (168). The same PCR as for the Surveyor assay was performed but without rehybridizing the PCR fragment. Instead, it was purified using the NucleoSpin® Gel and PCR Clean-up kit (Macherey-Nagel). The purified product was sequenced using nested primers (mHao1.int1.F1 and mHao1.ex2.R1, Table 2) and the resulting chromatograms were analyzed. The TIDE online tool compared the chromatograms of unmodified WT control sequences and the chromatogram of indel-containing modified sequences in the specific DSB site for a specific gRNA. Finally, an estimation of indel percentage in that specific chromatogram was obtained.

3.14.3 Next generation sequencing (NGS)

To further analyze off-target sites, the most likely off-target sites for each selected gRNA were determined using Benchling software (www.benchling.com) (Table 4). A total of 7 off-target candidates were selected for each gRNA. Primers spanning on-target and off-target sites for each gRNA were used to amplify relevant sequences by nested PCR. Briefly, 50 ng of genomic DNA was first amplified using specific primers using a KAPA HiFi HotStart ReadyMix PCR Kit (Kapa Biosystems) and purified using the Agencourt AMPure XP system (Beckman Coulter). Then, for each gRNA, equal amounts of purified amplicons from the same sample were mixed. Nested PCR was performed using 10 ng of PCR mix and universal primers with specific barcodes for each sample were used to generate Illumina amplicons. PCR products were purified as described above. A final library was generated by mixing equal amounts of the second PCR products and sequenced on Illumina MiSeq (2 × 250 bp paired end) at >10,000 × coverage at amplified regions. Data were processed according to standard Illumina sequencing analysis procedures. Processed reads were aligned to the reference (mm10) using bowtie2. Reads that did not map to the reference were

discarded. Insertions and/or deletions were determined by comparison of reads against the reference using the CrispRVariants R-based toolkit (167).

3.15 Western blot

After liver protein extraction and quantification (described in section 3.7.3), 20 µg of each extract were mixed with a loading buffer (containing 30% glycerol, SDS and DTT) and boiled for 5 minutes. The samples were loaded on 15% polyacrylamide gels and electrophoresis was used for protein separation by size. Subsequently, proteins were transferred to a nitrocellulose membrane (BioRad 162-0112). Membranes were stained using Ponceau Red dye to check the transference. After washing the dye with water, membranes were blocked using a Blocking Solution (ThermoFisher Scientific, # 37536) during 1 hour at RT on a shaker. Primary antibody (Table 3) diluted in blocking solution at the appropriate dilution was added and incubated ON while shaking at 4ºC. The membrane was washed 3 times using Tris-buffer saline (TBS)-Tween 20 0.05% for 10 minutes each wash. HRP-conjugated secondary antibody was added at the corresponding dilution in blocking solution and membranes were incubated 1 hour at RT on a shaker. After 4 washes of 10 minutes in TBS-Tween 20 0.05%, the peroxidase signal was developed using SuperSignal West Femto Maximum Sensitivity Substrate (ThermoFisher Scientific, # 34095) and Odyssey Fc (LI-COR) imaging system for image generation.

3.16 Oxalate measurement

Oxalate levels were measured using an oxalate kit (Trinity Biotech, # 591-D) according to manufacturer's instructions. Briefly, the urines were mixed 1:1 with 8% activated charcoal diluted in the assay diluent, and treated for at least 10 minutes at RT, shaking occasionally. The activated charcoal eliminated the compounds of the urine that interfered with the reaction. After centrifugation the supernatant was transferred to a new tube, and 5 µL of the samples or standards (Oxalate Standard 0.5 mM, Trinity Biotech, # 591-3) were mixed with 100 µL of reagent A and 10 µL of reagent B. The oxalate contained in the samples was metabolized by oxalate oxidase producing H_2O_2, which was used by the peroxidase in a redox reaction in which a chromogen is oxidized to a colored compound. The absorbance was measured at 595 nm and the oxalate concentration was calculated comparing absorbance with the standard curve. Oxalate µg per 24 hour was calculated using the oxalate concentration and the urine volume.

3.17 Glycolate measurement

This procedure was performed in Dr. Salido's laboratory at the University of La Laguna, Tenerife (Spain). Glycolate concentration in charcoal-treated urine samples was measured in a colorimetric assay using recombinant GO enzyme in 50 mM potassium phosphate buffer pH 7, coupled with HRP in the presence of sulfonated-DCIP and 4-aminoantipyrine (Sigma Aldrich) as chromogens, and measuring the absorbance relative to a glycolate standard curve 515 nm (168).

3.18 Immunostaining

Liver samples were fixed in 4% paraformaldehyde (PFA) for 24-48 hours. After the dehydration of the tissue by the incubation in increasing alcohol concentrations, the samples were embedded in paraffin blocks. The analysis of GO expression by immunohistochemistry (IHQ) was carried out in Dr. Salido's laboratory at the University of La Laguna, Tenerife (Spain) using Benchmark ultra (Ventana) equipment and reagents. Antigen retrieval was performed at 95ºC in high pH buffer (CC1, Ventana) for 24 min., and followed by incubation with anti-GO rabbit serum diluted 1:500 during 28 min at 37ºC. Next, a polymeric HRP-conjugated anti-rabbit IgG secondary antibody (Ventana) was used and a chromogenic signal was developed with DAB and copper enhancement (Ventana).

3.19 Statistical analysis

All results are represented as mean ± standard error of the mean (SEM). Sample sizes are noted in figure legends. All animals with successful intravenous injection were included in the study analysis and those animals with unsuccessful injection were excluded. Graphs and statistical analyses were performed using GraphPad Prism 5.0. Mann Whitney test was the test of choice to compare two groups. Kruskal Wallis test with Dunn's post-test was used to analyze differences between more than two groups. The Friendman test with Signs post-test was used for comparison between different administration groups at different times. p values smaller than 0.05 were considered significant.

4. RESULTS

4.1 Generation of a hyperoxaluria model in healthy WT animals

Animal models of disease are essential to determine the efficacy and the safety of novel treatments. The preclinical development of a drug has to include toxicity tests in clinically relevant animal models to determine the maximum dose that can be administered to patients in the absence of adverse events. NHPs are considered one of the best models to test the safety of a drug, including gene therapy drugs, due to similarities with humans in the immune response, metabolism and their large size (169). The main goal of our work is to develop new, efficient and safe treatments for PH1. Although a mouse model of PH1 is available, it has important differences with PH1 patients, such as the immune response or the oxalate metabolism. Despite thousands of preclininal studies in mice and NHPs using AAV vectors to target the liver, in none of them a T cell response against the vector capsid was detected; however, in several gene therapy trials for hemophilia B, T cell responses were developed leading to total or partial elimination of transgene expression (124,128). To investigate the oxalate metabolism, PH1 mice need to be challenged with precursors of oxalate in order to generate high enough oxalate levels to damage the kidneys, most likely because the GFR in mice is higher than in humans (101). In patients, the overproduction of oxalate is constant, leading to a continuous insult to the kidneys and development of urolithiasis, nephrocalcinosis and ESRD. In the PH1 animal model, none of these symptoms were observed, and only nephrocalcinosis developed in challenged animals (101).

In the present work, we decided to try to develop a PH model in macaques for the study of the efficacy of novel treatments. It is known that secondary hyperoxalurias are caused by an increase in oxalate or its precursor's intake in the organism (170). Different precursors can be taken up with the diet, such as HP. Therefore, we hypothesized that the oral administration of a diet highly rich in HP could lead to an increase in oxalate synthesis and its excretion in urine. Thus, one of the goals of this work was to develop a dietary hyperoxaluria.

4.1.1 A diet-induced hyperoxaluria model in WT mice

First, as proof of concept, WT C57BL/6 male animals were challenged by the administration of a HP-rich solid food. Three different HP concentrations were used, 1%, 3% and 5%. Before the administration of the HP-rich diet a basal urine sample was collected, and then, the animals were fed for 3 days with HP. During the experiment the animals were kept in metabolic cages in groups of 2 mice per cage and 24-hour urine samples were collected every day (Figure 20A). Oxalate measurement in urine revealed a significant increase of this metabolite during the feeding with the diets containing 3% and 5% HP in comparison to basal levels and to animals that received no HP or

low HP (1%) in their diet. After the elimination of HP from the diet oxalate levels returned to normal within 24-48 hours (Figure 20B).

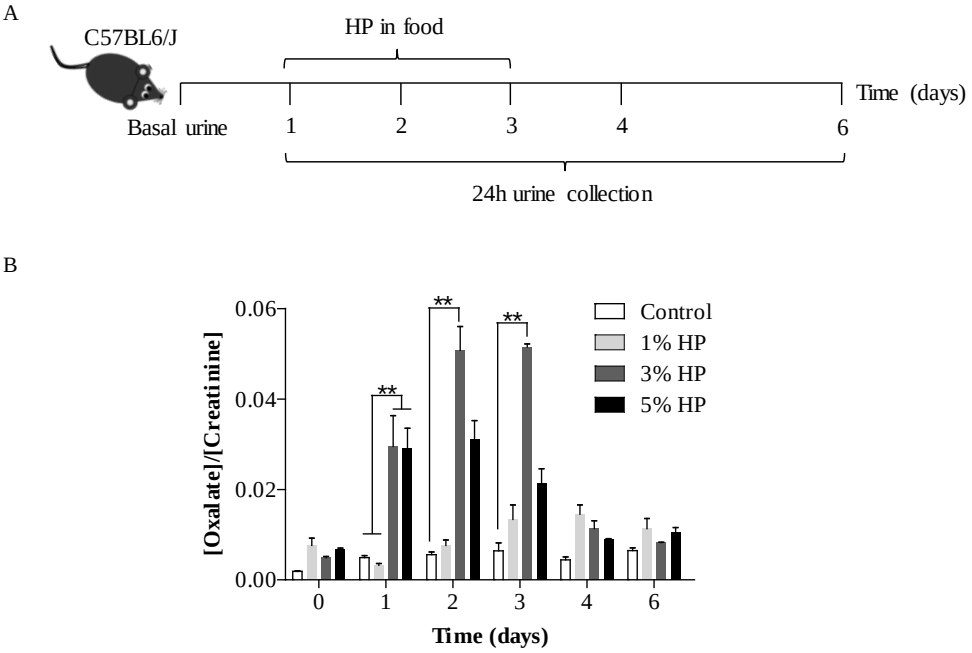

Figure 20. Set-up of a model of dietary hyperoxaluria in C57BL/6 mice. A) Schematic representation of the experimental procedure: urine collection and HP administration. B) Oxalate levels measured as oxalate concentration normalized to creatinine concentration in the urine of animals that received no HP or different concentrations of HP in food. Data of 4 urines per group are shown as mean ± SEM. Kruskal Wallis analysis was used to analyze differences between groups. ** = $p<0.01$.

4.1.2 Acute hyperoxaluria in *Macaca fascicularis*

For the generation of the model in macaques, 4 *Macaca fascicularis* males were fed with a dose of HP corresponding to 1% of their body weight. The HP dose was diluted in 100 mL of yogurt and each animal received 3 doses over 3 consecutive days. Three-hour urine samples were obtained daily during the course of the experiment and serum samples at days 0, 3, 5 and 7 and oxalate concentration was measured (Figure 21A). Urine oxalate progressively increased after each HP administration and returned to normal 48 hours after the last dose (Figure 21B). The hepatic damage marker ALT rose after HP treatment, although it was not significant and the levels were maintained within the reference normal values (0-138 U/L) (Figure 21C).

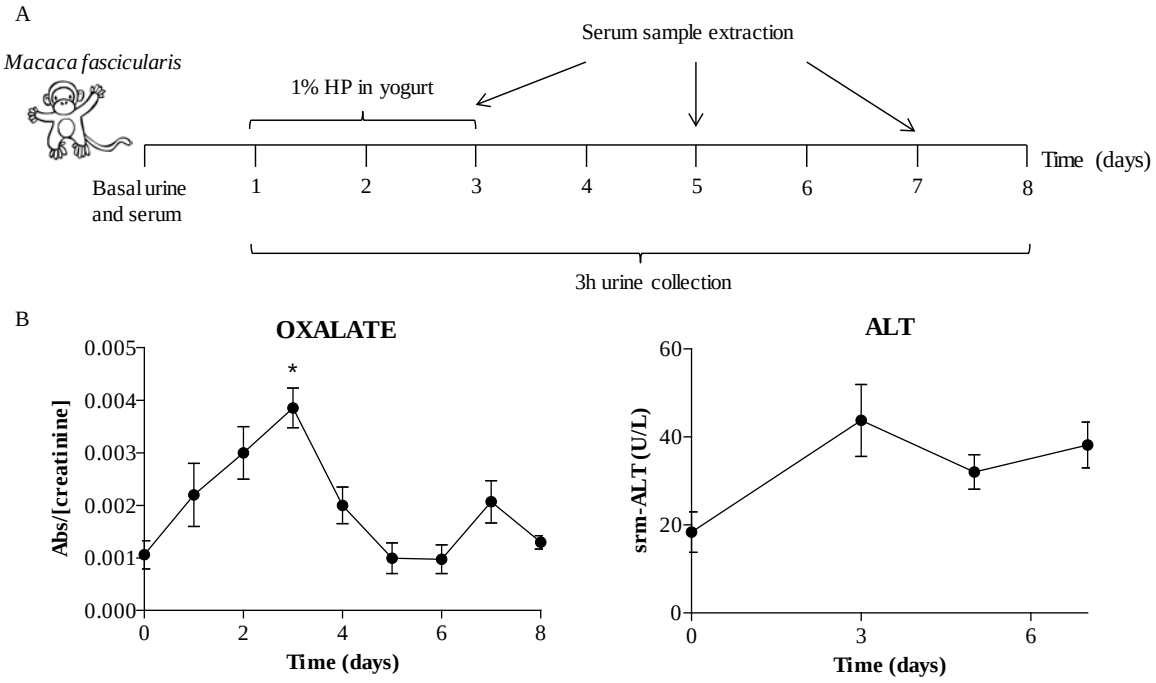

Figure 21. Set-up of a model of dietary hyperoxaluria in *Macaca fascicularis*. A) Experimental design of the HP challenge and urine and serum collection. B) Oxalate levels measured as oxalate absorbance normalized to urine creatinine concentration. Results are shown as mean ± SEM of the data obtained from 4 animals. Kuskal Wallis was used to compare oxalate levels between different days and differences were considered significant (p=0.003). Data are given as mean ± SEM. Dunn's post-test revealed statistical difference between day 3 and basal levels. * = p<0.05. C) Serum ALT levels (U/L). Data of 4 NHPs are shown as mean ± SEM. p=0.075, no significance was obtained following Kruskal Wallis analysis.

4.1.3 Analysis of the therapeutic effect of gene therapy in a C57BL/6 diet-induced hyperoxaluria model

It was shown that the gene therapy for the treatment of PH1 in the *Agxt*$^{-/-}$ preclinical model for the disease is effective (80). Thus, the usefulness of the C57BL/6 diet-induced hyperoxaluria model was evaluated in male animals treated with AAV5 vectors expressing AGT or an irrelevant gene (Factor IX (FIX)) and compared to saline-treated animals. HP challenge was performed in all the groups and oxalate was measured in 24-hour urines. As shown in Figure 22, oxalate levels (normalized to creatinine) were the same in all groups and the overexpression of AGT in WT animals did not confer any advantage during a HP challenge. In conclusion, the diet-induced hyperoxaluria model could not be used to evaluate therapies directed at decreasing oxalate. The lack of positive results in mice led us not to test this approach in monkeys.

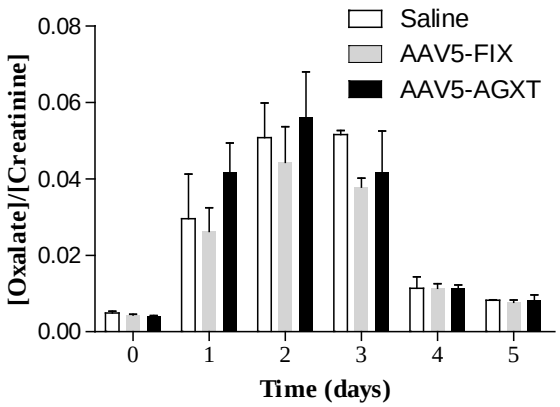

Figure 22. Oxalate levels (measured as concentration normalized to creatinine) in C57BL/6 mice treated with different vectors and challenged with 3% HP for 3 days. Data are shown as mean ± SEM of 2 pooled urines per group. Kruskal Wallis test was performed to analyze differences between groups for each day, no significant differences were observed.

4.2 Optimization of glyoxylate pathway overloading in the PH1 animal model

As described PH1 mice require the administration of a high concentration of oxalate precursors to accumulate oxalate in urine and to develop the disease (101). Before testing the efficacy of the potential treatment we first established the experimental conditions for the challenge.

4.2.1 L-hydroxyproline challenge

The protocol tested in WT C57BL/6 animals was transferred to PH1 animals. However, the animals did not eat the HP food. For this reason, HP diluted in water was administered by oral gavage, but it was toxic for the animals and 80% of them died 24 hours after the procedure.

4.2.2 Ethylene glycol (EG) challenge

As HP was not applicable in the PH1 model we decided to move to a different challenge strategy using EG administration.

4.2.2.1 Oral gavage

Animals received a single dose of 15.5 mg of EG by oral administration. The analysis of oxalate concentration in urine revealed an increase in oxalate levels that was sustained for at least 3 days after the gavage (Figure 23). Males of different ages were used for this experiment and an age-dependent oxalate increase was observed. Older animals were more sensitive to the EG challenge (Figure 23), displaying significantly higher oxalate urine levels compared to age-matched WT animal. Therefore, all subsequent experiments were performed in 12-14 weeks-old animals.

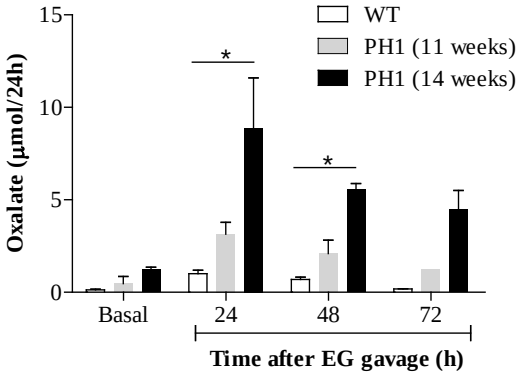

Figure 23. Set-up of the EG gavage challenge in PH1 animals. Oxalate levels measured as µmol/24 hour in C57BL/6 WT animals and PH1 animals after an EG challenge (15.5 mg). Data of at least 3 individual urines per group are shown as mean ± SEM. Kruskal Wallis test was significant for 24h (p=0.0302) and 48h (p=0.0181) points. Dunn's post-test revealed significant differences between WT and 14 week-old PH1 groups. * = p<0.05.

4.2.2.2 Oral uptake in drinking water

Sustained low EG dose administration was tested in order to mimic a scenario more closely resembling the one found in PH1 patients. For this purpose, 0.5% (v/v) EG was added to the drinking water of the animals during 13 days. 24-hour urine was collected every 3 days. As shown in Figure 24A, oxalate was significantly higher in the urines of PH1 mice and the highest peack of oxalate was obtained at day 3 after the addition of EG into the drinking water. On days 7 and 10 the oxalate level remained high compared to WT control animals. The urine volume increased in both groups during the challenge due to an increased osmosis of the hyperoxaluric urine (Figure 24B). However, on day 13 after the start of the challenge, the oxalate levels in the urine dropped because of a deterioration of the health status of the PH1 animals, which presented tremor and absence of movement. In addition, during the challenge the water intake increased in the control group because of the increased diuresis, while in PH1 animals it remained stable (Figure 24C). This could explain the bad state of the animals. Therefore, it was decided to shorten the challenge to a maximum of 10 days in order to not stress the animals in excess.

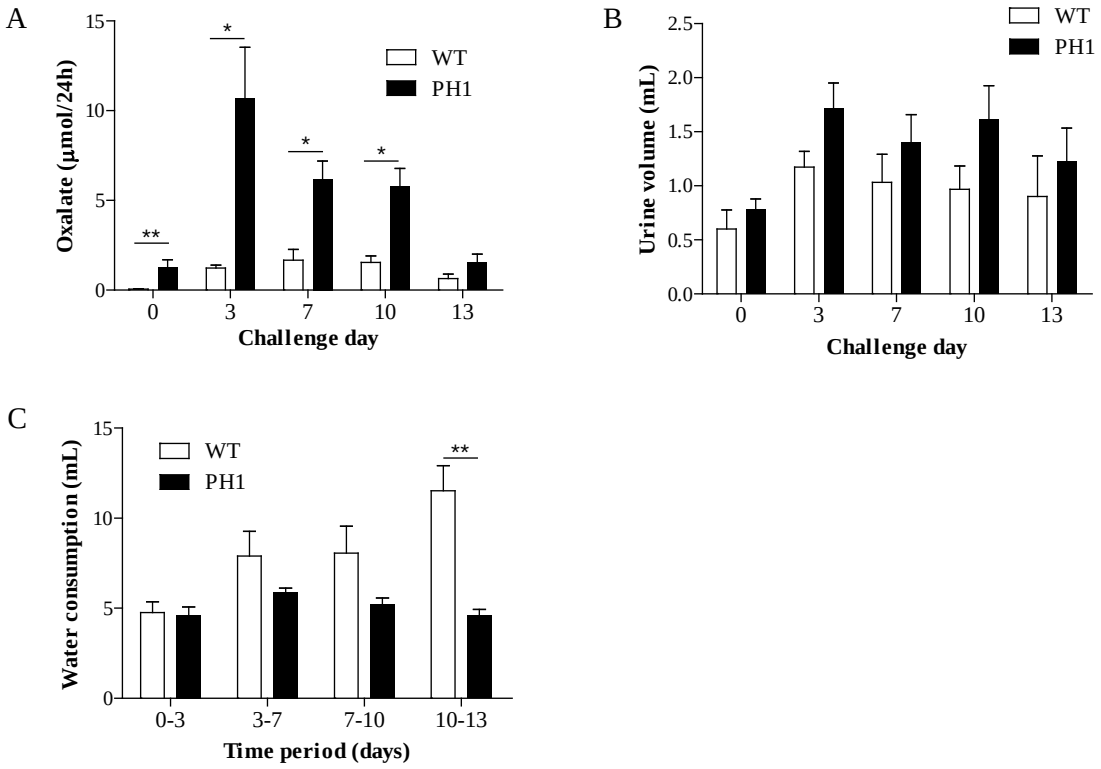

Figure 24. Set-up of EG challenge in PH1 animals. A) Oxalate levels (µmol/24 hours) in C57BL/6 WT and in PH1 animals during 13 days of challenge. Mann Whitney test revealed significant differences between the two groups on days 0, 3, 7 and 10. B) Urine volume during the EG challenge, measured in mL. Statistical analysis by Mann Whitney test revealed no significant differences for each day. C) Water intake of each animal in the experiment, measured in mL. Mann Whitney test revealed significant differences on day 13 ($p=0.0095$). A-C) At least 3 data points were obtained per group and they are shown as mean ± SEM.
* = $p<0.05$, ** = $p<0.01$.

4.3 Optimization of gene therapy for PH1

One of the objectives of this thesis was to optimize gene therapy for PH1, and for this purpose, we evaluated two different approaches. First, the transgene AGXT was codon optimized to achieve higher AGT protein levels. Then, different routes of administration of the vector were developed with the aim of increasing liver transduction efficiency.

4.3.1 Human *AGXT* codon optimization

Codon optimization can be used to increase the expression levels of a recombinant protein. The sequence is modified using the codon with the highest affinity for the tRNA of a particular amino acid, thus obtaining an optimized translation (133). Codon optimization has been used in gene therapy to achieve faster and higher transgene expression levels (128,134).

A

Treatment	Dose	n
Saline	-	5
AAV5-AGXT WT	10^{14} vg/kg	5
AAV5-coAGXT	10^{14} vg/kg	6

B

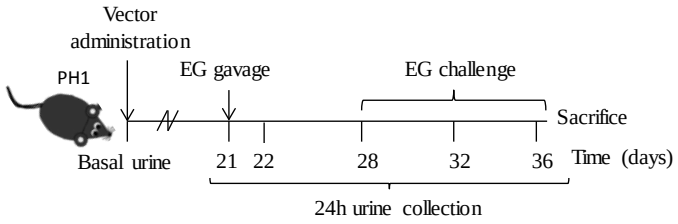

Figure 25. Experimental design of a study to compare the therapeutic efficacy of the WT or codon optimized version of the human *AGXT* gene. A) Distribution of PH1 animals into 3 groups. B) Experimental timeline of urine collection, EG gavage and challenge.

Here we have used a codon optimized human AGXT (coAGXT) targeted to the liver by an AAV5, which was produced by a Dutch company of gene therapy, uniQure. uniQure tested the constructs *in vitro* and concluded that the use of coAGXT resulted in a higher protein production than WT AGXT (data not shown). Taking into account *in vitro* data, the therapeutic efficacy of the vector carrying the coAGXT was compared with the one carrying the WT AGXT sequence. 12 week-old male PH1 animals were divided into 3 groups of at least 5 mice per group. The control group received saline solution, and the other two groups were administered with AAV5 containing either coAGXT or AGXT WT (Figure 25A). In addition, the urines of four C57BL/6 mice were collected during the experiment as control to determine normal urine oxalate levels. Twenty one days after the administration of the vectors, individual urines were collected using metabolic cages (Figure 25B). As shown in Figure 26A, 3 weeks after the treatment oxalate tended to be lower treated PH1

mice compared with PH1 animals, even though it was not significant and the levels were not toally normalized compared to WT animals. Next, all animals were challenged by EG gavage as described. After the gavage, the same trend was maintained: Treated animals showed less oxalate in urine than PH1 animals, but still higher than WT healthy controls (Figure 26B). One week after the gavage (28 days after the treatment), the oxalate in urine returned to basal levels and an EG challenge was started by the administration of EG in drinking water. On day 4 of the challenge, again the same trend was observed. However, the oxalate levels in AAV5-treated animals were the same as in WT animals by the day 8 of challenge, which indicated a normalization of levels (Figure 26C). No significance was found when analyzing the oxalate of treated groups, but probably this is an effect of the number of animals in the experiment. At the end of the study it was concluded that there was no difference in therapeutic efficacy between both versions of the transgene. Therefore, the codon optimization of *AGXT* sequence did not have a therapeutic advantage.

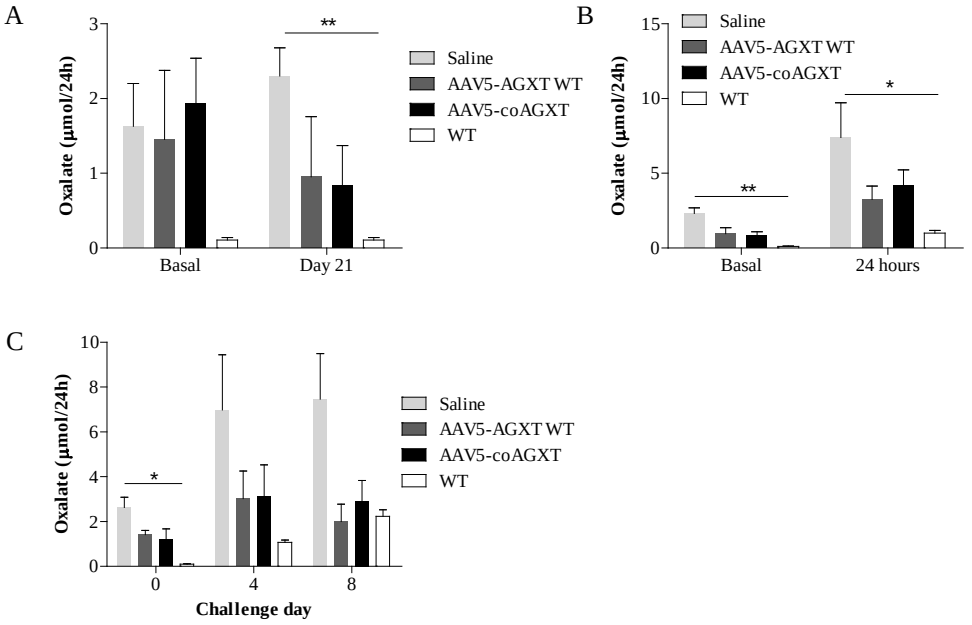

Figure 26. Codon-optimized AGXT does not provide a therapeutic advantage over the WT form. Oxalate levels measured as µmol/24 hour in the animals that received saline or the therapeutic vectors 21 days after vector administration (A), after a 15.5mg EG gavage (B) and during 8-day EG challenge (C). Data ($n \geq 3$) are shown as mean ± SEM. Kruskal Wallis testing gave significant differences in all cases and Dunn's post-test was performed. * = $p<0.05$, ** = $p<0.01$.

Finally, animals were sacrificed on day 36 and transduction was analyzed in the livers. In Figure 27A the amount of viral genomes in the liver is shown, which is the same in the groups treated with AAV5 but independent of the transgene used. Specific WT AGXT and coAGXT transcripts were also detected by qPCR (Figure 27B and 27C) and were higher for WT AGXT. AGT protein levels were analyzed by WB and the protein levels were the same in all the AAV-treated mice (Figure 27D). Thus, the infection and the transgene expression were the same between the two treated groups, explaining the absence of differences in the therapeutic efficacy. Exceptionally, one mouse in the AAV5-AGXT WT group was not properly infected, which presented low viral genome presence and lower AGT mRNA and protein levels.

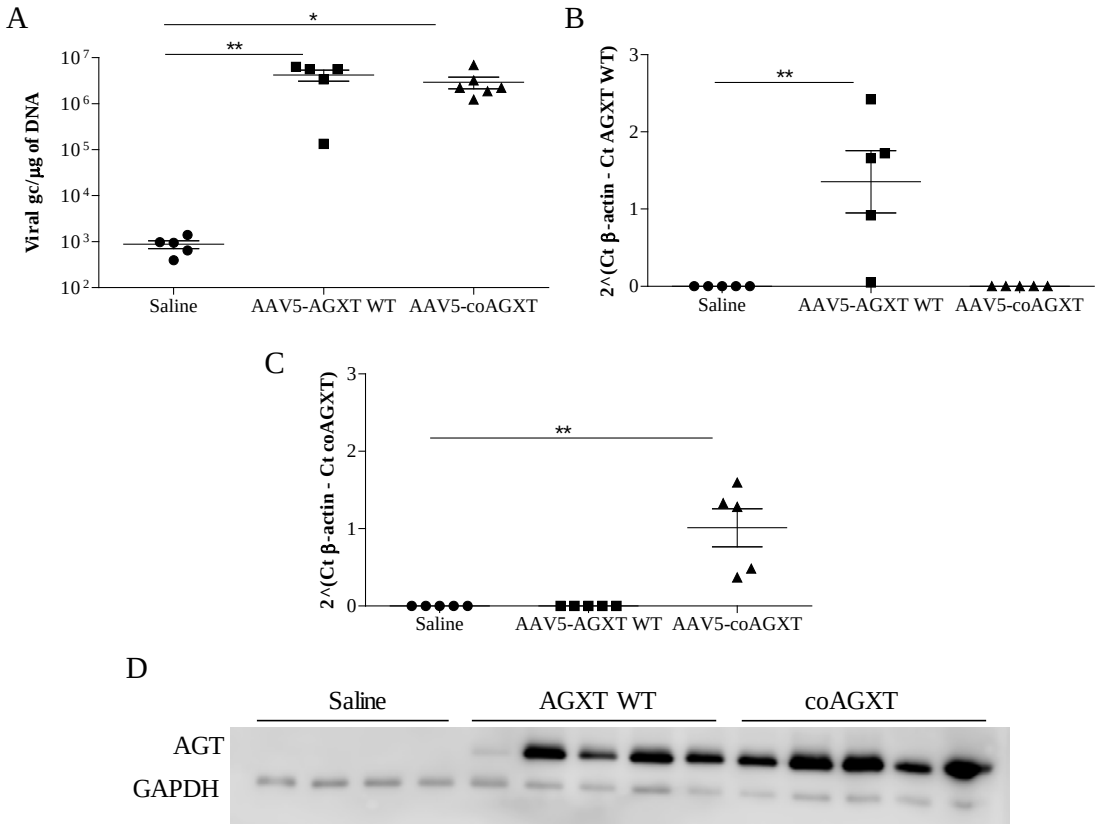

Figure 27. Analysis of liver transduction by AAV5-WT AGXT and AAV5-coAGXT vectors. A) Measurement of viral genome copies per µg of total genomic DNA. Kruskal Wallis test was significant (p=0.0063) and Dunn's post-test revealed higher genome copies in the groups treated with the vectors. B) RT-qPCR quantification of WT AGXT mRNA copies in livers. Kruskal Wallis test revealed significant differences between groups (p=0.0019). C) RT-qPCR detection of coAGXT mRNA. Kruskal Wallis test was significant (p=0.0025). D) WB detection of AGT expression in the livers of the treated mice. A-C) Data are shown as mean ± SEM of at least 5 animals per group. * = $p<0.05$, ** = $p<0.01$.

4.3.2 Improvement of AAV-mediated liver transduction efficiency by changing the route of administration

The results presented in this part were published in the journal Human Gene Therapy- Clinical Development (171).

Due to the need of transducing a high percentage of hepatocytes in order to cure the PH1, new routes for AAV administration were tested in an animal model with a similar hepatic structure as humans: *Macaca fascicularis*. Furthermore, not only transduction efficiency but also the safety of the different procedures was evaluated: biochemical and hematological toxicity, viral shedding and the immune response against the vector were determined. Two new routes of administration were tested and compared to the intravenous (IV) route. A vector expressing a secreted reporter protein was used to be able to follow transgene expression over time. Thus, an AAV5 expressing human secreted embryonic alkaline phosphatase (SEAP) under the control of the liver specific promoter α-1-antitrypsin was used, AAV5-AAT-SEAP.

4.3.2.1 Procedure

Two animals were administered with the AAV5-AAT-SEAP vector in the saphenous vein (**IV** group). A second group (n=3) received the vector by direct administration via the suprahepatic vein (**SHV**) using a balloon catheter for blood flow obstruction: a 3 cm incision was performed in the right jugular area of the animal and the jugular vein was exposed and cannulated by venotomy. The balloon catheter was then introduced until reaching the right branch of the SHV. Fluorography images were taken using a contrast medium in order to visualize the area where the vector was administered (Figure 28A). Once the catheter was in place, the balloon was blown up and the vector was administered in two boli: half of the total dose diluted in 10 mL was administered and the balloon remained inflated during 5 minutes, then it was deflated and normal blood flow was restored during 2 minutes. The second half of the dose was administered using the same procedure. The third group (**HA** group) was composed of three animals that received the vector via the hepatic artery (HA) with blood outflow occlusion by a balloon catheter in the SHV. In short, one balloon catheter was placed in the SHV as described above and a second balloon catheter was placed in the HA. To perform this procedure, a 3 cm incision was made in the inguinal area of the animal, the femoral artery was exposed and a catheter was introduced until reaching the right branch of the HA. Subsequently the vector was administered in two boli via the catheter placed in the right HA in the same way as described for group two. Figure 28B shows the area where the vector was infused. The procedure could only be performed on the right branch of SHV or HA due to the small size of the

left SHV branch, where balloon inflation was too dangerous. Thus only 40% of the liver could be reached (Figure 28). All procedures were carried out under general anesthesia.

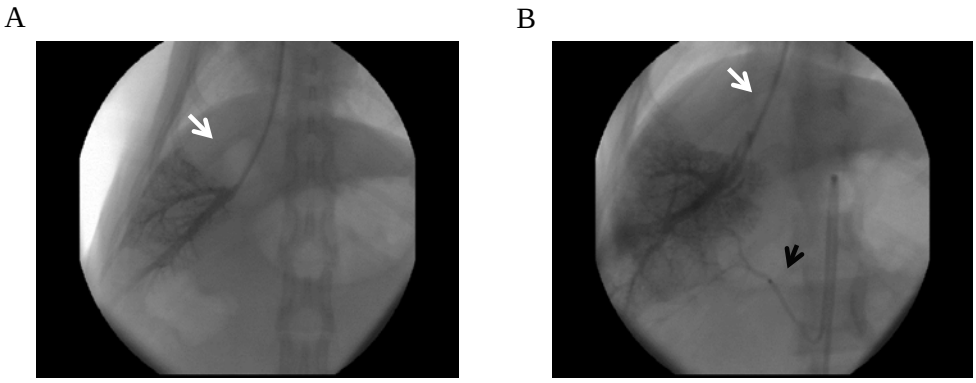

Figure 28. Fluorography images obtained during vector administration using the new routes. A) SHV injection of the vector. A balloon catheter (white arrow) was introduced into the right SHV. Administration of contrast medium visualizes the area where the vector was administered. B) A balloon catheter (white arrow) was introduced into the right SHV and second catheter was introduced into the right HA, via which administration of the vector was performed (black arrow). Balloon occlusion in the right SHV was maintained during administration.

4.3.2.2 Safety of the different procedures

The macaques tolerated the procedure well, they quickly recovered from the anesthesia and the incisions healed properly. All presented with normal weight gain and activity (food and water intake, social behavior) during the 4 months of the experiment until sacrifice. A complete hematological profile was analyzed in treated animals before and the first days after the administration of the vector. In general, in white blood cell lineages (WBC) no important alterations due to the administration of high amount of virus were observed (Figure 29). More importantly, the new routes did not elicit any affects that differed from those observed for the IV route. The same was true for the red blood cells (RBC) and related parameters, such as the hematocrit (Figure 30). Platelets and coagulation were also not affected by the injections (Figure 31).

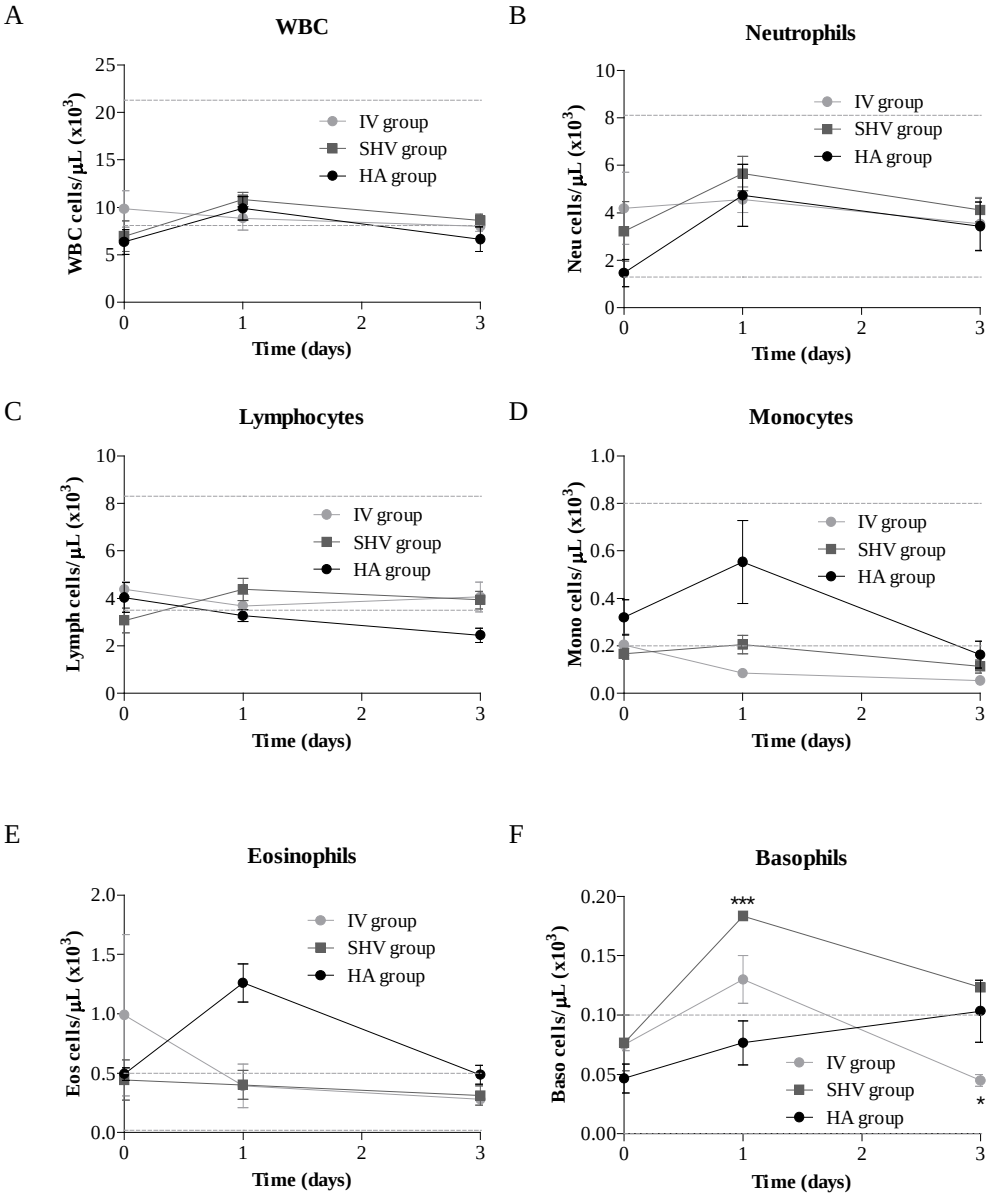

Figure 29. Hematological profile of WBC in the animals receiving the AAV5-AAT-SEAP by different routes of administration. Quantification of the number of WBC (A), neutrophils (B), lymphocytes (C), monocytes (D), eosinophils (E) and basophils (F). Data are shown as mean ± SEM. Friedman test was performed to analyze differences in cell populations between groups over time. Significance was obtained for basophils and no difference was observed in the other cell types. *** = $p<0.001$.

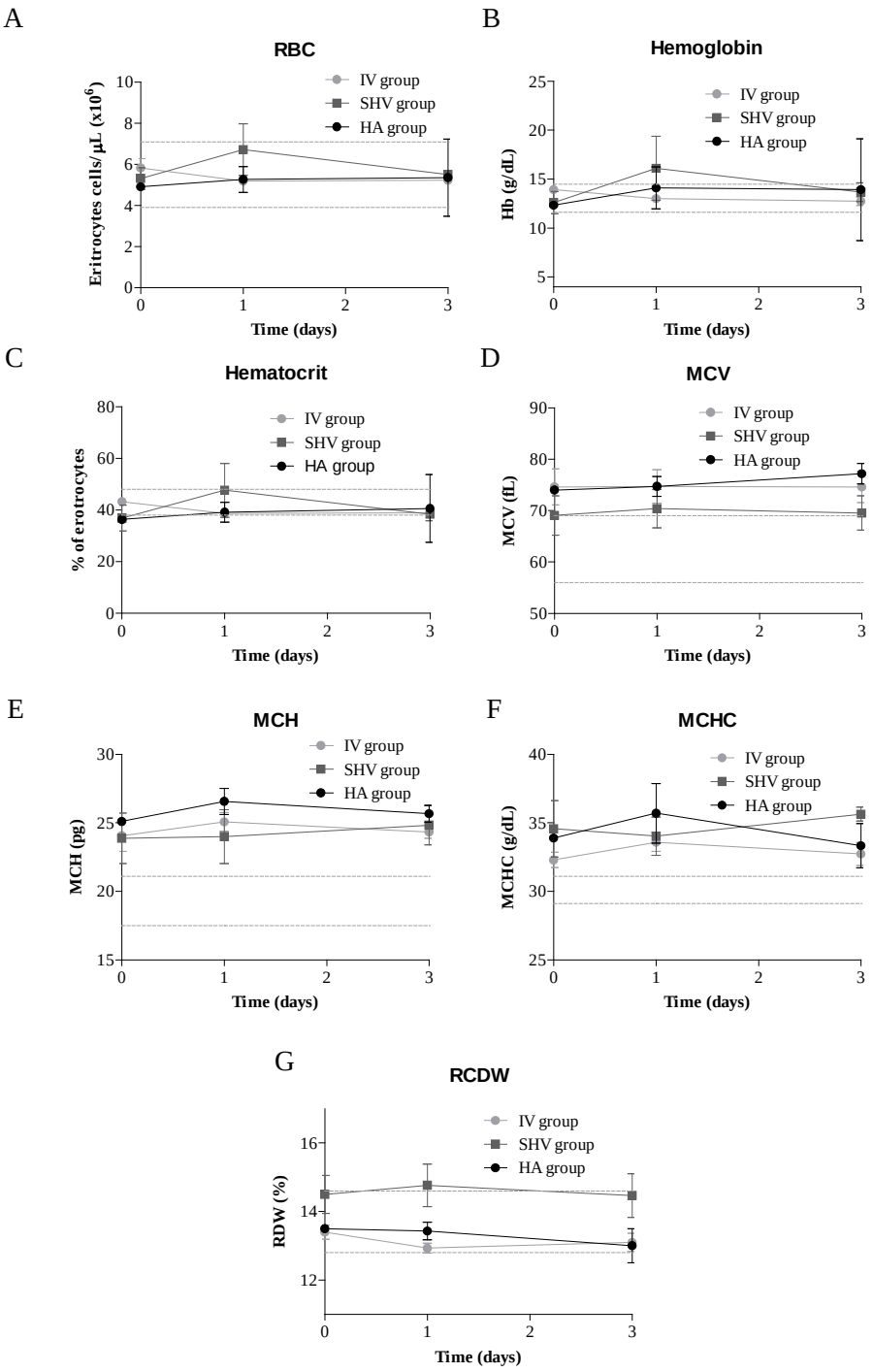

Figure 30. RBC and related parameters after the administration of the vector. Measurement of RBC number (A) and the related parameters hemoglobin (B), hematocrit (C), mean corpuscular volume (MCV) (D), mean corpuscular hemoglobin (MCH) (E), mean corpuscular hemoglobin concentration (MCHC) (F) and red cell distribution width (RCDW) (G). Data are shown as mean ± SEM. Friedman test revealed no significant differences between groups in any of the measured parameters.

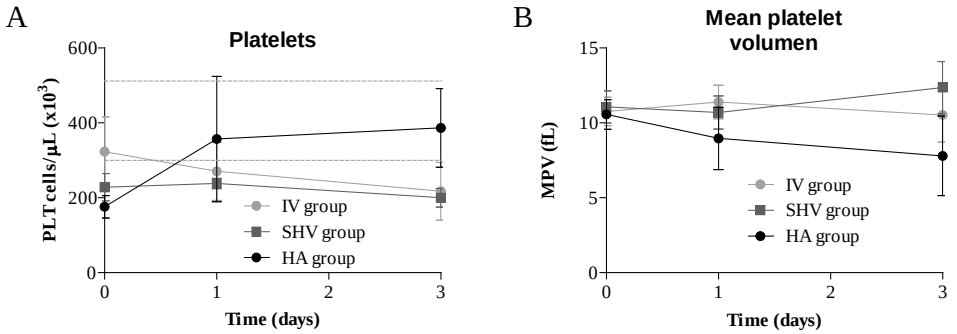

Figure 31. Measurement of the number of platelets (A) and the mean platelet volume (B) in the NHP treated via different administration routes. Data are shown as mean ± SEM. No significant differences were observed with the Friedman test.

The follow-up in the first week included the measurement of several biochemical parameters in order to analyze hepatic and renal functions. Neither was affected by the administration of the virus and all parameters analyzed in serum remained constant: albumin, total protein, bilirubin, GGT, urea and creatinine (Figure 32A-F). However, some liver damage was induced in the animals that received the vector by the new routes, as reflected in increased ALT (Figure 33A) and AST (Figure 33B) levels after the vector administration (even to above the maximum reference values).

This effect was resolved by day 7 after administration and these parameters were stable and between the normal ranges during the 4 months of the experiment (Figure 33). The death of a small portion of hepatocytes because of the increased intrahepatic pressure during the balloon occlusion cannot be excluded and can possibly explain for the increase of ALT and AST concentrations in serum.

Overall, no important toxicity was associated with the new routes of administration.

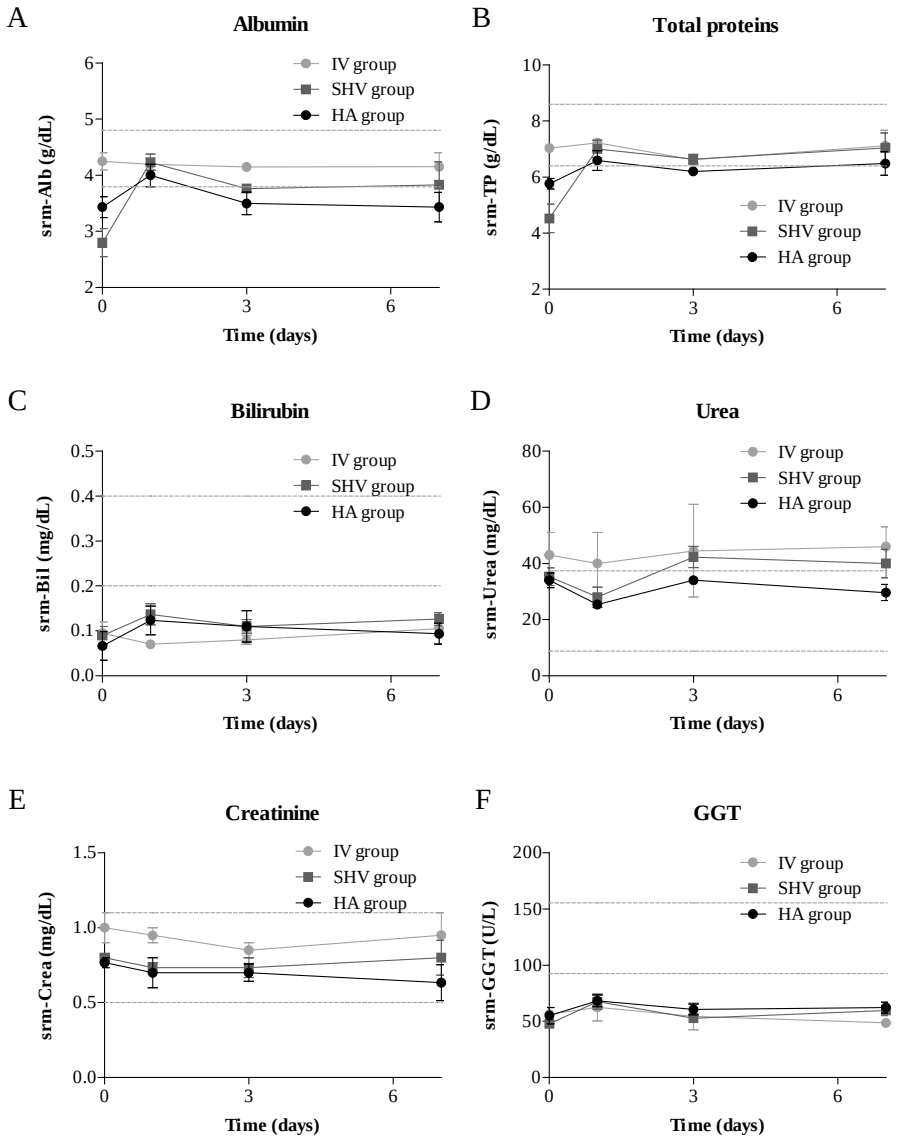

Figure 32. Biochemical serum profile during the first week after the administration of the vector. Measurement of (A) albumin concentration (g/dL), (B) total protein concentration (g/dL), (C) bilirubin (mg/dL), (D) urea (mg/dL), (E) creatinine (mg/dL) and (F) GGT (U/L). Data are shown as mean ± SEM. Friedman test was chosen to compare the groups during time and any significant difference was found. Dotted lines indicate the normal range.

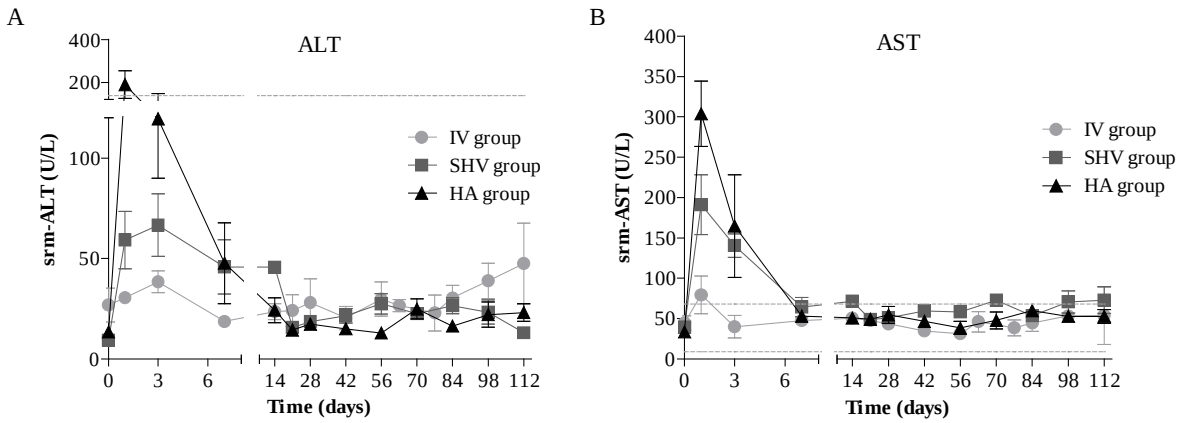

Figure 33. 4-month follow-up of transaminase levels. A) ALT measurement (U/L) and (B) AST measurement (U/L). Data are shown as mean ± SEM. Friedman test revealed no differences between groups during the experiment.

4.3.2.3 Viral shedding

The elimination of the vector was analyzed in different body fluids, such as urine, feces, saliva and nasal secretion. The presence of the virus was also measured in serum in order to monitor the clearance of the vector. The animals receiving the vector by the SHV route eliminated more amount of virus in feces than the other animals (Figure 34B). However, the HA injection triggered higher vector presence in urine and saliva during the first days after the administration (Figure 34A and 34C), and slightly less vector in the serum 24 hours after the treatment (Figure 34E). No differences were observed in the elimination of the vector in the nasal secretion (Figure 34D). Surprisingly, the animals that were administered using the new routes cleared the vector more slowly from the blood (Figure 34E).

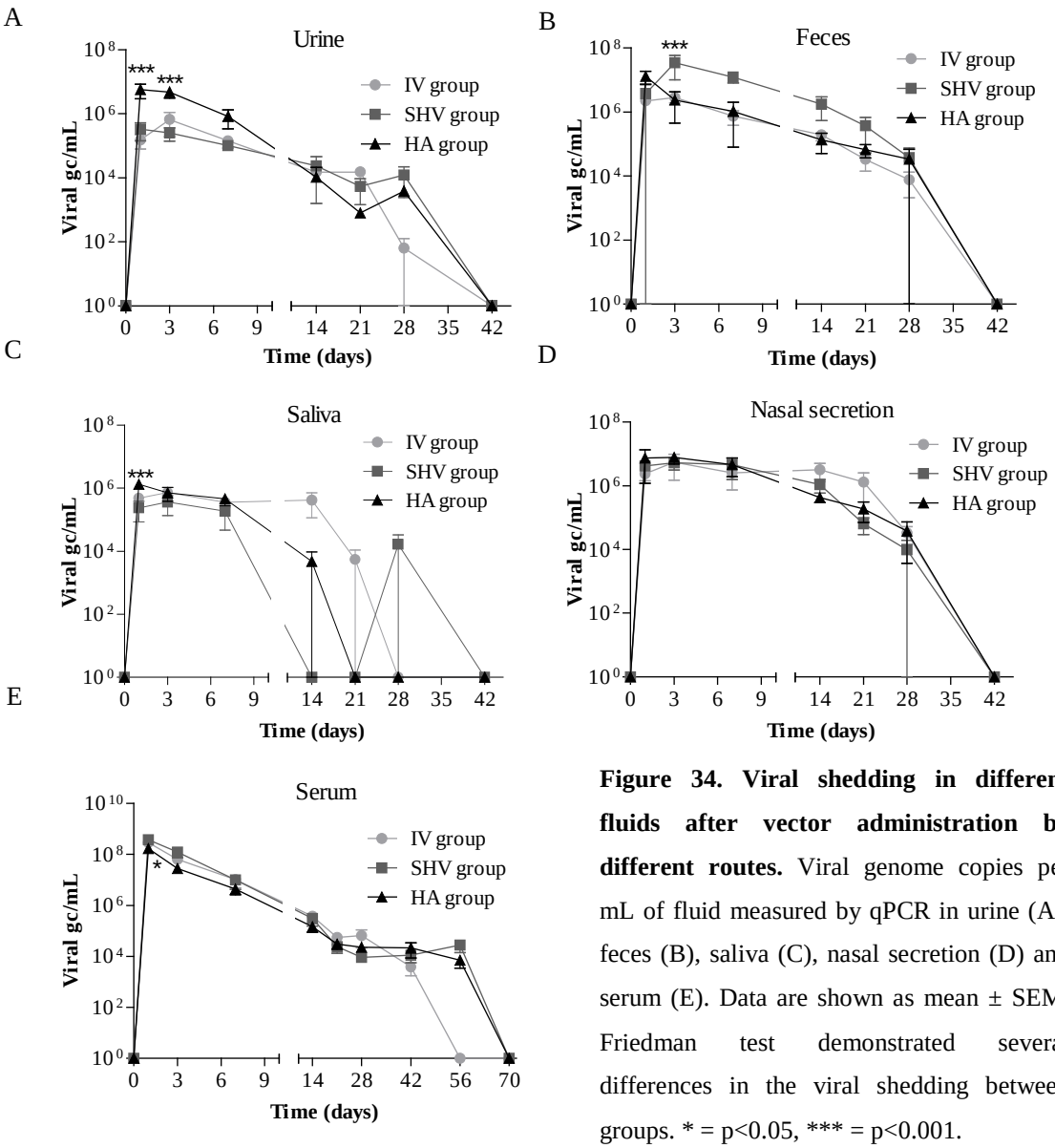

Figure 34. Viral shedding in different fluids after vector administration by different routes. Viral genome copies per mL of fluid measured by qPCR in urine (A), feces (B), saliva (C), nasal secretion (D) and serum (E). Data are shown as mean ± SEM. Friedman test demonstrated several differences in the viral shedding between groups. * = $p<0.05$, *** = $p<0.001$.

4.3.2.4 Immune response against AAV5 capsid

Antibody levels in serum were measured to analyze the humoral immune response against the capsid of AAV5. Total specific antibodies (neutralizing and binding antibodies) were increased in all animals after vector administration (Figure 35A). However, some of the animals from the 'new routes' groups developed higher antibody levels but the differences were not statistically significant. The same trend was observed for neutralizing antibody levels (Figure 35B).

IFN-γ ELISpot assay was used to determine the presence of T lymphocytes reactive against AAV5. The analysis was performed in peripheral blood mononuclear cells (PBMCs) extracted from one animal from the IV group and two animals from the other two groups. No AAV5-specific response was detected, neither before nor after the administration of the vector (Figure 35C-E).

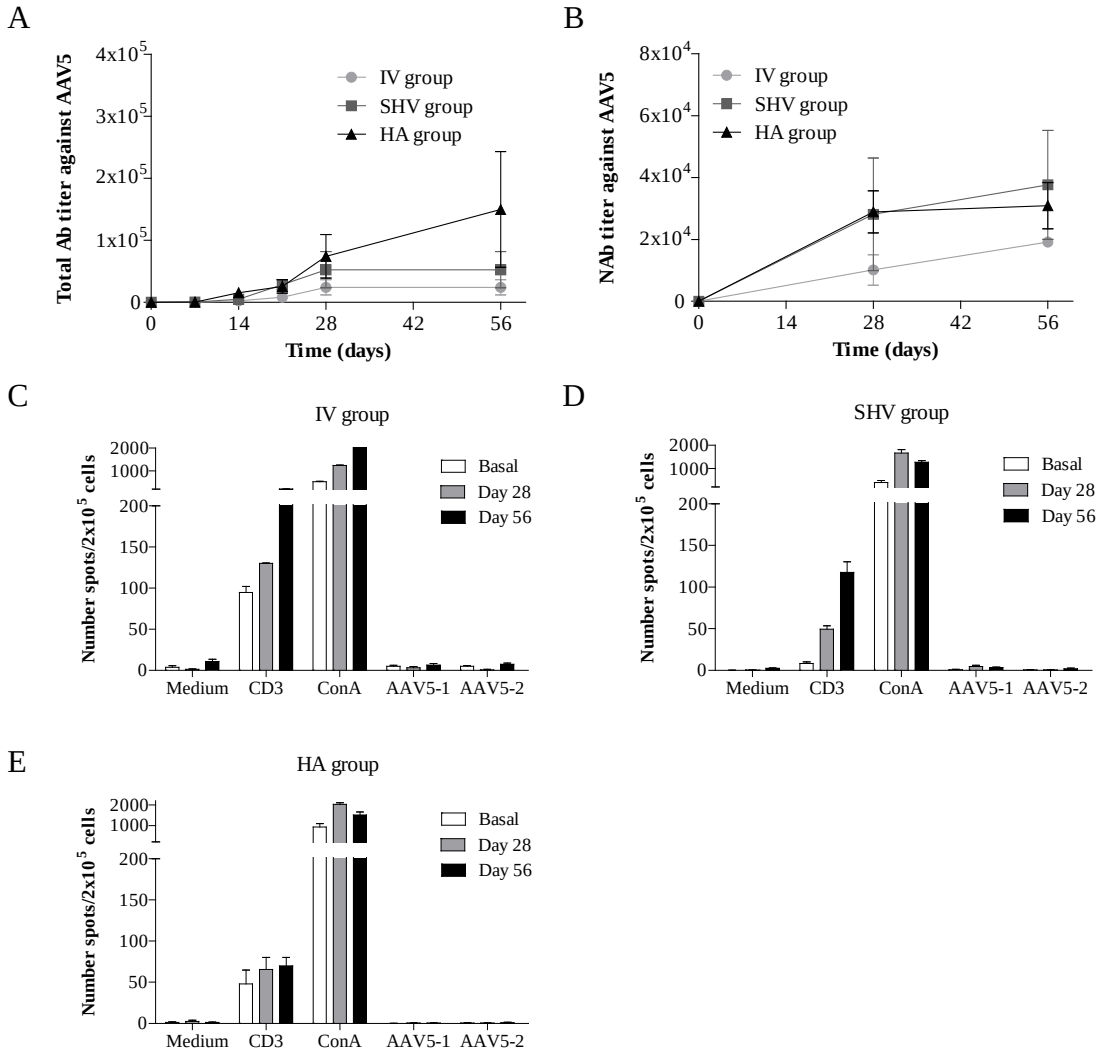

Figure 35. Analysis of the immune response against AAV5. A) Titration of total antibodies against AAV5 by ELISA. B) Titration of neutralizing antibodies (Nabs) against the vector by *in vitro* neutralization assay. Data are shown as mean ± SEM. Kruskal Wallis test was no significant for A and B. C-E) ELISpot analysis of the number of PBMCs responsive to AAV5 peptides in some of the animals from each group. Data are shown as mean ± SEM.

4.3.2.5 Transgene expression

As mentioned, SEAP is a secreted protein, whose phosphatase activity can be measured in serum samples. Therefore, SEAP activity was monitored during the 4 months of the experiment and it was significantly higher in animals administered using the new routes (Figure 36A). In addition, the normal alkaline phosphatase (ALP) activity was measured in serum, where the total alkaline phosphatase activity was measured, i.e. endogenous ALP plus exogenous SEAP. These measurements matched with the result obtained in the analysis of SEAP activity (Figure 36B).

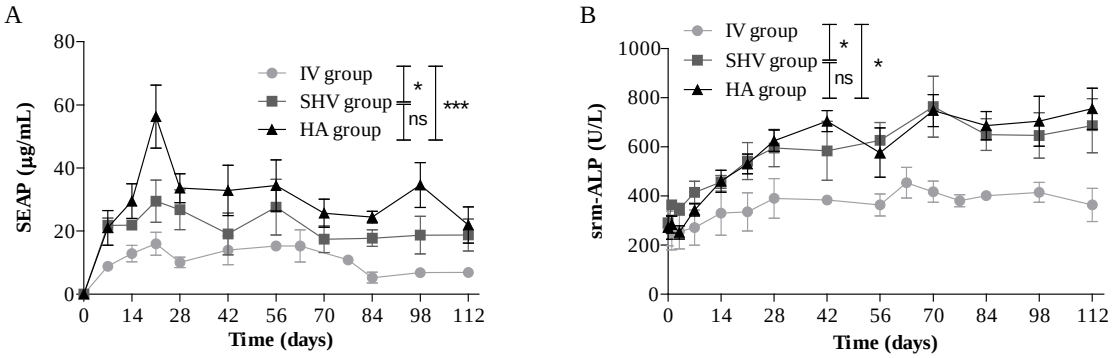

Figure 36. Monitoring of transgene expression in the serum in the 4-month follow-up after the administration of the vector. A) Measurement of specific activity of SEAP in serum. Data are shown as mean ± SEM. Kruskal Wallis test (p= 0.0002) and Dunn's post-test were used to analyze the differences between groups. B) Measurement of ALP in serum (U/L). Data are shown as mean ± SEM. Kruskal Wallis (p=0.0054) and Dunn's tests determined the statistical differences between groups. * = $p<0.05$, *** = $p<0.001$.

4.3.2.6 Liver transduction

As the direct administration in the liver was performed on the right side, samples from 8 different liver sections (from I to VIII) were collected at necropsy (Figure 37A). In addition, each section was subdivided in smaller pieces (depending on the size of the section), and a total of 30 different samples were obtained. This way, the spatial distribution of the vector was investigated. The transduction of the vector was analyzed by measuring the presence of viral DNA and the expression of SEAP at mRNA level in each piece. In the systemic administration the vector infected the liver in a homogenous way (Figure 37B). In contrast, animals receiving the vector via direct administration to the vascular system of the right side of the liver presented with higher infection rates in the sections located at the site of administration (sections V-VIII). Moreover, the overall viral genomes were significantly higher in animals administered via the new routes. Similar results were obtained for SEAP mRNA quantification, although significance was not reached (Figure 37C).

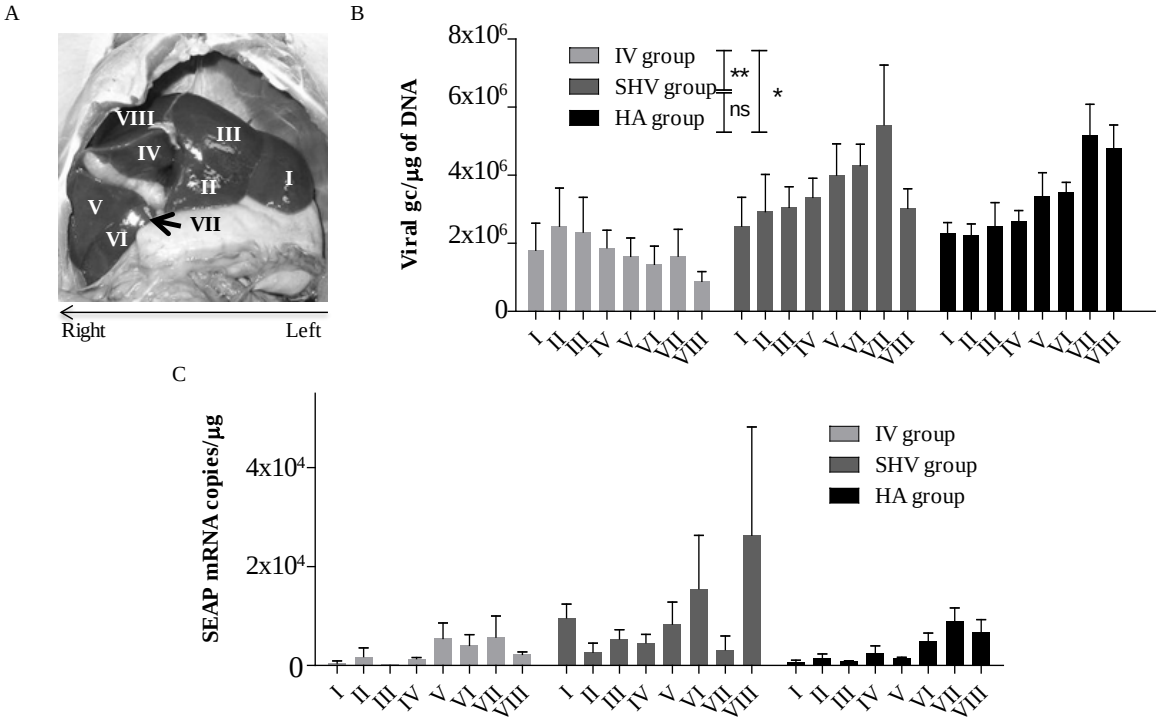

Figure 37. Analysis of the spatial transduction of the liver. A) Image showing the pattern followed to dissect the liver in 8 regions and perform posterior analysis. B) Quantification of viral genome copies in each region of the liver. Data are shown as mean ± SEM. Kruskal Wallis test (p=0.0016) and Dunn's post-test were used to compare the groups. C) qPCR analysis of the expression of SEAP in each liver region was analyzed. Data are shown as mean ± SEM. Kruskal Wallis test revealed no significant differences (p= 0.0827). * = $p<0.05$, ** = $p<0.01$.

4.3.2.7 Vector biodistribution

The presence of viral genomes was also assessed in further 21 organs in order to analyze if the route of administration changed the biodistribution profile of the vector. As shown in Figure 38, vector copy numbers were highest in liver and adrenal glands, followed by heart, gall bladder and inguinal lymph nodes (ILN). No statistically significant differences were observed although there were trends in organ distribution depending on the route. Adrenal glands were more preferentially transduced in the SHV and HA groups, in which copy numbers were very similar to data obtained in liver ($3.5x10^6$ gc/µg in liver and $2x10^6$ gc/µg in adrenal glands). Analysis of gall bladder and spleen also revealed the same trend.

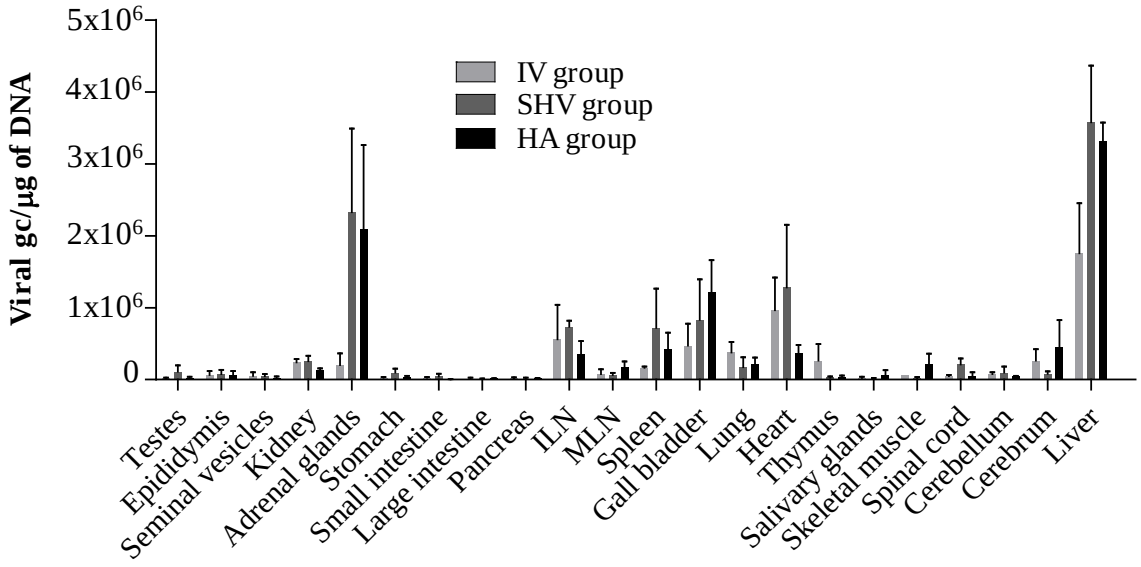

Figure 38. Biodistribution of the vector. Quantification of viral genome copies per µg of genomic DNA in 22 organs. Results are shown as mean ± SEM. Kruskal Wallis test for each organ revealed no significant differences between administration routes.

4.4 CRISPR/Cas9-mediated substrate reduction therapy (SRT) for PH1

As mentioned in 'Introduction' section, our main goal was to develop new therapies for PH1. The inhibition of GO is being used as an efficient and safe SRT strategy for PH1 (78,86,87). GO is a peroxisomal enzyme encoded by *HAO1* gene and catalyzes the conversion of glycolate into glyoxylate. It has been demonstrated that the inhibition of *Hao1* by siRNAs *in vivo* reduces oxaluria in the PH1 animal model. The only side effect observed so far has been a non-pathological increase in glycolate, which is eliminated into the urine without causing kidney damage. Moreover, this approach is being currently tested in clinical trials to treat PH1 patients. Our hypothesis is that same therapeutic effect can be obtained by decreasing GO levels using CRISPR/Cas9-mediated *Hao1* gene disruption. These systems could be used to generate DSBs in the *Hao1* gene that will be subsequently repaired by the error-prone NHEJ mechanism. This will lead to the disruption of the gene, and as a consequence, to a decrease in the expression of the protein.

4.4.1 Experimental design

As mentioned in the 'Material and Methods' section, two gRNAs targeting the second exon of the murine *Hao1* gene were designed and cloned into a vector expressing SaCas9 under the control of the hepatospecific thyroxin binding globulin (TBG) promoter flanked by AAV ITRs. This plasmid was used to produce AAV8 particles, a highly liver-tropic AAV serotype (80).

Table 7. Summary of the experimental groups in CRISPR/Cas9-mediated SRT studies: mouse strain, treatment, group ID and dose of vector.

Strain	Treatment	Group ID	Dose
PH1	PBS	Saline	-
PH1	AAV8-SaCas9	Cas9	$5x10^{12}$ vg/kg
PH1	AAV8-SaCas9-*Hao1*-g1	*Hao1*-g1	$5x10^{12}$ vg/kg
PH1	AAV8-SaCas9-*Hao1*-g2	*Hao1*-g2	$5x10^{12}$ vg/kg
C57BL/6	-	WT	-

To study the efficacy of this treatment in PH1 animals, experimental groups as outlined in Table 7 were formed: Two groups received the therapeutic vectors with different gRNAs against *Hao1* (*Hao1*-g1 and *Hao1*-g2), and as control groups, one group received the vehicle (Saline) while the

other received the vector expressing the SaCas9 without any gRNA (Cas9). An untreated C57BL/6 WT animal group was also included. In all the groups the respective vector was administered intravenously at a dose of $5x10^{12}$ vg/kg.

4.4.2 *In vivo Hao1* gene disruption and protein reduction in the liver

First, groups of 12-14 week-old male PH1 mice (n=5) were treated with the different vectors as described above and were sacrificed 4 weeks later.

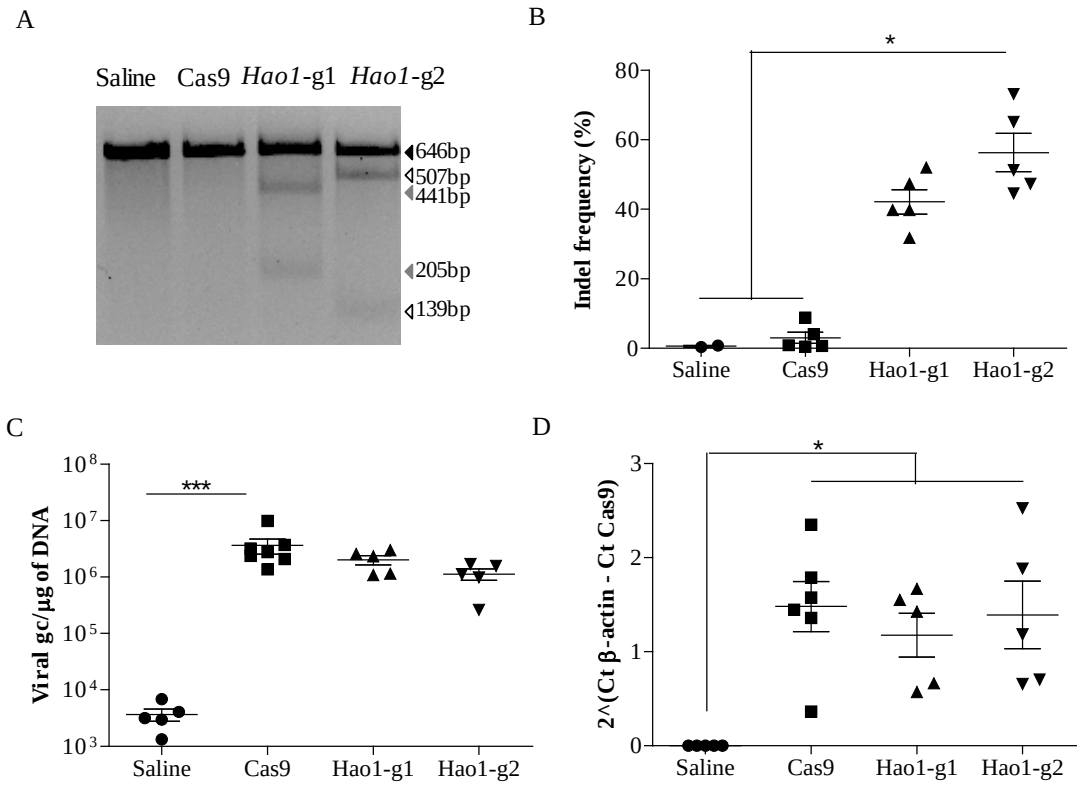

Figure 39. Specific *Hao1* gene disruption with AAV8-SaCas9-*Hao1*-gRNA treatment. A) 2% agarose gel separation of the fragments obtained after the Surveyor assay. B) Quantification of indel percentage by sequencing and TIDE analysis. C) Viral genome copies per µg of total DNA in the livers of the treated animals. D) Quantification of Cas9 mRNA copies by qPCR normalized to GAPDH mRNA. Results are presented as mean ± SEM of at least 5 mice per group. Kruskal Wallis and Dunn's post-test were the tests of choice to analyze differences between groups.

Indel generation was analyzed by Surveyor assay and TIDE analysis using genomic DNA extracted from the livers as a template. As shown in Figure 39A, indels were detected by Surveyor, with each gRNA having a different pattern of digestion. This is due to the different location of the targeted

regions in exon 2 of the *Hao1* gene. TIDE analysis allowed the quantification of the percentage of indels generated in the targeted regions (Figure 39B), which was around 50% in the animals treated with AAV8-SaCas9-*Hao1*-g1 and AAV8-SaCas9-*Hao1*-g2. The level of AAV liver transduction was similar in all vector-treated groups, since the viral genome copies and Cas9 mRNA expression levels were statistically not different (Figure 39C-D).

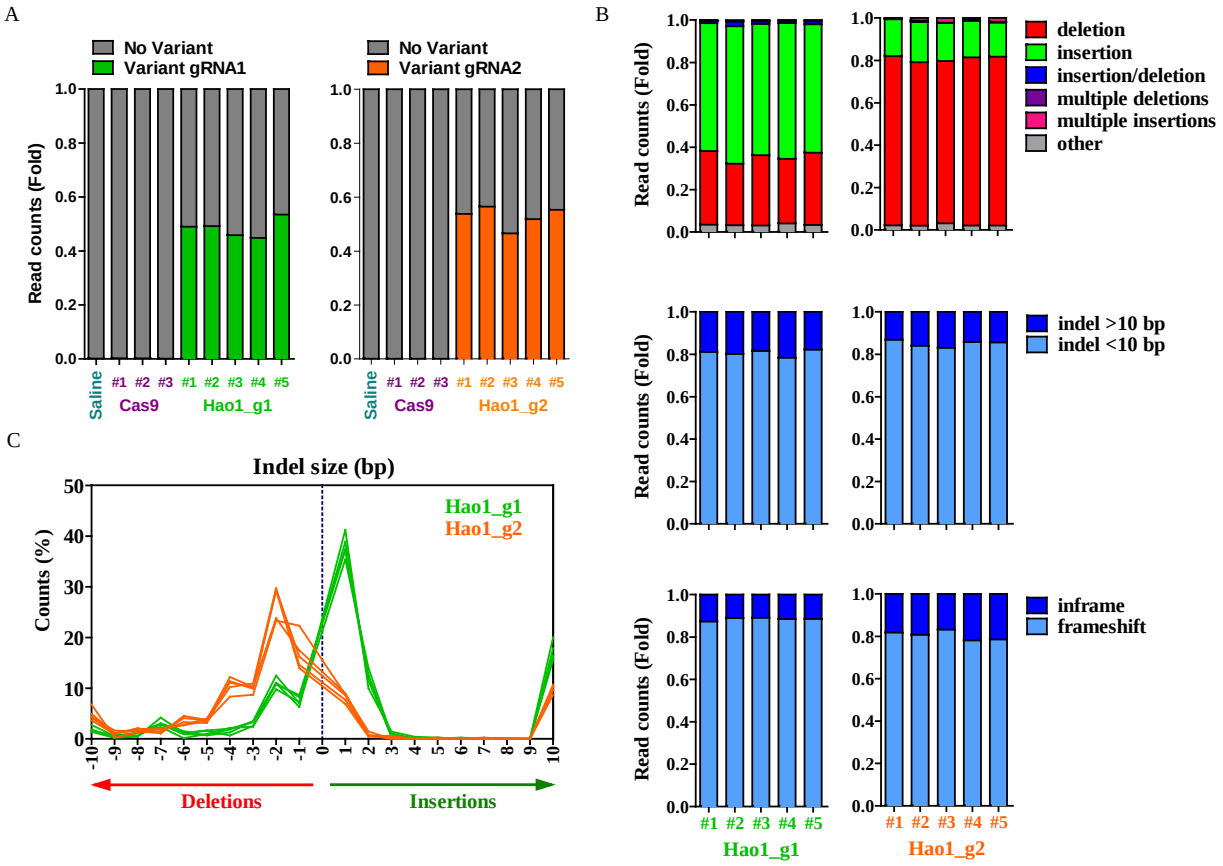

Figure 40. NGS of the on-target region of *Hao1*-g1 and *Hao1*-g2. A) Frequency of CRISPR/Cas9-introduced variants introduced in *Hao1* gene analyzed by NGS in one mouse treated with saline, three treated with AAV8-SaCas9 and five treated with AAV8-SaCas9-*Hao1*-gRNA (5 animals per gRNA). B) Characterization of the variants according to their modification type, size and frameshift potential in the animals presenting indels. C) Distribution of indel size in base pairs (bp) for each gRNA.

A more profound analysis of indels was performed by NGS. An average of 26,503 and 52,234 reads were obtained from the specific regions targeted by *Hao1*-g1 and *Hao1*-g2, respectively. Deep sequencing of animals receiving gRNAs against *Hao1* (n=5 per gRNA) confirmed previously observed indel frequencies determined by TIDE (with an indel average of 48.46 ± 3.41% for *Hao1*-g1 and 52.81 ± 3.85% for *Hao1*-g2) (Figure 40A). The most common mutations for both gRNAs

were indels smaller than 10bp (average of 80.66% for *Hao1*-g1 and 85.03% for *Hao1*-g2), occurring around positions −3 to +3 relative to the cleavage site and triggering a frameshift (with 88.45% and 80.42% frequencies), which explained the reduction in protein levels (Figure 40B). Interestingly, indel distribution was different within gRNAs, being *Hao1*-g1 prone to introduce insertions of 1bp, while *Hao1*-g2 induced 2bp deletions more frequently (Figure 40C). Moreover, although insertions were predominantly introduced at position +1 for both gRNAs, deletions were more widely distributed. These differences in the indel distribution might be due to the regions the gRNAs are targeting. Since *Hao1*-g1 is targeting the 5' end of the exon 2 of the gene, splicing regulatory regions of the intron-exon junction could affect NHEJ repair.

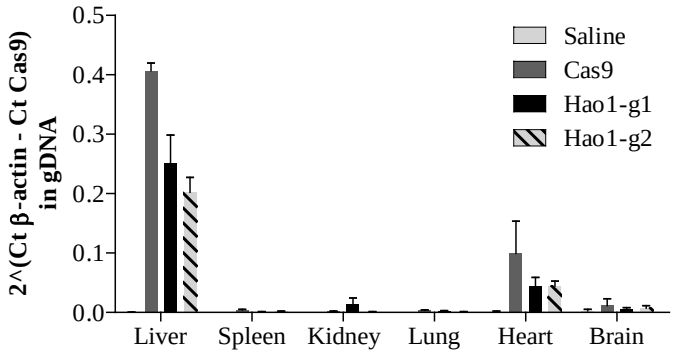

Figure 41. Distribution of the vector in the principal organs. Measurement of viral genomes related to GAPDH by qPCR. Results are shown as mean ± SEM (n=3).

The biodistribution of viral genomes copies was also analyzed (Figure 41). As expected, AAV8 preferentially infected the liver, even though some vector could be detected in other organs such as the heart.

Next, the effect of the indels on the expression of GO was analyzed. As shown in Figure 42A, *Hao1* mRNA levels were similar among all PH1 groups, independent of the treatment. The absence of differences correlates with the fact that the majority of the indels were small and therefore transcription and mRNA levels were not affected. However, no GO protein was detected in the livers of animals that had received the treatment with vectors expressing the gRNAs (Figure 42B and 42C). This clearly indicates that the indels generated by the CRISPR/Cas9 system induced no changes at the transcriptional level but a reduction of the protein to undetectable levels by WB and IHC.

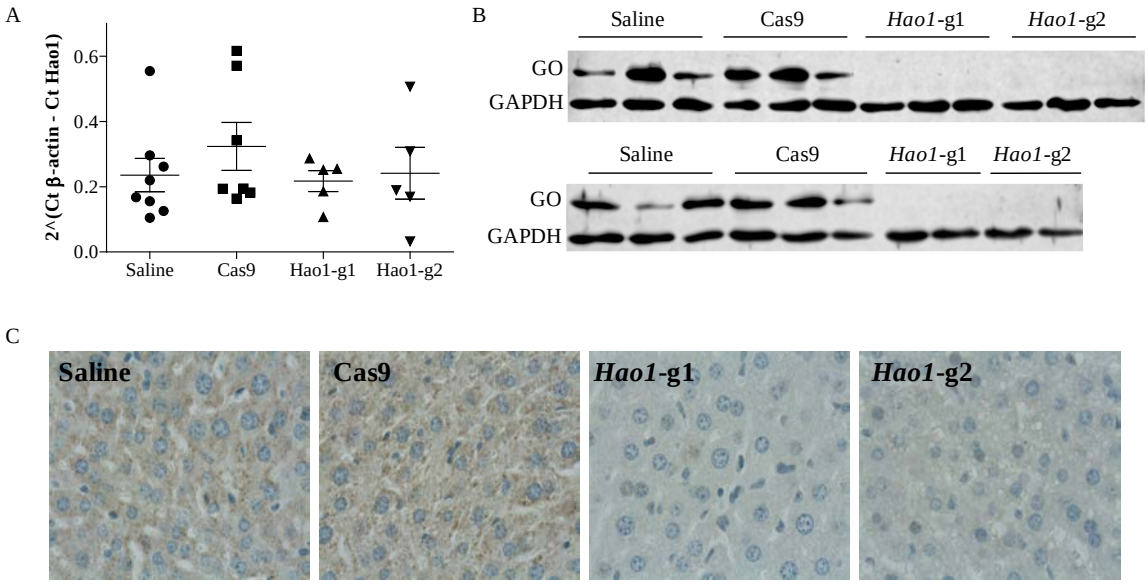

Figure 42. Effect of *Hao1* gene disruption on the mRNA and protein expression. A) Quantification of the mRNA expression of *Hao1*. Data are shown as mean ± SEM (n≥5). Kruskal Wallis analysis was not significant (p=0.1020). B) Detection of GO and GAPDH proteins by WB in liver protein extracts. C) IHC of GO in liver sections of one animal per group.

4.4.3 Therapeutic efficacy of GO reduction 1 month after treatment

In order to explore the therapeutic efficacy of the CRISPR/Cas9 vectors, treated mice were challenged 21 days after AAV administration with 0.5% EG in drinking water during 10 days (Figure 43A). Urine samples were collected before the challenge and on days 3 and 7. Urine oxalate and glycolate levels were measured at different time points before and after EG challenge. After challenge, in spite of the variability inside groups, PH1 animals treated with saline or with AAV8-SaCas9 generally displayed significantly higher oxalate levels in urine than AAV8-SaCas9-*Hao1*-gRNA-treated animals. Oxalate levels were very similar in AAV8-SaCas9-*Hao1*-gRNA treated- and WT animals (Figure 43B). As expected, glycolate levels were increased in the AAV8-SaCas9-*Hao1*-gRNAs group (Figure 43C). However, this difference was not clear by day 7 of the challenge because of high levels obtained in the saline group. This phenomenon is also observed in PH1 patients and it is possible that it is caused by the presence of extremely high glyoxylate levels. This leads to a saturation of the LDH enzyme and hence the activation of GRHPR that converts glyoxylate into glycolate will occur. Water intake was monitored while the animals were kept in metabolic cages and no difference was observed between groups (Figure 43D).

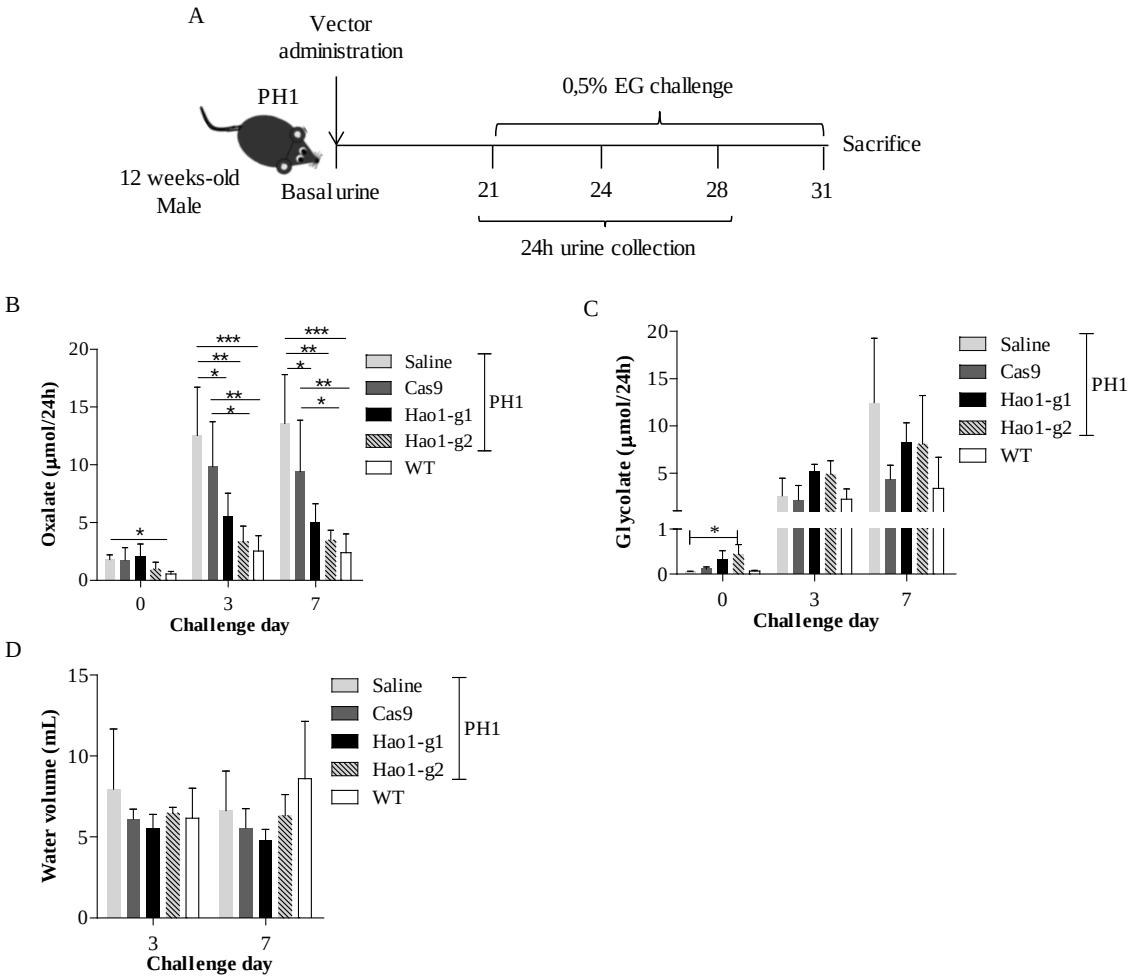

Figure 43. Analysis of the short-term therapeutic efficacy of the treatment with AAV8-SaCas9-*Hao1*-gRNAs. A) Experimental procedure: 21 days after the administration of the vector an EG challenge was performed during 10 days. B) Measurement of urine oxalate levels (µmol/24 hours) on days 0, 3 and 7 of the EG challenge. C) Measurement of water intake during the challenge (mL/24 hours). All data are shown as mean ± SEM (n≥3). Kruskal Wallis test was employed to analyze differences between group. * = p<0.05, ** = p<0.01, *** = p<0.001.

In addition, the treatment was able to prevent the nephrocalcinosis (NC) caused by a 10-day EG challenge as shown by the staining of CaOX crystals in the renal parenchyma (Table 8 and Figure 44A), which was lower or non-existent in treated mice. The controls that presented with NC had high urea levels in serum associated with kidney damage (Figure 44B). Animals were also weighed during the challenge, and weights remained stable in gRNA-treated and WT animals, while control animals lost weight by day 7 of challenge (Figure 44C).

Table 8. Number of mice that accumulated CaOx crystals in the kidneys and severity of nephrocalcinosis after 10 days of EG challenge.

Treatment	Development of NC	Severity
Controls	3 of 8	Severe
Hao1-g1	1 of 5	Mild
Hao1-g2	0 of 5	None

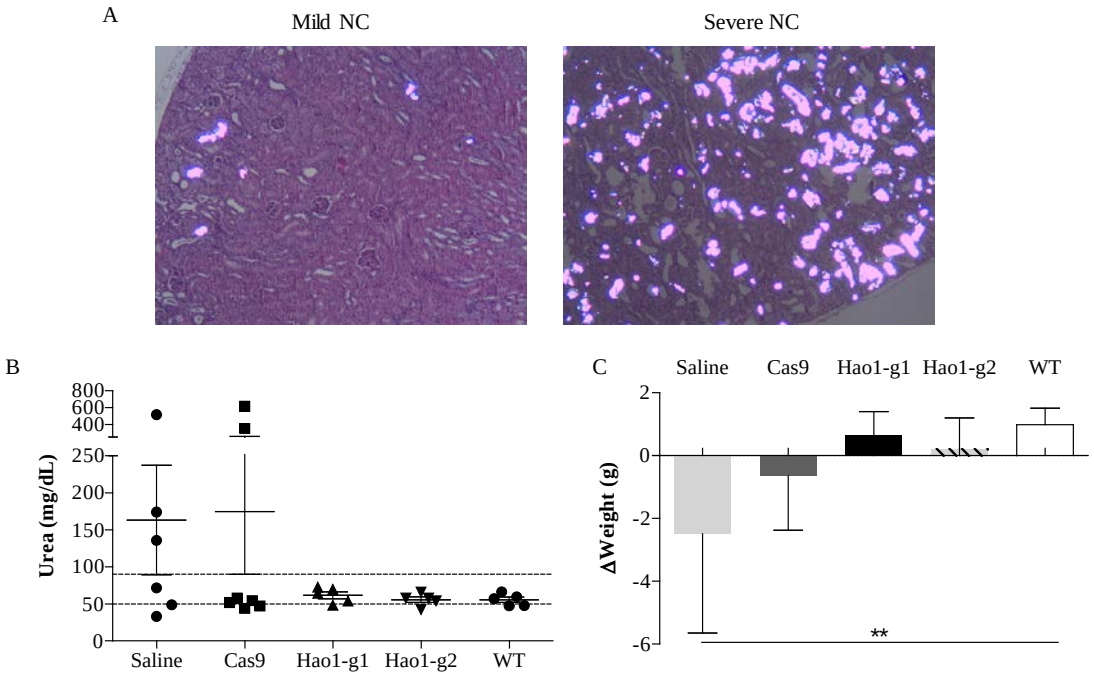

Figure 44. Analysis of toxic effect of EG challenge 1 month after the treatment. A) Examples of kidneys with mild (left) or severe (right) NC. B) Serum urea levels (mg/dL). Normal reference values are 49.9-90.15 mg/dL (dashed lines). C) Change in body weight after the challenge. Kruskal Wallis analysis (p=0.0033) showed significant differences only between Saline and WT group. All data are shown as mean ± SEM for each group (n≥5) and were analyzed by Kruskal Wallis statistical analysis. ** = p<0.01.

Moreover, a second challenge was performed in another set of animals two weeks after the first challenge, both over 7 days. During the double challenge, therapeutic efficacy was maintained since oxalate levels remained low in the group treated with gRNA (Figure 45A). Water intake was also similar among groups (Figure 45B).

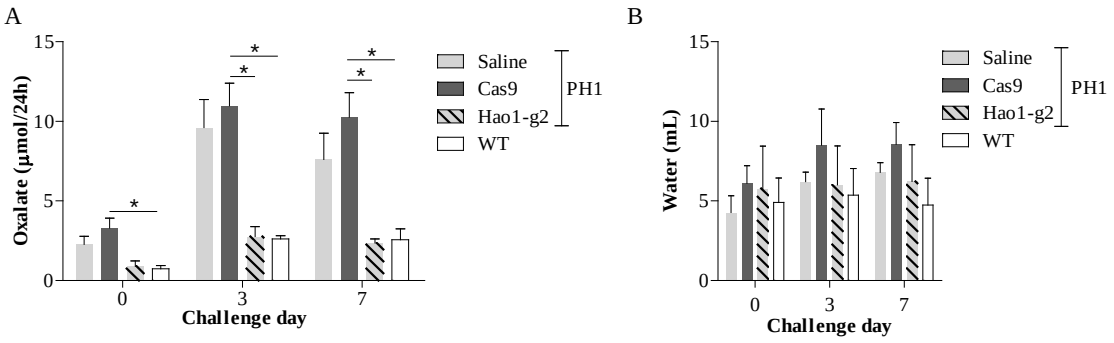

Figure 45. Therapeutic efficacy after a double EG challenge. A) Oxalate levels in 24-hour urines during the double challenge. B) Water uptake (mL in 24 hours) during the second EG challenge. Data are shown as mean ± SEM (n=5) and Kruskal Wallis was employed to compare the data. * = $p<0.05$.

4.4.4 Therapeutic efficacy of GO reduction in male PH1 mice 4 months after treatment

One of the advantages of CRISPR/Cas9 therapies is the lifelong effect, since the modifications are performed at genomic DNA level and remain after cell division. In order to prove if this holds true in for our approach, treated and untreated PH1 animals were challenged with EG in drinking water 4 months after the administration of the vectors and urine samples were collected at different time points (day 0, 3 and 7 of challenge) (Figure 46).

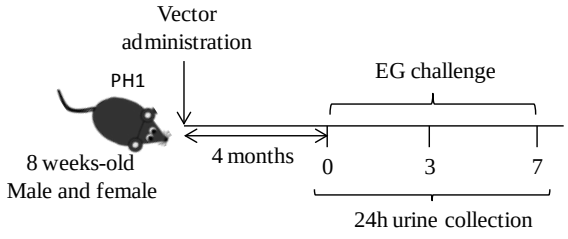

Figure 46. Scheme of experimental procedure to analyze the long-term efficacy of the treatment. The different treatments were administered to eight-week-old male and female animals and 4 months later a seven-day-long EG challenge was performed. Three 24-hour urine points were collected and the animals were sacrificed after the challenge.

After 4 months of treatment, basal oxalate levels were significantly lower in male animals treated with AAV8-SaCas9-*Hao1*-gRNAs and in the WT group compared to PH1 controls (animals that received Saline or AAV8-SaCas9) (Figure 47A), indicating an amelioration of the disease. Furthermore, animals that were administered with the therapeutic vectors displayed significantly higher levels of glycolate in urine (Figure 47B).

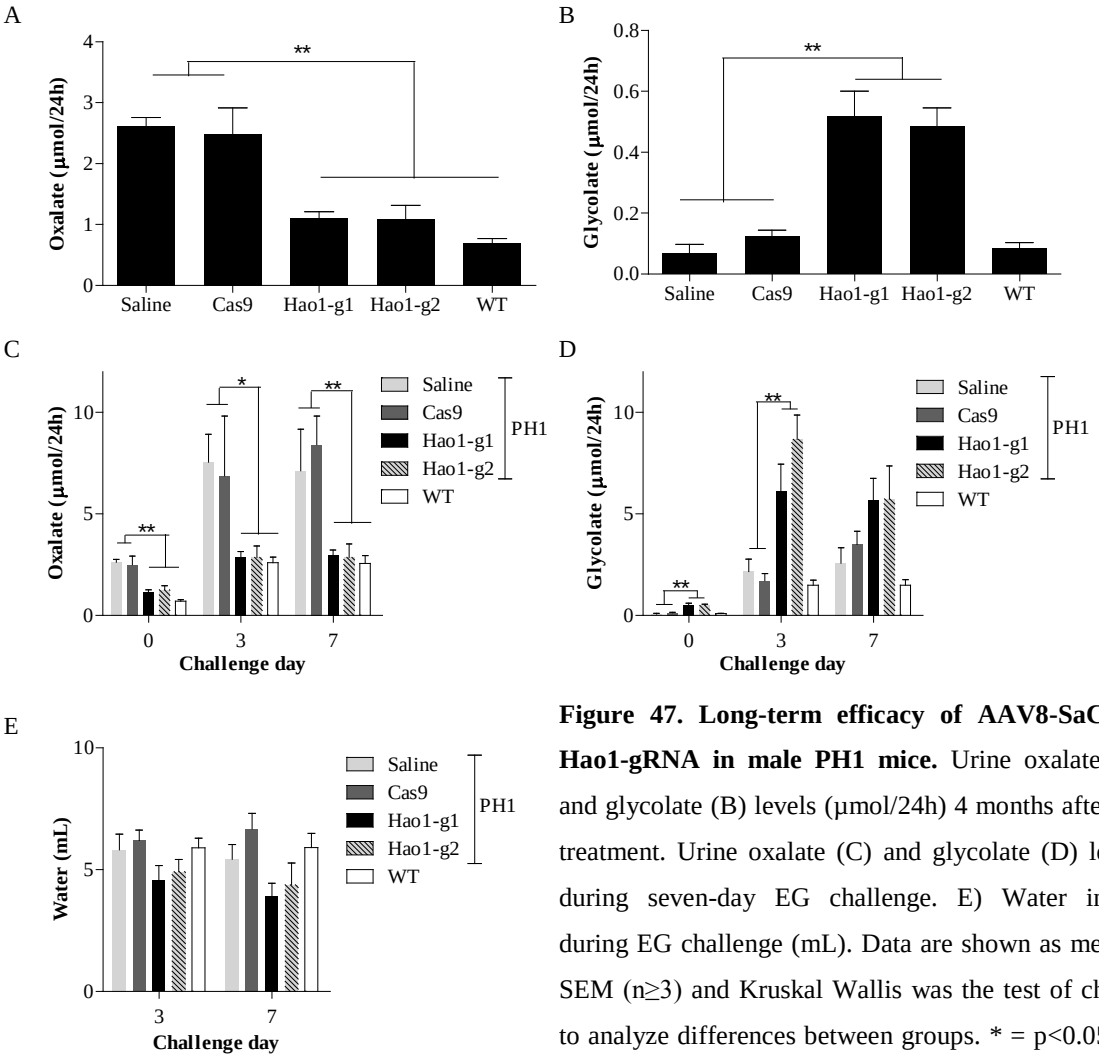

Figure 47. Long-term efficacy of AAV8-SaCas9-Hao1-gRNA in male PH1 mice. Urine oxalate (A) and glycolate (B) levels (µmol/24h) 4 months after the treatment. Urine oxalate (C) and glycolate (D) levels during seven-day EG challenge. E) Water intake during EG challenge (mL). Data are shown as mean ± SEM (n≥3) and Kruskal Wallis was the test of choice to analyze differences between groups. * = $p<0.05$, ** = $p<0.01$.

The same pattern was observed during the challenge. Even though the oxalate levels increased in all animals during the challenge, it was higher in control animals. Once again, urine oxalate levels in controls were heterogeneous resulting in a high variability. This phenomenon could be caused by the fact that the control animals were not healthy and did not produce normal volumes of urine. Nevertheless, the oxalate levels in treated animals were significantly lower and to the same as the levels obtained for WT healthy controls. Based on this a protection against the EG challenge can be concluded (Figure 47C). The glycolate amount was also significantly higher in animals treated with gRNAs (Figure 47D). To ensure the homogeneity of the challenge, the water intake was measured and no significant differences were observed between groups (Figure 47E).

It should be noted that two control animals displayed high urea levels in serum, which was probably due to the kidney impairment (Figure 48A). The presence of NC in kidneys was also analyzed and

complete protection was observed in treated animals. However, milder kidney damage than during the 1-month experiment was detected in controls, most likely because the challenge was shorter. Treated animals also did not suffer weight alterations during the challenge (Figure 48B).

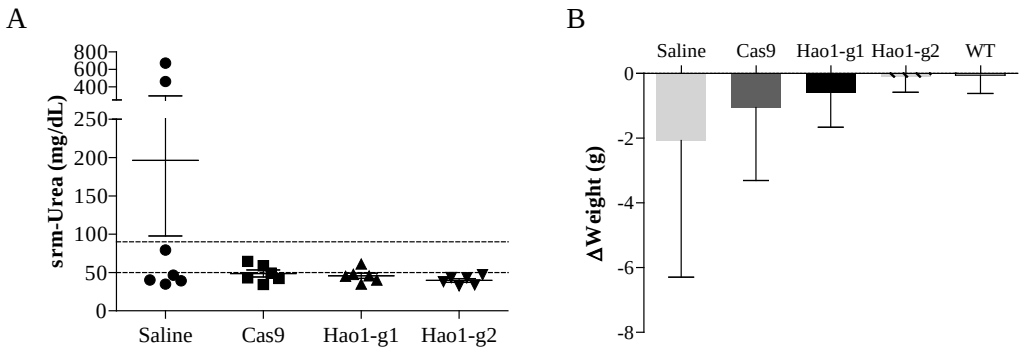

Figure 48. Toxicity of the EG challenge 4 months after the treatment with AAV8-SaCas9-*Hao1*-gRNA. A) Serum urea levels (mg/dL) and normal reference range (dashed lines, 49.9-90.15 mg/dL). B) Change in body weight during EG challenge. Mean ± SEM (n≥6) are shown for each groups and Kruskal Wallis test was not significant for both parameters.

After sacrifice, a molecular analysis was carried out in order to correlate the therapeutic effect with GO inhibition. The indel percentage was calculated using the tool TIDE, and, as shown in Figure 49A, most of the animals treated with AAV8-SaCas9-*Hao1*-gRNAs were positive for indels in the specific target site. However, some of the animals that had been treated with AAV8-SaCas9-*Hao1*-g2 (empty inverted triangles) had a lower indel percentage compared to the rest of the animals treated with the gRNAs, which had about 40-50% of indels. These animals also presented lower viral genome copy numbers (Figure 49B empty inverted triangles), lower Cas9 expression at mRNA level in the liver (Figure 49C empty inverted triangles) and almost no inhibition of GO by WB (Figure 49E marked with #). The analysis of the remaining gRNA-treated animals was in line with that obtained after short-term treatment. Interestingly, the relative quantification of *Hao1* mRNA showed a significant reduction in animals treated with the gRNAs, while the mRNA expression levels were higher in control animals (Figure 49D).

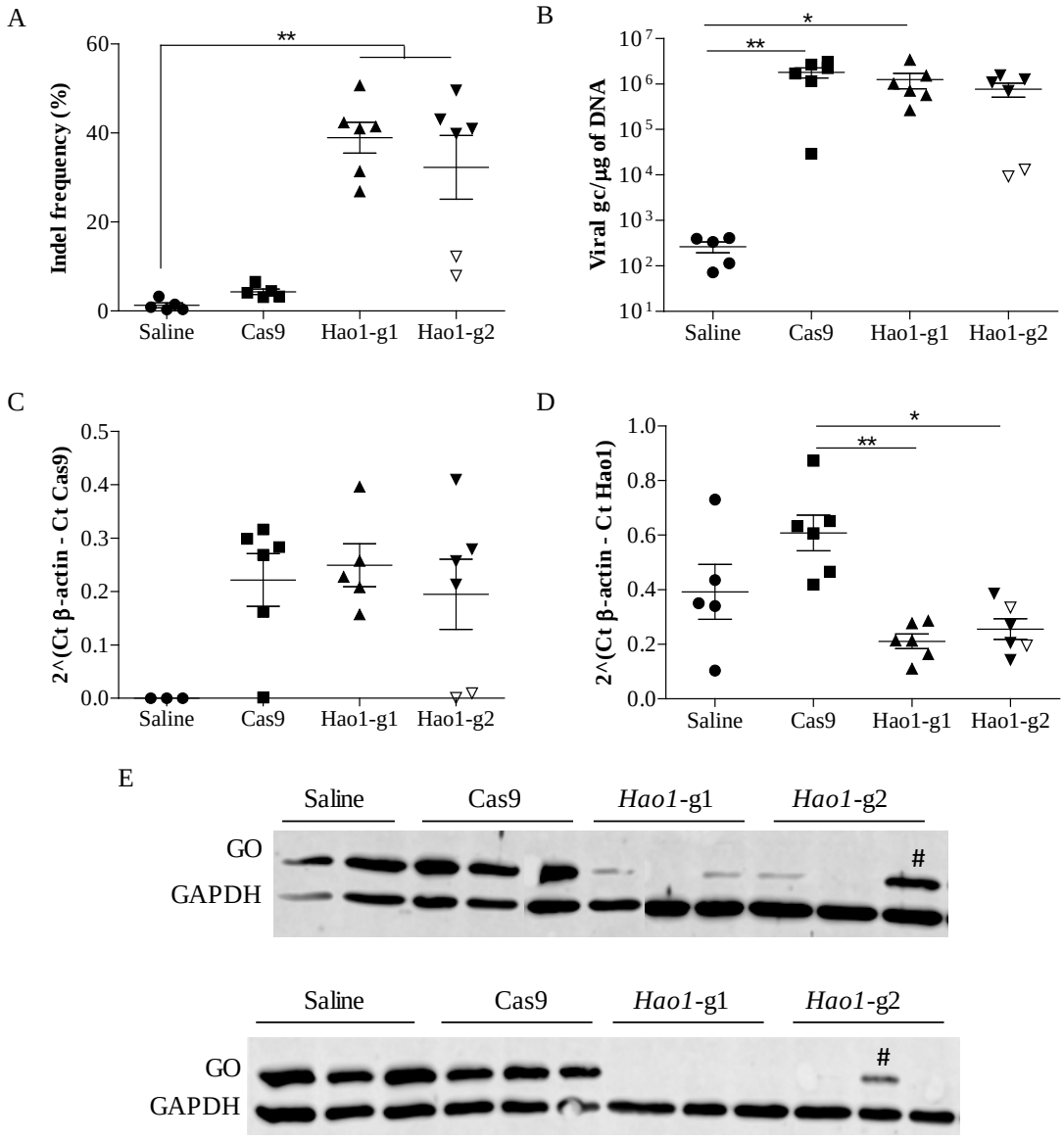

Figure 49. *Hao1* gene disruption and GO inhibition in the liver of treated and control male animals 4 months after treatment. A) The percentage of indel in the target site for *Hao1*-g1 and *Hao1*-g2. B-C) Transduction of the liver analyzed as viral genome copies (B) and SaCas9 mRNA expression (C). D) *Hao1* mRNA expression in the liver. All data are represented as mean ± SEM (n≥5). Kruskal Wallis was the analysis to compare the groups. E) WB analysis of GO and GAPDH protein expression in the liver. * = $p<0.05$, ** = $p<0.01$.

4.4.5 Therapeutic efficacy of GO reduction in female PH1 mice 4 months after the treatment

After studying the therapeutic efficacy of GO reduction in male mice, we next repeated the experiments using females. PH1 female mice were divided in the same treatment groups as before and they underwent the same procedures as males (Figure 46). Although not reaching significant, 4 months after treatment, oxalate levels were lower in gRNA-treated and in WT females than in controls (Figure 50A). This effect was likely due to the less severe phenotype that has been described for female PH1 mice (101). During the challenge, oxalate levels were increased in all animals, even though with a trend to be lower in animals treated with AAV8-SaCas9-*Hao1*-gRNAs; however no significant differences were observed (Figure 50B). As in experiments with males, water consumption was monitored and did not differ between groups (Figure 50C).

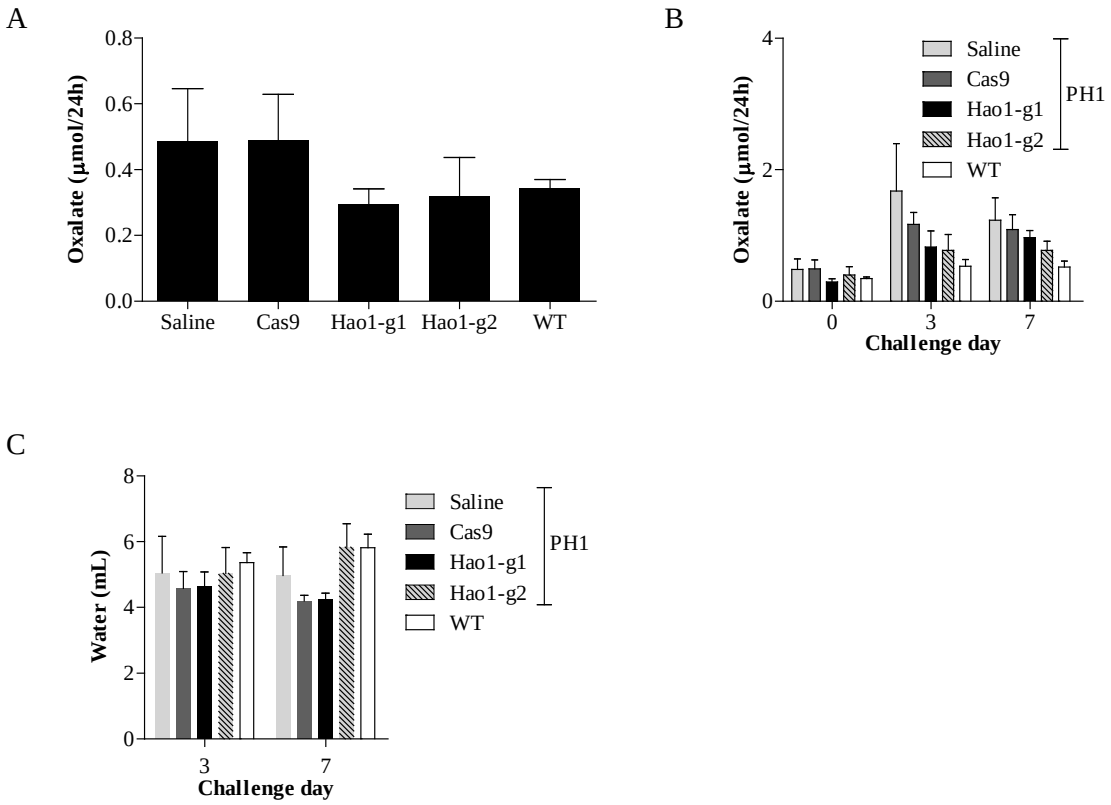

Figure 50. Long-term efficacy of the AAV8-SaCas9-*Hao1*-gRNA in female PH1 mice 4 months after treatment. A) Basal oxalate levels in females 4 months after treatment. B) Oxalate levels during EG challenge. C) Water consumption during EG challenge. Data are shown as mean ± SEM (n≥3) and Kruskal Wallis revealed no significant differences between groups.

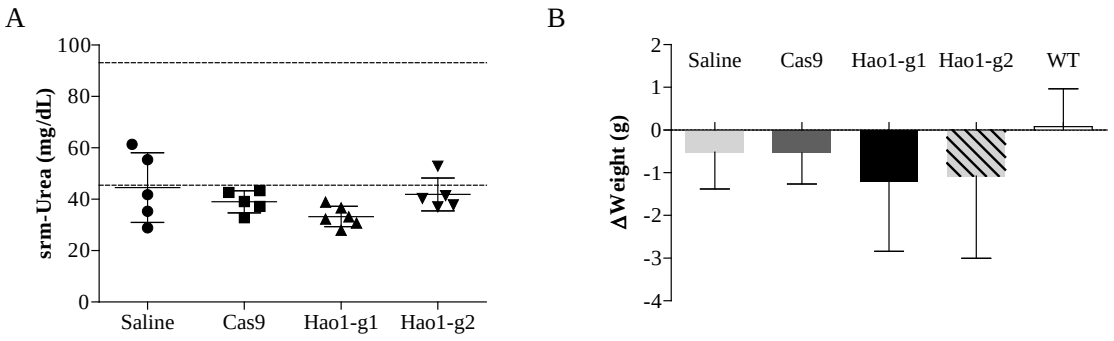

Figure 51. Effects of EG challenge on kidney function and weight in females. A) Urea levels (mg/dL) in serum, reference values were 45.46-93.2 mg/dL. B) Weight change during seven-day EG challenge. Data are represented as mean ± SEM (n≥5) and Kruskal Wallis test showed no significant results.

While urea levels were normal after the challenge (Figure 51A) and the changes observed in body weight were the homogeneous among groups (Figure 51B), the molecular analysis revealed an interesting difference in indels between the groups that received the gRNAs (Figure 52A). The group that received AAV8-SaCas9-*Hao1*-g2 had a similar indel frequency to that observed in males but females that received the AAV8-SaCas9-*Hao1*-g1 showed an indel frequency of around 20%, and therefore only about half of that observed in males. The transduction of the liver, measured as the presence of viral genome copies (Figure 52B), and the expression of Cas9 mRNA (Figure 52C) revealed a slight decrease in Cas9 expression in the *Hao1*-g1 group; therefore, explaining the observed differences in indel frequency (Figure 52C). *Hao1* mRNA analysis revealed a decreased expression in animals with a high percentage of indels (Figure 52D). GO protein expression was analyzed by WB and most of the female mice treated with AAV8-SaCas9-*Hao1*-gRNAs had a decrease into protein levels, but not a complete disappearance like in males (Figure 52E). Of note, one mouse of the AAV8-SaCas9-*Hao1*-g1 group, presented with low percentage of indels and also a low presence of viral particles in the liver (Figure 52A-B, empty triangle, and Figure 52E marked with #).

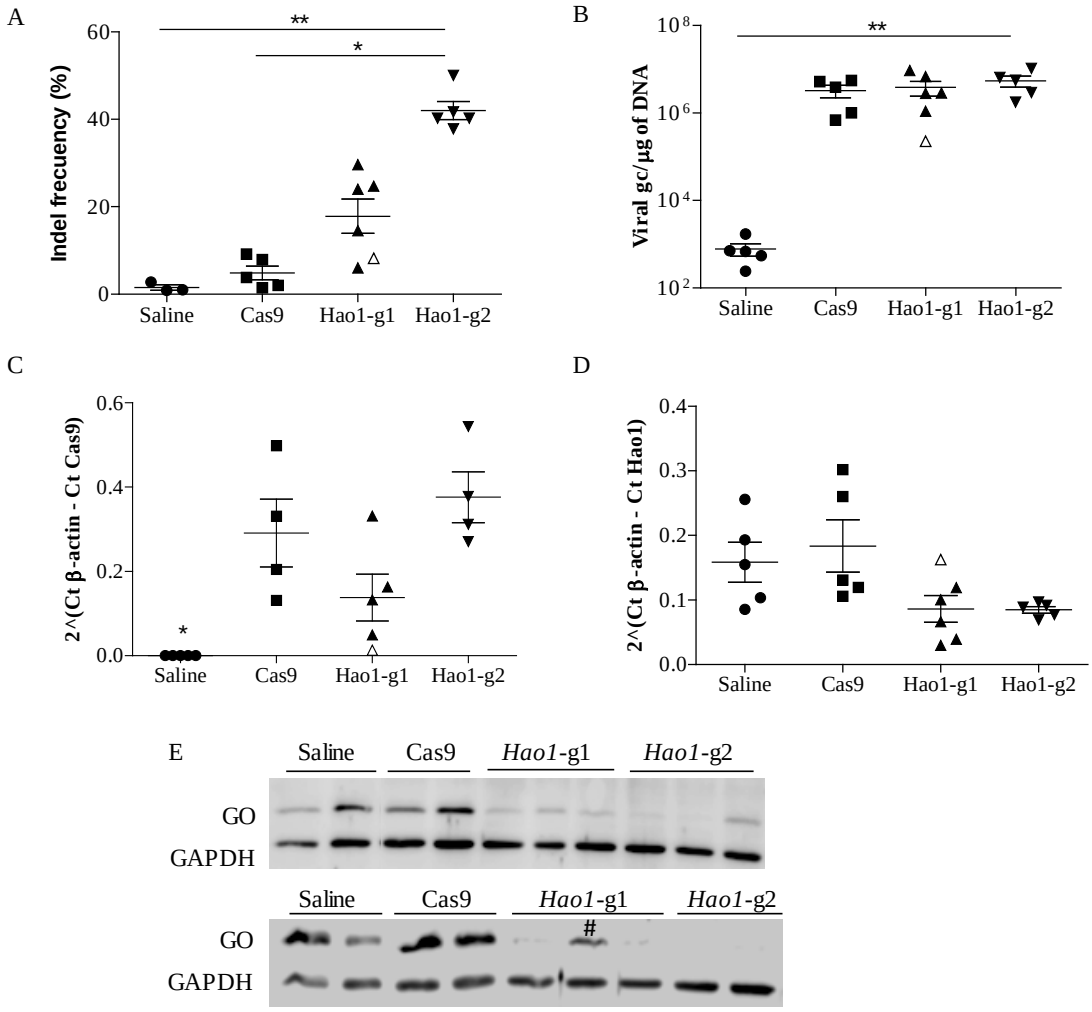

Figure 52. *Hao1* gene disruption and GO inhibition in the liver of female animals. A) Quantification of indel frequencies in the liver by TIDE. B-C) Analysis of liver transduction of AAV8 vectors by viral genome quantification (B) and Cas9 expression (C). D) *Hao1* mRNA expression by RT-qPCR. All the data are represented as mean ± SEM (n≥4) and Kruskal Wallis test was used to analyze differences between groups. E) GO and GAPDH expression analyzed by WB in liver protein extracts. * = $p<0.05$, ** = $p<0.01$.

4.4.6 Safety of CRISPR/Cas9-mediated SRT

Liver toxicity markers were analyzed in the sera of all animals treated with the AAV8-SaCas9-*Hao1*-gRNAs to exclude a possible toxic effect associated with the treatment. Serum ALT and bilirubin were analyzed in treated males after one month (Figure 53A and 53B), four months (Figure 54A and 54B) and the respective females (Figure 55A and 55B). Overall, no abnormality of either parameter could be detected and no difference was found between groups.

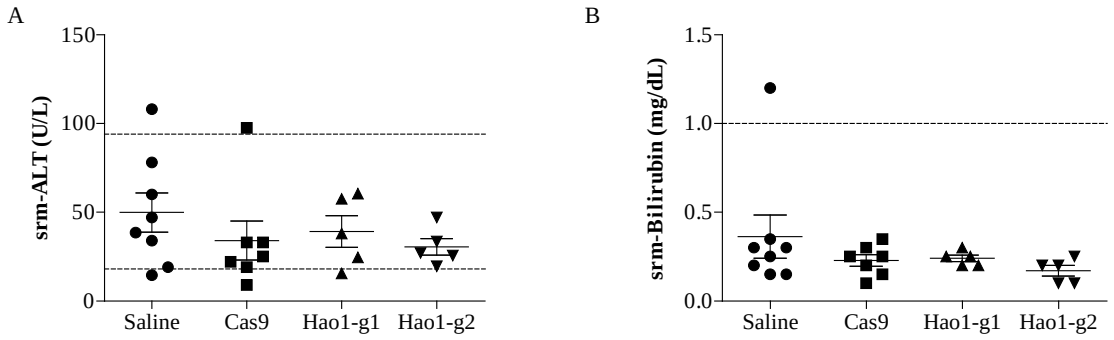

Figure 53. Analysis of short-term toxicity associated with SaCas9 expression in male mice. Serum ALT (A) and bilirubin (B) measurement after one month of treatment. Reference values are 18-94 U/L for ALT and 0-1 mg/dL for bilirubin (dashed lines). Data are shown as mean ± SEM. Kruskal Wallis test was used to analyze differences between groups.

Interestingly, after four months of treatment some of the animals – both treated (males and females) and mock-treated (males only) - a slight increase in ALT and/or bilirubin levels could be observed. Among the treated animals, this was the case of two males treated with the AAV8-SaCas9-*Hao1*-g2 (empty inverted triangles in Figures 49 and 54) and a female treated with the AAV8-SaCas9-*Hao1*-g1 (empty triangles in Figures 52 and 55). These mice presented also with lower levels of viral load, SaCas9 mRNA expression and indels in the *Hao1* gene. The reason of this damage remains unknown.

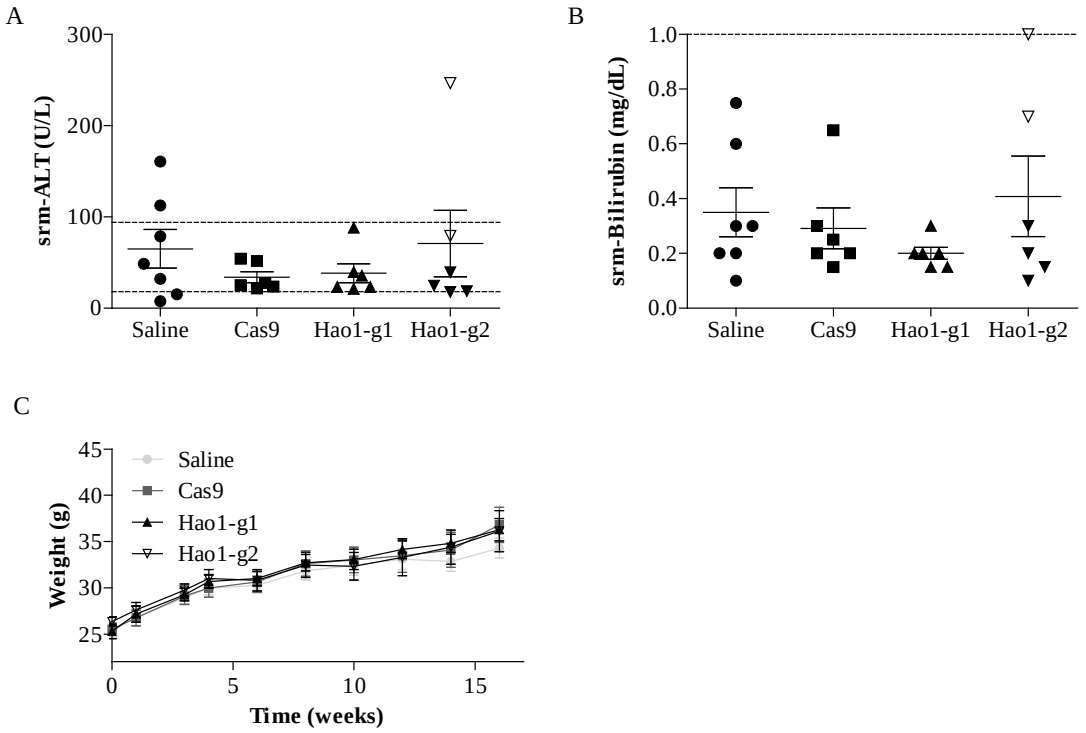

Figure 54. Analysis of long-term toxicity in male mice after 4 months. Measurement of liver toxicity-associated biochemical parameters in serum: ALT (A) and bilirubin (B). Reference values for ALT were 18-94 U/L and for bilirubin 0-1 mg/dL (dashed lines). Data are shown as mean ± SEM. Kruskal Wallis test revealed no significant differences. C) Monitoring of body weight during the 4 months between treatment and sacrifice. Friedman test revealed no significant differences between groups.

The body weight was also monitored in both sexes during the 4 months duration of the experiment. All animals grew according to the normal development of PH1 mice (Figure 54C and Figure 55C).

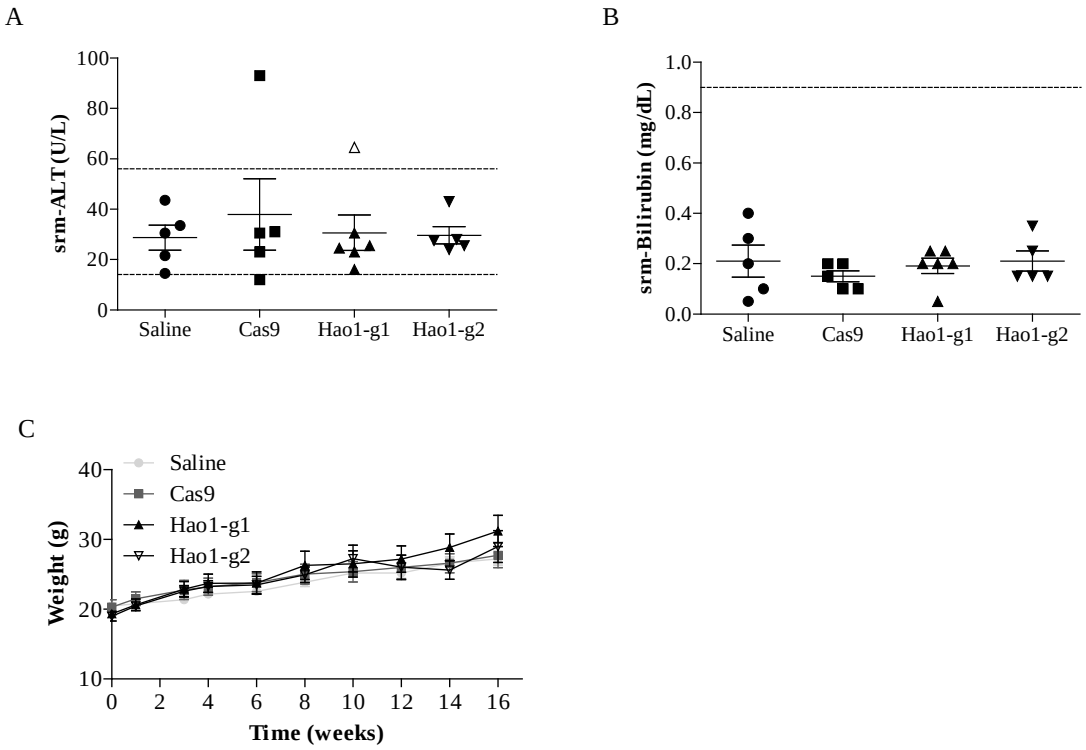

Figure 55. Analysis of toxicity in female mice after 4 months. Quantification of ALT (A) and bilirubin (B). Reference values for ALT were 14-56 U/L and for bilirubin 0-0.9 mg/dL. Mean ± SEM for each group are represented. Kruskal Wallis test was no significant for both parameters. C) Changes in body weight during the four months that lasted the experiment. Friedman test was no significant.

One of the main concerns regarding the therapies involving CRISPR/Cas9 is the possible genotoxic effect caused by unspecific indel generation in off-target sequences that are similar in sequence to the gRNA-targeted region. To address this issue, the predicted off-target regions scoring highest were sequenced by NGS in the genomic DNA of the liver of animals treated with Cas9 and the two different gRNAs and in some controls. Moreover, the off-target effect was analyzed in animals treated one and six months before the sacrifice, in order to discard a time-related increase in genotoxicity. In Tables 9 and 10 the indel frequency in the predicted top 7 off-target (OFT1-7) regions is shown and none of the gRNAs introduced modifications in the predicted off-target sequences (neither short- nor long-term after the treatment).

Table 9. Sequence variant frequencies (%) in the top 7 predicted off-targets for *Hao1*-g1.

Time of treatment	Average	ONT	OFT1	OFT2	OFT3	OFT4	OFT5	OFT6	OFT7
4 weeks	Saline	0,14	0,12	0,1	0,03	0,08	0,01	0,26	0,11
	Cas9	0,18	0,17	0,09	0,06	0,08	0,04	0,3	0,08
	Hao1-g1	48,46	0,18	0,08	0,05	0,08	0,04	0,29	0,08
6 months	Saline	0,14	0,12	0,1	0,03	0,08	0,01	0,26	0,11
	Cas9	0,24	0,18	0,07	0,06	0,07	0,04	0,28	0,07
	Hao1-g1	60,57	0,19	0,08	0,05	0,07	0,03	0,32	0,1

Saline: n=1. Cas9: n=3. *Hao1*-g1:n=5.

Table 10. Sequence variant frequencies (%) in top 7 predicted of targets for *Hao1*-g2.

Time of treatment	Average	ONT	OFT1	OFT2	OFT3	OFT4	OFT5	OFT6	OFT7
4 weeks	Saline	0,14	0,12	0,1	0,03	0,08	0,01	0,26	0,11
	Cas9	0,08	0,07	0,09	0,09	0,06	0,07	0,1	0,11
	Hao1-g2	52,81	0,08	0,09	0,08	0,06	0,06	0,13	0,11
6 months	Saline	0,14	0,12	0,1	0,03	0,08	0,01	0,26	0,11
	Cas9	0,08	0,07	0,09	0,1	0,08	0,06	0,11	0,12
	Hao1-g2	60,13	0,07	0,08	0,08	0,07	0,07	0,1	0,12

Saline: n=1. Cas9: n=3. *Hao1*-g2:n=5.

Indel frequencies in the on-target (ONT) site were also analyzed by NGS after 6 months of treatment (Figure 56 and Tables 9 and 10). Similar to the short-term experiment, an average of 20,026 and 79,731 reads were generated of the on-target region in exon 2 of *Hao1* gene for *Hao1*-g1 and *Hao1*-g2, respectively. The percentage of indels was around 60% (with a mean of 60.57% for *Hao1*-g1 and 60.13% for *Hao1*-g2), which was slightly higher than in the short-term analysis (Figure 56A). A possible reason could be the continuous expression of the Cas9 and the gRNAs in the livers. Once again, the majority of indels were smaller than 10 bp and produced frameshifts (Figure 56B), thus explaining the observed reduction in GO protein, and indel distribution was different within gRNAs (Figure 56C).

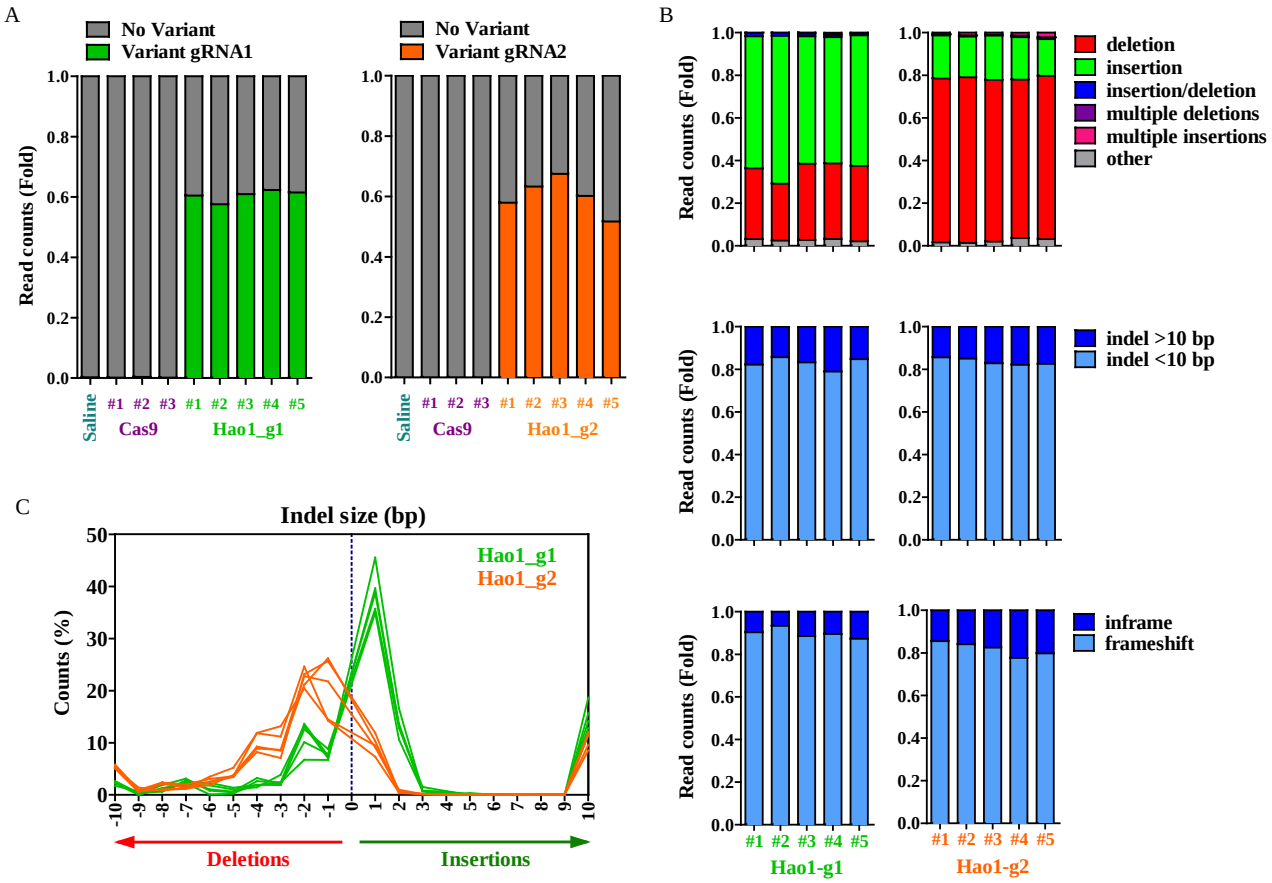

Figure 56. NGS of the on-target region of *Hao1*-g1 and *Hao1*-g2 6 months after the treatment. A) Frequency of CRISPR/Cas9-introduced variants in *Hao1* gene analyzed by NGS in one mouse treated with saline, three treated with AAV8-SaCas9 and five treated with AAV8-SaCas9-*Hao1*-gRNA (5 animals per gRNA). B) Characterization of the variants according to their modification type, size and frameshift potential in the animals presenting indels. C) Distribution of indel size in base pairs (bp) for each gRNA.

5. DISCUSSION

PH1 is an inborn error of the glyoxylate metabolism, characterized by the dysfunction of the peroxisomal enzyme AGT in the liver. It leads to an overproduction of oxalate, which subsequently forms CaOx stones in the kidney causing renal damage. Among PH1 patients the incidence of ESRD increases dramatically compared to the general population. One of the main concerns regarding PH1 is the low number of therapeutic approaches available in the clinical practice, which in most of the cases are palliative. Currently, the only curative treatment is liver transplantation, which is normally done together with kidney transplantation. Therefore, there is an urgent need to develop new strategies to cure these patients.

The main goal of this project was to find a therapeutic alternative to treat PH1 patients. Gene therapy has proven to be efficient in normalizing oxalate levels in the PH1 mouse model. Here, we have corroborated this finding and we have also demonstrated that it can be rendered more efficient by optimizing gene therapy treatment using direct injection in liver circulation. Furthermore, we have generated a completely new therapeutic strategy based on the newly discovered CRISPR/Cas9 system mediated SRT.

5.1 Development of new preclinical hyperoxaluria models

Any drug, including gene therapy products, has to be tested in representative animal models of disease during the preclinical development to determine the efficacy and potential adverse events that the treatment could have in humans. In the case of liver-directed gene therapy, NHPs are the most relevant animal model used for the preclinical assessment of safety due to the similarities in hepatic structure and response to drugs (169). It is not mandatory to perform the safety testing in a specific disease model, and in fact, in almost all cases it is not possible due to the lack of disease models in large animals such as NHPs. However, the ideal preclinical development of a drug would comprise a detailed study of both safety and efficacy in NHP.

In the case of PH1, a single mouse model has been developed (101) that is based on the elimination of the expression of AGT protein (*Agxt*$^{-/-}$ mice) and presents with a milder phenotype of the disease compared to humans. The animals have high oxalate levels in 24-hour urines, recapitulating the main alteration of the disease in PH1 patients. Urinary sediments also revealed the presence of oxalate crystals. However, they had a normal lifespan and they never developed kidney failure, not even nephrocalcinosis or urolithiasis. This phenomenon is explained by the fact that the GFR in mice is very high in relation to their body weight, hence allowing a faster detoxification of the oxalate and thereby decreasing the probability of formation of CaOx crystals in the tissue. Nevertheless, this handicap of the model can be solved by challenging the mice with precursors of

oxalate in the form of HP (83) and EG (101). Another fact that should be taken in consideration is that the phenotype observed in mice depends on their genetic background, which implicates that many other variables other than AGT activity are implicated in the progression and severity of the disease.

Our first goal was to generate a diet-induced hyperoxaluria model in NHPs, in which the safety and efficacy of an AAV-based gene therapy treatment can be analyzed. As known, HP is metabolized in the mitochondria to glycolate that is converted into glyoxylate in the peroxisome (Figure 1). Our working hypothesis was that an overexpression of the AGT protein in a healthy animal prevents an excessive production of oxalate induced by an oxalate precursor rich diet. Therefore, we first demonstrated in WT animals, mice and NHP, that a three-day overload challenge with HP led to an increased oxalate production and its subsequent elimination in urine. However, contrary to what we had expected, we observed that in mice an increase in the expression of AGT mediated by gene therapy was not able to decrease the elevated urine oxalate levels. Based on these findings, this diet-induced acute hyperoxaluria model was considered inadequate to explore the efficacy of gene therapy treatments in NHPs.

As a consequence, we decided to continue our analysis of the efficacy of new gene therapy and gene editing approaches using the *Agxt*$^{-/-}$ mouse model. As mentioned, PH1 animals have to be challenged with a precursor of oxalate to increase oxalate levels in urine and to generate nephrocalcinosis. During the set-up of both HP and EG challenges, a higher sensitivity to oxalate precursors was observed in PH1 mice. In the case of HP, the animals did not voluntarily take HP into solid diet, while the oral gavage resulted to be toxic and many animals died. In contrast, EG challenge could be applied, but if compared with previous published works, the dose had to be lowered and the time shortened in order to avoid the death of the animals (80,101). This phenomenon could be caused because living conditions of the animals could change between different animal facilities, for example, temperature variations could affect the volume of water consumed by the animal, increasing the amount of EG taken up by each animal.

5.2 Optimization of gene therapy for PH1

5.2.1 Human *AGXT* codon optimization

Many clinical trials have used codon optimized versions of genes to treat monogenic disorders with gene therapy (123,128), aiming at increasing the translation speed of the transgene, and as consequence, the amount of protein that is obtained. As known, the genetic code is degenerated, meaning that each protein can be potentially encoded by many versions of its mRNA by using

synonymous codons. It has been shown that different mRNA sequences translate into different amounts of the same protein because the relative abundance of the different tRNAs varies dramatically (133). Codon optimization of the transgene is based on the generation of synonymous mutations in order to generate codons recognized by the most abundant tRNAs.

For the purpose of our study, a codon optimized version of the human *AGXT* gene was generated (coAGXT) and compared to the WT version (AGXT WT). coAGXT was designed by the Dutch biotech company uniQure, which produced the AAV vectors carrying both the WT and the co versions of the AGXT cDNA, and the efficacy of both vectors was tested side by side. The analysis of protein levels revealed no translation advantage for coAGXT and this was reflected in the therapeutic efficacy, since oxalate levels were the same in the animals treated with either AAV-AGXT WT or coAGXT. In conclusion, the codon optimized version of the human *AGXT* gene used in this study did not generate a therapeutic advantage in mice.

A possible reason to explain why this approach did not induce higher protein levels and reduced oxaluria could be that the synonymous changes at mRNA levels were not a real optimization. Many scientists are concerned about the meaning and the consequences of synonymous codon changes (133,172) as they may affect the stability and conformation, post-translational modifications and the function of the proteins they encode. Moreover, a study published by Rosano *et al.* demonstrated that the overexpression of tRNAs corresponding to rare codons in *E.coli* led to increased protein levels but made this protein more prone to misfolding and aggregation (173). In fact, many examples of disease-associated synonymous mutations have been described (174). In this regard, the codon optimization of the *AGXT* gene has to be taken with extreme care, due to the tendency of AGT to misfold, resulting in mistargeting (44) or aggregation (17,64). The AGT protein has a complex structure and a minimal change leads to the destabilization of the complex folding and to problems in protein function (44). Therefore, a detailed analysis of the effect of codon optimization should be performed, which might be complicated due to the high number of possible synonymous changes.

Even though the dose inoculated in this experiment was higher than the dose used by Salido *et al.* (80), the therapeutic effect was smaller. Again, this differences could be explained by the different sensitivity to EG of the mice used for these experiments.

In conclusion, the codon optimization did not give a therapeutic advantage in the treatment of PH1. It has to be carefully considered by the field whether it is worth to try and optimize the *AGXT* gene with the goal of increasing the protein levels when running the risk of compromising the correct

folding of the protein. Moreover, AGT is intracellular and its malfunction leads to the overproduction of oxalate. Therefore, a high percentage of hepatocytes needs to be corrected in order to lower oxalate to non-damaging levels, implicating that the percentage of transduction may be more important than intracellular protein levels.

5.2.2 Improvement of AAV-mediated liver transduction efficiency by changing the route of administration

In order to increase the percentage of AAV-transduced hepatocytes, several strategies can be carried out. In this project, we hypothesized that a change of the administration route from intravenous to direct could trigger a higher transduction. In clinical trials of gene therapy treatments directed at the liver, intravenous administration was performed using AAV vectors with an increased liver tropism (123,128).

It is known that in rodents, hydrodynamic injection of naked DNA results in a significant percentage of transduced hepatocytes (145). The hydrodynamic injection is based on the administration of DNA diluted a large volume, which generates an increase in hepatic pressure that leads to the enlargement of the endothelial fenestrations, the formation of pores in the hepatocyte membrane and thus facilitates the entrance of the DNA (145). The same strategy can be employed to increase the transduction in treatments with AAV vectors. However, the hydrodynamic injection is impossible to perform in the same way in rodents and in bigger animals or humans. Some groups described different methods for mimicking this phenomenon in bigger animal models, such as NHP (141). These methods make use of introducing various catheters and balloons into the hepatic vessels in order to isolate the hepatic blood flow, to increase hepatic pressure and to administer the vector in a more targeted manner. Results were promising; however, these systems were only tested for HDAd delivery and not for AAV vectors.

In the present study, we demonstrated that the administration of an AAV serotype 5 using new routes directly targeting the liver resulted in a higher efficacy of transduction and increased transgene expression. We developed a new surgical method directly administering AAV into the hepatic blood flow. The innovation of the technique is that it did not require isolation of the whole liver, but instead a balloon catheter was placed in one of the branches of SHV and the vector was administered in two boli. This way the overall blood flow of the liver was not obstructed at the same time, which in previous studies was reported to cause a decrease in the blood pressure of the animals (141). The blood pressure of our animals was maintained at normal levels during the procedure (data not shown). However, unfortunately the animals of the study were not big enough

for the catheterization and balloon inflation of the left branch of the SHV. Consequently, we were forced to administer the whole vector dose on the right side. Nevertheless, in humans administration on both sides should not be impeded by vessel size. As a proof of principle we performed a pilot study using two hybrid pigs, which in size are closer to humans and the procedure was easily performed without causing damage (data not shown). However, the procedure needs to be tested further in bigger animals in order to determine whether one of the routes of administration will result in higher expression levels after AAV administration.

In summary, in comparison to IV injection, higher transgene levels were measured in the serum of the animals treated via the new routes. Moreover, the spatial distribution of the AAV genome load was analyzed in different liver sections, revealing higher transduction levels in the regions located on the right side of the liver, where the new administration procedure was performed. Therefore, the main goal of increasing liver transduction was achieved. However, the same experiment should be done using an intracellular reporter transgene that allows imaging of the transduction and the re-evaluation of the percentage of transduction.

Regarding the safety of the procedures, we only observed a slight increase in liver transaminases that resulted in no long-term damage for the animals. Interestingly, the viral shedding profile was found to be different between the three administration procedures. This could be a result of the procedure: In SHV administration the vector is administered against the blood flow and travels from the central vein to the edges of the lobule. An increased pressure from the central vein to the portal triad could push the vector into the bile ducts, which would explain a higher number of vector genome copies in the feces of animals from the SHV group. In contrast, HA administration follows the natural direction of the blood, from the portal triad to the central vein. An increase of vector in the urine of these animals could be explained by a retrograde escape of the vector through the inferior vena cava to the renal arteries during the balloon occlusion. Another interesting fact is that the clearance of the vector from the blood is delayed in all animals receiving the vector via the new routes. One possible explanation is that the vector may be retained in some microvessels coagulated during balloon occlusion and delivered later. This phenomenon could also explain the measurement of higher anti-AAV5 capsid antibody levels in some of the animals from the SHV and HA groups on day 56 after the administration. Regarding the biodistribution, no significant change was observed.

In addition, the routes described here can be adapted to other goals, such as the fluxing with saline before vector administration to empty the liver from blood and to allow transduction in presence of preexisting AAV-specific antibodies. Mimuro *et al.* successfully administered AAV8 particles to

NHPs with preexisting antibodies by injecting the vector directly into the portal vein (139). The portal vein confers an advantage over the HA as the hepatocytes are mainly supplied by portal blood, which composes around 70-80% of hepatic flow. In spite of the higher blood supply, portal vein administration is a more complicated procedure and it also bears a higher risk since a laparotomy has to be performed to reach the vein. Moreover, the use of a balloon catheter placed in the SHV would favor the retention of the vector in the liver vessels, eliminating the blood supply factor and favoring the infection of the hepatocytes in an antibody-free environment.

In conclusion, minimally invasive new routes of administration were developed and characterized for the administration of gene therapy vectors that triggered higher transduction of the liver in absence of adverse events.

5.3 CRISPR/Cas9-mediated substrate reduction therapy (SRT) for PH1

The last goal of this project was to develop novel therapeutic alternatives to treat PH1 based on the recently discovered CRISPR/Cas9 systems. As mentioned, these systems have been used to generate DSBs in the genomic DNA of eukaryotes, which are repaired by two cellular mechanisms, NHEJ and HDR.

The ideal gene editing treatment for a genetic disease in which a single gene is affected would be the correction of the specific mutation or the introduction of a correct copy of the gene in the genomic DNA; hence, HDR should be employed. However, HDR was found to be very inefficient in adult cells (165). To improve HDR efficacy some strategies have been suggested. First, it was shown that the treatment in newborns increased the percentage of HDR-edited hepatocytes from a maximum of 2.1% in adults to 20.1% in newborns (165). Other studies have demonstrated that the efficacy of HDR strategy increased due to the selection of corrected hepatocytes, such as in HT1 (163,164). Finally, pharmacological inhibitors of NHEJ pathway were tested to increase HDR frequency in cells, but this strategy has not yet been tested *in vivo* (175). Unfortunately, the strategies mentioned above cannot be applied in PH1. This disease is usually manifested during childhood, which makes the treatment of newborn impossible unless a newborn screening to search for mutations in *AGXT* gene is performed. In addition, in the case of PH1 the corrected hepatocytes have no selective advantage. In conclusion, the use of HDR to correct the metabolic disorder in PH1 requires the optimization of the HDR to obtain a high percentage of corrected hepatocytes.

Recently, a new strategy was described, making use of a mixture between NHEJ and HDR. Suzuki *et al.* called this process *homology-independent targeted integration* (HITI). It is based on the generation of DSBs both in the genomic locus and in the donor template flanking the fragment that is going to be introduced in the specific genomic site (176). The DSB is subsequently repaired by NHEJ but during the repair the donor DNA is introduced. This strategy needs to be further characterized before applying it as treatment.

The difficulties to employ HDR-based strategies led us to design an alternative therapy based on NHEJ, which has been proven to be very efficient in generating indels in the genomic DNA of hepatocytes (157,158,161,177). This strategy has been applied successfully, due to the high rate of NHEJ in adult non-dividing cells. Furthermore, previous experiences demonstrated that SRT using siRNAs targeting the *Hao1* gene could be an efficient treatment to reduce oxalate levels (78,86,87). These findings encouraged us to develop an *in vivo* treatment using CRISPR/Cas9 to knock out GO enzyme in the liver.

Our strategy offers some advantages over siRNA-based or small molecule-based inhibition. The most obvious problem of siRNAs and small molecules is the transient inhibition effect, implicating that the treatment has to be administered periodically during the life of the PH1 patient to avoid the overproduction of oxalate (86). In contrast, the strategy developed in this project had a long-term effect in the PH1 mouse model as a consequence of the introduction of permanent changes in the DNA, which are also transferred during cell division. Another concern related to siRNAs or small molecules could be the potential unspecific knock down of other mRNAs or miRNAs with sequence similarities or inhibition of other protein. However, this is a risk that is also taken in CRISPR/Cas9-based therapies, where the nuclease can generate DSBs in other genomic regions leading to unknown effects.

We chose GO as a target due to previous data indicating that it is a safe and efficient target to reduce of oxalate production in PH1 (78). However, it is not the only possible target for SRT. Another enzyme, hydroxyproline dehydrogenase (HYPDH), is the catalyst in the metabolism of hydroxyproline. When Li *et al.* knocked down HYPDH with siRNAs *in vivo* in PH1 animal model, they were able to reduce urine oxalate. In humans, the HYPDH-deficiency is considered a benign error of metabolism (92). Even though this strategy would avoid the production of oxalate from hydroxyproline, oxalate would be still generated from glycolate precursors. Another possible candidate for inhibition is lactate dehydrogenase, or LDH, which is the enzyme that oxidizes glyoxylate to oxalate. Nevertheless, being an enzyme that is also involved in other metabolic

processes, the safety of inhibiting LDH is doubtful. In addition, the effect of the accumulation of glyoxylate is currently unknown.

Permanent inhibition of an enzyme may be associated with the development of unwanted side effects. However, GO deficiency was detected in a patient, who presented with non-pathogenic gycolic aciduria as the only symptom, which was induced by the high amount of glycolate synthesized in the liver, which eliminated in the urine (90). Therefore, GO deficiency was considered a benign inborn error of metabolism. In addition, glycolate is a very soluble molecule (calcium glycolate is approximately 15,000-fold more soluble than calcium oxalate) and can easily be excreted into the urine without causing any damage to the kidneys (91).

Taking into account these findings, we designed a *Hao1*-specific CRISPR/Cas9 system based on SaCas9 and gRNAs specific for the exon 2 of the murine *Hao1* gene, which was then packaged into AAV8 vectors to facilitate hepatic delivery in PH1 mice. The system was able to efficiently generate indels in the targeted locus, which was translated into a dramatic decrease of GO protein levels in the liver. In addition, GO reduction was found to be therapeutic as a reduction of oxalate in urine was observed and the kidneys were protected against the accumulation of CaOx crystals during an EG challenge. This phenotypic effect was maintained over time until at least 4 months after administration of the vectors. Interestingly, long-term experiments in males revealed that oxalate levels were normalized to levels observed in WT animals. These results indicate that the major part of glyoxylate is produced by GO. As expected, glycolate levels were higher in the urine of animals in which the GO had been knocked out.

In a publication of Li *et al.*, increased oxalate levels were observed in the urine of WT mice treated with a siRNA *in vivo* to knock down *Hao1* (83). They hypothesized that this phenomenon could be a compensatory mechanism to reduce glycolate, where the glycolate is reabsorbed in the kidney and converted to oxalate in a GO-independent manner. In accordance to this experimental observations, it has been recently diagnosed a GO-deficient patient with unexplained hyperoxaluria (91). This patient was born from consanguineous parents, she was diagnosed for congenital hyperinsulinism and she underwent several hepatic problems. Although *AGXT*, *GRHPR* and *HOGA1* genes were not mutated, the genetic background of the patient was problematic and the hyperoxaluria could not be attributed to the defect in GO. The authors hypothesized that it could be caused by the inhibition of GRHPR activity, which is the enzyme implicated in PH2 and it is also inhibited in absence of HOGA1 activity in PH3 patients. They also suggested that the metabolic environment could be altered due to the hyperinsulinism. In contrast to these results, in our experience, when GO was knocked out in PH1 animals the oxalate levels decreased to normal oxalate levels.

As mentioned, there is a lot of concern about the possible off-target effects of CRISPR/Cas9 therapies. However, the high-throughput sequencing of the top 7 *in silico* predicted off-targets of the gRNAs employed in this study revealed no alterations in sequences that are similar to the gRNA-targets and that are followed by the NNGRRT PAM sequence. However, this gives no warranty of safety since Schaefer *et al.* reported many unexpected off-target cleavages *in vivo* (178). Nevertheless, these results have been controversial because the vast majority of indels found in this study were single nucleotide variants (SNV), which can be generated during the repair of a DSB caused by the cleavage by Cas9 but it is a very rare event (179). Moreover, the off-target sites seemed to be independent of the sequence targeted by the gRNA and the presence of the PAM sequence. In conclusion, there still is neither clear evidence nor enough long-term experience to confirm that the expression of CRISPR/Cas9 systems in eukaryotic cells is not genotoxic. In order to elucidate if the treatment proposed in this thesis is safe, more profound studies need to be performed. The treatment has to be tested in NHP, which are more similar to humans than mice, and in-depth study of genomic changes must be performed by whole genome sequencing to ensure that there is no off-target effect.

Some technical issues should be addressed at this point, as there is a gap between the quantification of indels by TIDE or NGS and the resulting observed effect on protein levels. We found an average of approximately 50-60% of indels in the exon 2 of the *Hao1* gene, while in most of the animals the GO protein was undetectable by IHC and WB. A possible explanation for this phenomenon is that the population of cells analyzed differs between the techniques using genomic DNA and the techniques assessing protein. The *Hao1* gene is present in all cell types, independently of the expression of the gene, while SaCas9, being under the control of the TBG promoter, is only expressed in hepatocytes. Hence *Hao1* can only be edited in hepatocytes. Genomic DNA is extracted from the whole liver, where about 50% of the cell composition corresponds to hepatocytes and therefore non-edited DNA of other cell types interferes with the results of the sequencing. However, *Hao1* expression is hepatocyte-specific, implicating that protein expression occurs only in hepatocytes and thus detection is not altered by other cell populations. Various strategies can be applied to analyze indels only in hepatocytes: Firstly, hepatocytes can be isolated using a perfusion system and circulating collagenase to eliminate circulating- as well as epithelial cells. Alternatively hepatocytes can be sorted by flow cytometry. Another method would be the analysis of indels in cDNA; since *Hao1* is only expressed in hepatocytes, *Hao1* mRNA found in the liver originates from this cell type. This technical issue has also been observed by other groups (157).

A limitation of our studies is that we were not able to prove the therapeutic efficacy in female PH1 animals. Oxalate levels were monitored in females 4 months after treatment during an EG challenge. Although there was a trend to a reduction in oxalate levels in treated females, no significant evidence of efficacy was observed in treated mice *versus* sex-matched PH1 controls. As explained, the disease phenotype in the PH1 mouse model is milder in the females (101), which led us to conclude that the EG dose administered may not have been high enough to increase oxalate levels. The milder phenotype of females could be caused by a difference in GO levels between males and females, which were lower in female PH1 animals compared with age-matched males. Further experiments have to be carried out to set up a new challenge for females and elucidate the effects of the treatment. In addition, in female studies it could be observed that *Hao1*-g1 produced indels less efficiently than *Hao1*-g2, while in males it was the same. This difference might be due to the lower Cas9 expression observed in the female *Hao1-g1* group, probably due to a technical problem during the administration of the vector.

For the present study, AAV8 were chosen as vectors because of their high liver tropism (80), which allowed analyzing the efficacy of the new treatment strategies. Also, AAV vectors have been used as proof-of-concept of the efficacy of CRISPR/Cas9-mediated SRT. One of the advantages of AAV-based gene therapies is the long-term transgene expression (128), although this is not a requisite for CRISPR/Cas9-based strategies: On the contrary, a transient expression of the Cas9 nuclease is sufficient to introduce the modifications of interest in the genomic DNA and reduces the possibility of having an undesired off-target effect. Moreover, a sustained expression of a foreign protein, which originated from bacteria, could promote the development of immune responses against transduced hepatocytes.

Taken together, the next steps in the development of CRISPR/Cas9-based PH1 treatment should be focused on the optimization of the administration method in order to achieve transient Cas9 expression. Several strategies could fulfill this goal. For example, the therapeutic AAV vectors could be administered to newborns. It is known that the AAV genomes are diluted during liver growth and renewal, implicating a loss of transgene expression. Yang *et al.* demonstrated that the administration of Cas9-expressing AAVs in newborns triggered a transient expression of the nuclease because of dilution effect during the growth of the liver (165). However, to date PH1 is not part of the routine screening of newborn and only diagnosed once symptoms occur, which currently excludes this option. Another way of expressing Cas9 transiently could be the switch to other viral vectors, such as first generation adenovirus. These vectors were also tested with Cas9 and a progressive loss of genomes and expression of the nuclease were reported (158). The main problem

of adenovirus is their induction of an acute immune reaction and a related high probability of immunoreactivity against Cas9 (159). Merienne *et al.* described a self-inactivating Cas9 consisting of the simultaneous expression of a gRNA targeting the gene of interest and a gRNA targeting the sequence of the Cas9 itself (181). This strategy would decrease the probability of having an off-target effect of the Cas9 but the protein would be still expressed and an immune response could be developed. Lastly, some groups have expressed Cas9 transiently using nanoparticles of different composition to direct the mRNA of Cas9 to the liver (164,182,183).

In this context it needs to be mentioned that in three of our long-term treated males and in one female several observations were made that hint at an immune response producing liver damage. Said animals presented with high levels of ALT and bilirubin in the serum, which is an indicator of liver damage. Molecular analysis revealed that in these mice the transduction of the liver was lower compared to the ones that had received the same treatment. In addition, the percentage of detected indels was also lower. These results could indicate the destruction of transduced hepatocytes. However, we were not able to analyze the response against SaCas9 protein due to the absence of proper tools. Others have investigated the host response against Cas9 protein. One publication analyzed the immune response against SpCas9 when it was expressed in muscle using AAV9 as carrier (184). In this study the development of a cellular and humoral immune response against SpCas9 was observed. However, it is known that the expression of a foreign protein in the liver leads to the development of tolerance for the transgene (185,186), while the probability to induce immune responses against the transgene is higher in the muscle. Moreover, recent findings indicate that antibody-mediated and T-cell-mediated responses against this protein are developed in humans infected with *S.pyogenes* or *S.aureus* (180). In conclusion, we should analyze the response in the PH1 animals, but certain tools, as pure SaCas9 protein or a peptide library, should be produced to study the host response.

In conclusion, the treatment described here was demonstrated to be efficient in reducing urinary oxalate levels and kidney damage, and no evidence of toxicity related to the knocking out of GO enzyme could be observed.

It needs to be explored whether this strategy could be applied to reduce oxalate levels in secondary hyperoxalurias (SH), which are caused by an excessive exogenous absorption of oxalate or its precursors. In these cases, the reduction of endogenous oxalate synthesis would contribute to the reduction of total oxalate. However, the inhibition of GO with CRISPR/Cas9 is permanent and an in-depth study has to be done to assess whether this therapy would be beneficial for SH or comes with a high risk.

Finally, we would like to note that CRISPR/Cas9-based therapies are still far of their application in the clinical practice. However, these systems comprise a precise tool that can be easily modified to generate very efficient and effective treatments for inherited diseases. Therefore, more research must be performed to understand, develop and take advantage of CRISPR/Cas9-based gene editing.

6. CONCLUSIONS

CONCLUSIONS

1. The administration of L-hydroxyproline with the diet causes dietary hyperoxaluria in WT mice and NHPs. However, this model is not useful for the analysis of the efficacy of gene therapy for PH1.
2. The codon optimization of human *AGXT* delivered by an AAV5 vector did not improve the therapeutic efficacy achieved with the WT sequence.
3. The direct administration of AAV5 vectors into the hepatic blood flow using balloon catheters to increase the exposure to the vector is minimally invasive, improved liver transduction and did not reveal any toxic effect in NHPs.
4. A CRISPR/Cas9-based strategy was designed to inhibit GO protein as SRT for PH1. SaCas9 expression in the liver and GO-specific gRNAs delivered with AAV8 vectors produced an efficient *Hao1* gene disruption and GO protein reduction.
5. The inhibition of GO was able to reduce oxalate levels and protected the mice against accumulation of CaOx crystals in renal parenchyma.
6. The continuous expression of SaCas9 protein in the liver of PH1 mice was safe and generated no off-target indels in the highest scoring predicted off-target sites.

CONCLUSIONES

1. La administración de L-hidroxiprolina en la dieta causa hiperoxaluria en ratones y NHPs. Pero este modelo no es adecuado para analizar la eficacia de la terapia génica dirigida a PH1.
2. La optimización de codones del gen humano *AGXT* expresado mediante un AAV5 no incrementa la eficacia terapéutica obtenida con la secuencia WT.
3. La administración directa de vectores AAV5 en el torrente sanguíneo hepático mediante catéteres con balón para incrementar la exposición al vector es un método mínimamente invasivo que mejora la transducción del hígado y no mostró efecto tóxico en NHPs.
4. Una estrategia de SRT mediante la inhibición de GO basada en CRISPR/Cas9 fue diseñada para el tratamiento de la PH1. La expresión en el hígado de la proteína SaCas9 y gRNAs específicas para GO mediante un AAV8 genera eficientemente errores en el gen *Hao1* y disminuye los niveles de la proteína GO.
5. La inhibición de GO redujo el oxalato en orina y protegió a los ratones frente a la acumulación de cristales de CaOx en el parénquima renal.
6. La expresión sostenida de la nucleasa SaCas9 en el hígado de los ratones PH1 es segura y no genera errores en las secuencias off-target predichas.

7. BIBLIOGRAPHY

1. Whittamore JM, Hatch M. The role of intestinal oxalate transport in hyperoxaluria and the formation of kidney stones in animals and man. Urolithiasis. 2017;45:89–108.

2. Hatch M, Freel RW. Intestinal transport of an obdurate anion: oxalate. Urol Res. 2005;33:1–16.

3. Knauf F, Ko N, Jiang Z, Robertson WG, Van Itallie CM, Anderson JM, et al. Net intestinal transport of oxalate reflects passive absorption and SLC26A6-mediated secretion. J Am Soc Nephrol. 2011;22(12):2247–55.

4. Freel RW, Whittamore JM, Hatch M. Transcellular oxalate and Cl- absorption in mouse intestine is mediated by the DRA anion exchanger Slc26a3, and DRA deletion decreases urinary oxalate. Am J Physiol - Gastrointest Liver Physiol. 2013;305:520–7.

5. Freel RW, Hatch M, Green M, Soleimani M. Ileal oxalate absorption and urinary oxalate excretion are enhanced in Slc26a6 null mice. Am J Physiol - Gastrointest Liver Physiol. 2006;290:719–28.

6. Jiang Z, Asplin JR, Evan AP, Rajendran VM, Velazquez H, Nottoli TP, et al. Calcium oxalate urolithiasis in mice lacking anion transporter Slc26a6. Nat Genet. 2006;38(4):474–8.

7. Pey AL, Albert A, Salido E. Protein homeostasis defects of alanine-glyoxylate aminotransferase: new therapeutic strategies in primary hyperoxaluria type I. Biomed Res Int. 2013;2013:1–19.

8. Bergsland KJ, Zisman AL, Asplin JR, Worcester EM, Coe FL. Evidence for net renal tubule oxalate secretion in patients with calcium kidney stones. Am J Physiol - Ren Physiol. 2011;300:311–8.

9. Holmes RP, Ambrosius WT, Assimos DG. Dietary oxalate loads and renal oxalate handling. J Urol. 2005;174:943–7.

10. Kopp N, Leumann E. Changing pattern of primary hyperoxaluria in Switzerland. Nephrol Dial Transplant. 1995;10(12):2224–7.

11. Cochat P, Deloraine A, Rotily M, Olive F, Liponski I, Deries N. Epidemiology of primary hyperoxaluria type 1. Nephrol Dial Transplant. 1995;10(8):3–7.

12. Van Woerden CS, Groothoff JW, Wanders RJA, Davin J-C, Wijburg FA. Primary

hyperoxaluria type 1 in The Netherlands: prevalence and outcome. Nephrol Dial Transplant. 2003;18:273–9.

13. Hoppe B, Langman CB. A United States survey on diagnosis, treatment, and outcome of primary hyperoxaluria. Pediatr Nephrol. 2003;18:986–91.

14. Akrawi DS, Li X, Sundquist J, Sundquist K, Zö Ller B, Jia Z. Familial Risks of Kidney Failure in Sweden: A Nationwide Family Study. PLoS One. 2014;9(11):1–17.

15. Hori T, Egawa H, Kaido T, Ogawa K, Uemoto S. Liver Transplantation for Primary Hyperoxaluria Type 1: A Single-center Experience during Two Decades in Japan. World J Surg. 2013;37:688–93.

16. M'dimegh S, Omezzine A, M'barek I, Moussa A, Mabrouk S, Kaarout H, et al. Mutational Analysis of Agxt in Tunisian Population with Primary Hyperoxaluria Type 1. Ann Hum Genet. 2017;81:1–10.

17. Santana A, Salido E, Torres A, Shapiro LJ. Primary hyperoxaluria type 1 in the Canary Islands: A conformational disease due to I244T mutation in the P11L-containing alanine:glyoxylate aminotransferase. PNAS. 2003;100(2):7277–82.

18. Mandrile G, Robbiano A, Giachino DF, Sebastiano R, Dondi E, Fenoglio R, et al. Primary hyperoxaluria: report of an Italian family with clear sex conditioned penetrance. Urol Res. 2008;36:309–12.

19. Takayama T, Nagata M, Ichiyama A, Ozono S. In-Depth Topic Review Primary Hyperoxaluria Type 1 in Japan. Am J Nephrol. 2005;25:297–302.

20. Kamoun A, Lakhoua R. End-stage renal disease of the Tunisian child: epidemiology, etiologies, and outcome. Pediatr Nephrol. 1996;10:479–82.

21. Salido E, Pey AL, Rodriguez R, Lorenzo V. Primary hyperoxalurias: Disorders of glyoxylate detoxification. Biochim Biophys Acta. 2012;1822(9):1453–64.

22. Verhulst A, Asselman M, Persy VP, Schepers MSJ, Helbert MF, Verkoelen CF, et al. Crystal retention capacity of cells in the human nephron: involvement of CD44 and its ligands hyaluronic acid and osteopontin in the transition of a crystal binding- into a nonadherent epithelium. J Am Soc Nephrol. 2003;13:107–15.

23. Hoppe B, Beck BB, Milliner D. The Primary Hyperoxalurias. Kidney Int. 2009;75(12):1264–71.

24. Schepers MSJ, Van Ballegooijen ES, Bangma CH, Verkoelen CF. Crystals cause acute necrotic cell death in renal proximal tubule cells, but not in collecting tubule cells. Kidney Int. 2005;68:1543–53.

25. Schepers MSJ, Van Ballegooijen ES, Bangma CH, Verkoelen CF. Oxalate is toxic to renal tubular cells only at supraphysiologic concentrations. Kidney Int. 2005;68:1660–9.

26. Brooks ER, Hoppe B, Milliner DS, Salido E, Rim J, Krevitt LM, et al. Assessment of Urine Proteomics in Type 1 Primary Hyperoxaluria. Am J Nephrol. 2016;43:293–303.

27. Hoppe B, Kemper MJ, Bokenkamp AB, Portale AA, Cohn RA, Langman CB. Plasma calcium oxalate supersaturation in children with primary hyperoxaluria and end-stage renal failure. Kidney Int. 1999;56:268–74.

28. Cochat P, Hulton S-A, Acquaviva C, Danpure CJ, Daudon M, De Marchi M, et al. Primary hyperoxaluria Type 1: indications for screening and guidance for diagnosis and treatment. Nephrol Dial Transpl. 2012;27:1729–36.

29. Leumann E, Hoppe B. The primary hyperoxalurias. J Am Soc Nephrol. 2001;12(9):1986–93.

30. Harambat J, Fargue S, Acquaviva C, Gagnadoux M-F, Janssen F, Liutkus A, et al. Genotype–phenotype correlation in primary hyperoxaluria type 1: the p.Gly170Arg AGXT mutation is associated with a better outcome. Kidney Int. 2010;77(5):443–9.

31. Cochat P, Liutkus A, Fargue S, Basmaison O, Ranchin B, Rolland M-O. Primary hyperoxaluria type 1: still challenging! Pediatr Nephrol. 2006;21:1075–81.

32. Cochat P. Primary hyperoxaluria type 1. Kidney Int. 1999;55:2533–47.

33. Habbig S, Beck BB, Hoppe B. Nephrocalcinosis and urolithiasis in children. Kidney Int. 2011;80(10):1278–91.

34. Leumann E, Hoppe B. Primary hyperoxaluria type 1: is genotyping clinically helpful? Pediatr Nephrol. 2005;20:555–7.

35. Williams E, Rumsby G. Selected Exonic Sequencing of the AGXT Gene Provides a Genetic

Diagnosis in 50% of Patients with Primary Hyperoxaluria Type 1. Clin Chem. 2007;53(7):1216–21.

36. Sato M, Toné S, Ishikawa T, Purdue PE, Danpure CJ, Minatogawa Y. Functional analysis of the 5'-flanking region of the human alanine:glyoxylate aminotransferase gene AGXT. Biochim Biophys Acta. 2002;1574:205–9.

37. Oppici E, Montioli R, Cellini B. Liver peroxisomal alanine:glyoxylate aminotransferase and the effects of mutations associated with Primary Hyperoxaluria Type I: An overview. Biochim Biophys Acta. 2015;1854(9):1212–9.

38. Lumb MJ, Danpure CJ. Functional Synergism between the Most Common Polymorphism in Human Alanine:Glyoxylate Aminotransferase and Four of the Most Common Disease-causing Mutations. J Biol Chem. 2000;275(46):36415–22.

39. Cellini B, Montioli R, Voltattorni C. Human liver peroxisomal alanine:glyoxylate aminotransferase: Characterization of the two allelic forms and their pathogenic variants. Biochim Biophys Acta. 2011;1814(11):1577–84.

40. Coulter-Mackie MB, Tung A, Henderson HE, Toone JR, Applegarth DA. The AGT gene in Africa: a distinctive minor allele haplotype, a polymorphism (V326I), and a novel PH1 mutation (A112D) in black Africans. Mol Genet Metab. 2003;78:44–50.

41. Xue H, Fujie M, Sakaguchiţ T, Oda T, Ogawa H, Kneer N, et al. Flux of the L-Serine Metabolism in Rat Liver. The predominant contribution of serine dehydratase. J Biol Chem. 1999;274(23):16020–7.

42. Montioli R, Fargue S, Lewin J, Zamparelli C, Danpure CJ, Voltattorni C, et al. The N-terminal extension is essential for the formation of the active dimeric structure of liver peroxisomal alanine:glyoxylate aminotransferase. Int J Biochem Cell Biol. 2012;44(3):536–46.

43. Oppici E, Montioli R, Lorenzetto A, Bianconi S, Voltattorni CB, Cellini B. Biochemical analyses are instrumental in identifying the impact of mutations on holo and/or apo-forms and on the region(s) of alanine:glyoxylate aminotransferase variants associated with Primary Hyperoxaluria Type I. Mol Genet Metab. 2012;105:132–40.

44. Zhang X, Roe SM, Hou Y, Bartlam M, Rao Z, Pearl LH, et al. Crystal Structure of

Alanine:Glyoxylate Aminotransferase and the Relationship Between Genotype and Enzymatic Phenotype in Primary Hyperoxaluria Type 1. J Mol Biol. 2003;331:643–52.

45. Cellini B, Montioli R, Oppici E, Astegno A, Voltattorni CB. The chaperone role of the pyridoxal 5'-phosphate and its implications for rare diseases involving B6-dependent enzymes. Clin Biochem. 2014;47(3):158–65.

46. Danpure CJ. Variable peroxisomal and mitochondrial targeting of alanine: glyoxylate aminotransferase in mammalian evolution and disease. BioEssays. 1997;19(4):317–26.

47. Holbrook JD, Birdsey GM, Yang Z, Bruford MW, Danpure CJ. Molecular Adaptation of Alanine : Glyoxylate Aminotransferase Targeting in Primates. Mol Biol Evol. 2000;17(3):387–400.

48. Danpure CJ. Primary hyperoxaluria type 1: AGT mistargeting highlights the fundamental differences between the peroxisomal and mitochondrial protein import pathways. Biochim Biophys Acta. 2006;1763:1776–84.

49. Miyajima H, Oda T, Ichiyama A. Induction of Mitochondrial Serine:Pyruvate Aminotransferase of Rat Liver by Glucagon and Insulin through Different Mechanisms. J Biochem. 1989;105:500–4.

50. Caldwell EF, Mayor LR, Thomas MG, Danpure CJ. Diet and the frequency of the alanine:glyoxylate aminotransferase Pro11Leu polymorphism in different human populations. Hum Genet. 2004;115:504–9.

51. Fargue S, Lewin J, Rumsby G, Danpure CJ. Four of the most common mutations in primary hyperoxaluria type 1 unmask the cryptic mitochondrial targeting sequence of alanine:glyoxylate aminotransferase encoded by the polymorphic minor allele. J Biol Chem. 2013;288(4):2475–84.

52. Motley A, Lumb MJ, Oatey PB, Jennings PR, De Zoysa PA, Wanders RJA, et al. Mammalian Alanine/Glyoxylate Aminotransferase 1 Is Imported into Peroxisomes via the PTS1 Translocation Pathway. Increased Degeneracy and Context Specificity of the Mammalian PTS1 Motif and Implications for the Peroxisome-to-Mitochondrion Mistargeting of. J Cell Biol. 1995;131(1):95–109.

53. Huber PAJ, Birdsey GM, Lumb MJ, Prowse DTR, Perkins TJ, Knight DR, et al.

Peroxisomal Import of Human Alanine:glyoxylate Aminotransferase Requires Ancillary Targeting Information Remote from Its C Terminus. J Biol Chem. 2005;280(29):27111–20.

54. Mesa-Torres N, Tomic N, Albert A, Salido E, Pey AL. Molecular Recognition of PTS-1 Cargo Proteins by Pex5p: Implications for Protein Mistargeting in Primary Hyperoxaluria. Biomolecules. 2015;5:121–41.

55. Williams EL, Acquaviva C, Amoroso A, Chevalier F, Coulter-Mackie M, Monico CG, et al. Primary hyperoxaluria type 1: update and additional mutation analysis of the AGXT gene. Hum Mutat. 2009;30(6):910–7.

56. Pey AL, Salido E, Sanchez-Ruiz JM. Role of low native state kinetic stability and interaction of partially unfolded states with molecular chaperones in the mitochondrial protein mistargeting associated with primary hyperoxaluria. Amino Acids. 2011;41:1233–45.

57. Mesa-Torres N, Fabelo-Rosa I, Riverol D, Yunta C, Albert A, Salido E, et al. The Role of Protein Denaturation Energetics and Molecular Chaperones in the Aggregation and Mistargeting of Mutants Causing Primary Hyperoxaluria Type I. PLoS One. 2013;8(8):1–14.

58. Lage MD, Pittman AMC, Roncador A, Cellini B, Tucker CL. Allele-specific characterization of alanine: Glyoxylate aminotransferase variants associated with primary hyperoxaluria. PLoS One. 2014;9(1–9):e94338.

59. Monico CG, Rossetti S, Schwanz HA, Olson JB, Lundquist PA, Dawson DB, et al. Comprehensive Mutation Screening in 55 Probands with Type 1 Primary Hyperoxaluria Shows Feasibility of a Gene-Based Diagnosis. J Am Soc Nephrol. 2007;18(6):1905–14.

60. Purdue PE, Takada Y, Danpure CJ. Identification of Mutations Associated with Peroxisome-to-Mitochondrion Mistargeting of Alanine/Glyoxylate Aminotransferase in Primary Hyperoxaluria Type 1. J Cell Biol. 1990;111(6):2341–51.

61. Danpure CJ, Rumsby G. Molecular aetiology of primary hyperoxaluria and its implications for clinical management. Expert Rev Mol Med. 2004;6(1):1–16.

62. Lumb MJ, Drake AF, Danpure CJ. Effect of N-terminal a-Helix Formation on the Dimerization and Intracellular Targeting of Alanine:Glyoxylate Aminotransferase. J Biol Chem. 1999;274(29):20587–96.

63. Cellini B, Montioli R, Paiardini A, Lorenzetto A, Voltattorni CB. Molecular Insight into the

Synergism between the Minor Allele of Human Liver Peroxisomal Alanine:Glyoxylate Aminotransferase and the F152I Mutation. J Biol Chem. 2009;284(13):8349–58.

64. Danpure CJ, Purdue PE, Fryer P, Griffiths S, Allsop J, Lumb MJ, et al. Enzymological and Mutational Analysis of a Complex Primary Hyperoxaluria Type I Phenotype Involving Alanine:Glyoxylate Aminotransferase Peroxisome-to-Mitochondrion Mistargeting and Intraperoxisomal Aggregation. Am J Hum Genct. 1993;53:417–32.

65. Pirulli D, Puzzer D, Ferri L, Crovella S, Amoroso A, Ferrettini C, et al. Molecular analysis of hyperoxaluria type 1 in Italian patients reveals eight new mutations in the alanine : glyoxylate aminotransferase gene. Hum Genet. 1999;104:523–5.

66. Tarn AC, Schnakenburg C Von, Rumsby G. Primary hyperoxaluria type 1: Diagnostic relevance of mutations and polymorphisms in the alanine:glyoxylate aminotransferase gene (AGXT). J Inher Metab Dis. 1997;20:689–96.

67. Montioli R, Roncador A, Oppici E, Mandrile G, Giachino DF, Cellini B, et al. S81L and G170R mutations causing Primary Hyperoxaluria type I in homozygosis and heterozygosis: an example of positive interallelic complementation. Hum Mol Genet. 2014;23(22):5998–6007.

68. Cellini B, Bertoldi M, Montioli R, Paiardini A, Borri Voltattorni C. Human wild-type alanine:glyoxylate aminotransferase and its naturally occurring G82E variant: functional properties and physiological implications. Biochem J. 2007;408:39–50.

69. Nishiyama K, Funai T, Yokota S, Ichiyama A. ATP-Dependent Degradation of a Mutant Serine:Pyruvate/Alanine:Glyoxylate Aminotransferase in a Primary Hyperoxaluda Type 1 Case. J Cell Biol. 1993;123(5):1237–48.

70. Bergstralh EJ, Monico CG, Lieske JC, Herges RM, Langman CB, Hoppe B, et al. Transplantation Outcomes in Primary Hyperoxaluria. Am J Transplant. 2010;10(11):2493–501.

71. Hamm LL. Renal handling of citrate. Kidney Int. 1990;38:728–35.

72. Leumann E, Hoppe B, Neuhaus T. Management of primary hyperoxaluria: efficacy of oral citrate administration. Pediatr Nephrol. 1993;7:207–11.

73. Milliner DS, Eickholt J, Bergstralh E, Wilson D, Smith L. Results of long-term treatment

with orthophosphate and pyridoxine in patients with primary hyperoxaluria. NEJM. 1994;331(23):1553–8.

74. Fargue S, Rumsby G, Danpure CJ. Multiple mechanisms of action of pyridoxine in primary hyperoxaluria type 1. Biochim Biophys Acta. 2013;1832:1776–83.

75. Hoyer-Kuhn H, Kohbrok S, Volland R, Franklin J, Hero B, Beck BB, et al. Vitamin B6 in primary hyperoxaluria I: first prospective trial after 40 years of practice. Clin J Am Soc Nephrol. 2014;9(3):468–77.

76. Lorenz EC, Lieske JC, Seide BM, Meek AM, Olson JB, Bergstralh EJ, et al. Sustained pyridoxine response in primary hyperoxaluria type 1 recipients of kidney alone transplant. Am J Transplant. 2014;14(6):1433–8.

77. Fargue S, Knight J, Holmes RP, Rumsby G, Danpure CJ. Effects of alanine:glyoxylate aminotransferase variants and pyridoxine sensitivity on oxalate metabolism in a cell-based cytotoxicity assay. Biochim Biophys Acta. 2016;1862(6):1055–62.

78. Martin-Higueras C, Luis-Lima S, Salido E. Glycolate Oxidase Is a Safe and Efficient Target for Substrate Reduction Therapy in a Mouse Model of Primary Hyperoxaluria Type I. Mol Ther. 2016;24(4):719–25.

79. Castello R, Borzone R, D'Aria S, Annunziata P, Piccolo P, Brunetti-Pierri N. Helper-dependent adenoviral vectors for liver-directed gene therapy of primary hyperoxaluria type 1. Gene Ther. 2015;23(2):129–34.

80. Salido E, Rodriguez-Pena M, Santana A, Beattie SG, Petry H, Torres A. Phenotypic correction of a mouse model for primary hyperoxaluria with adeno-associated virus gene transfer. Mol Ther. 2011;19(5):870–5.

81. Mesa-Torres N, Tomic N, Albert A, Salido E, Pey AL. Molecular recognition of PTS-1 cargo proteins by Pex5p: implications for protein mistargeting in primary hyperoxaluria. Biomolecules. 2015;5(1):121–41.

82. Holmes RP, Assimos DG. Glyoxylate synthesis, and its modulation and influence on oxalate synthesis. J Urol. 1998;160:1617–24.

83. Li X, Knight J, Fargue S, Buchalski B, Guan Z, Inscho EW, et al. Metabolism of 13C5-hydroxyproline in mouse models of Primary Hyperoxaluria and its inhibition by RNAi

therapeutics targeting liver glycolate oxidase and hydroxyproline dehydrogenase. Biochim Biophys Acta. 2016;1862:233–9.

84. Recalcati S, Menotti E, Kühn LC. Peroxisomal targeting of mammalian hydroxyacid oxidase 1 requires the C-terminal tripeptide SKI. J Cell Sci. 2000;114:1625–9.

85. Jones JM, Morrell JC, Gould SJ. Identification and characterization of HAOX1, HAOX2, and HAOX3, three human peroxisomal 2-hydroxy acid oxidases. J Biol Chem. 2000;275(17):12590–7.

86. Dutta C, Avitahl-Curtis N, Pursell N, Larsson Cohen M, Holmes B, Diwanji R, et al. Inhibition of Glycolate Oxidase With Dicer-substrate siRNA Reduces Calcium Oxalate Deposition in a Mouse Model of Primary Hyperoxaluria Type 1. Mol Ther. 2016;24(4):770–8.

87. Liebow A, Li X, Racie T, Hettinger J, Bettencourt BR, Najafian N, et al. An Investigational RNAi Therapeutic Targeting Glycolate Oxidase Reduces Oxalate Production in Models of Primary Hyperoxaluria. J Am Soc Nephrol. 2017;28(2):494–503.

88. Shirfule AL, Sangamwar AT, Khobragade CN. Exploring glycolate oxidase (GOX) as an antiurolithic drug target: Molecular modeling and in vitro inhibitor study. Int J Biol Macromol. 2011;49(1):62–70.

89. Wang M, Xu M, Long Y, Fargue S, Southall N, Hu X, et al. High throughput cell-based assay for identification of glycolate oxidase inhibitors as a potential treatment for Primary Hyperoxaluria Type 1. Sci Rep. 2016;6:1–12.

90. Frishberg Y, Zeharia A, Lyakhovetsky R, Bargal R, Belostotsky R. Mutations in HAO1 encoding glycolate oxidase cause isolated glycolic aciduria. J Med Genet. 2014;51(8):526–9.

91. Clifford-Mobley O, Rumsby G, Kanodia S, Didi M, Holt R, Senniappan S. Glycolate oxidase deficiency in a patient with congenital hyperinsulinism and unexplained hyperoxaluria. Pediatr Nephrol. 2017;32(11):2159–63.

92. Pelkonen R, Kivirikko KI. Hydroxyprolinemia: an apparently harmless familial metabolic disorder. N Engl J Med. 1970;283(9):451–6.

93. Albert A, Yunta C, Arranz R, Peña Á, Salido E, Valpuesta JM, et al. Structure of GroEL in Complex with an Early Folding Intermediate of Alanine Glyoxylate Aminotransferase. J

Biol Chem. 2010;285(9):6371–6.

94. Oppici E, Montioli R, Dindo M, Maccari L, Porcari V, Lorenzetto A, et al. The Chaperoning Activity of Amino-oxyacetic Acid on Folding- Defective Variants of Human Alanine:Glyoxylate Aminotransferase Causing Primary Hyperoxaluria Type I.

95. Hatch M, Gjymishka A, Salido EC, Allison MJ, Freel RW. Enteric oxalate elimination is induced and oxalate is normalized in a mouse model of primary hyperoxaluria following intestinal colonization with Oxalobacter. Am J Physiol - Gastrointest Liver Physiol. 2011;300(3):461–9.

96. Hoppe B, Beck B, Gatter N, Von Unruh G, Tischer A, Hesse A, et al. Oxalobacter formigenes: a potential tool for the treatment of primary hyperoxaluria type 1. Kidney Int. 2006;70:1305–11.

97. Hoppe B, Groothoff JW, Hulton S-A, Cochat P, Niaudet P, Kemper MJ, et al. Efficacy and safety of Oxalobacter formigenes to reduce urinary oxalate in primary hyperoxaluria. Nephrol Dial Transpl. 2011;26:3609–15.

98. Hoppe B, Niaudet P, Salomon R, Harambat J, Hulton S-A, Van ’t Hoff W, et al. A randomised Phase I/II trial to evaluate the efficacy and safety of orally administered Oxalobacter formigenes to treat primary hyperoxaluria. Pediatr Nephrol. 2017;32:781–90.

99. Milliner D, Hoppe B, Groothoff J. A randomised Phase II/III study to evaluate the efficacy and safety of orally administered Oxalobacter formigenes to treat primary hyperoxaluria. Urolithiasis. 2017;

100. Jiang J, Salido EC, Guha C, Wang X, Moitra R, Liu L, et al. Correction of Hyperoxaluria by Liver Repopulation With Hepatocytes in a Mouse Model of Primary Hyperoxaluria Type-1. Transplantation. 2008;85(9):1253–60.

101. Salido EC, Li XM, Lu Y, Wang X, Santana A, Roy-Chowdhury N, et al. Alanine-glyoxylate aminotransferase-deficient mice, a model for primary hyperoxaluria that responds to adenoviral gene transfer. PNAS. 2006;103(48):18249–54.

102. Behnam JT, Williams EL, Brink S, Rumsby G, Danpure CJ. Reconstruction of human hepatocyte glyoxylate metabolic pathways in stably transformed Chinese-hamster ovary cells. Biochem J. 2006;394:409–16.

103. Zapata-Linares N, Rodriguez S, Salido E, Abizanda G, Iglesias E, Prosper F, et al. Generation and characterization of human iPSC lines derived from a Primary Hyperoxaluria Type I patient with p.I244T mutation. Stem Cell Res. 2016;16(1):116–9.

104. Ginn SL, Alexander IE, Edelstein ML, Abedi MR, Wixon J. Gene therapy clinical trials worldwide to 2012 - an update. J Gene Med. 2013;15(2):65–77.

105. Naldini L. Ex vivo gene transfer and correction for cell-based therapies. Nat Rev Genet. 2011;12:301–15.

106. Cavazzana M, Six E, Lagresle-Peyrou C, André-Schmutz I, Hacein-Bey-Abina S. Gene Therapy for X-Linked Severe Combined Immunodeficiency: Where Do We Stand? Hum Gene Ther. 2015;27(2):108–16.

107. Hartmann J, Schüßler-Lenz M, Bondanza A, Buchholz CJ. Clinical development of CAR T cells—challenges and opportunities in translating innovative treatment concepts. EMBO Mol Med. 2017;9(9):1183–97.

108. Nathwani AC, Davidoff AM, D Tuddenham EG. Advances in Gene Therapy for Haemophilia. Hum Gene Ther. 2017;28(11):1004–12.

109. Atchison RW, Casto BC, McD Hammon W. Adenovirus-Associated Defective Virus Particles. Science (80-). 1965;149(3685):754–6.

110. Gao G, Zhong L, Danos O. Exploiting Natural Diversity of AAV for the Design of Vectors with Novel Properties. Methods Mol Biol. 2012;807:93–118.

111. Salganik M, Hirsch ML, Samulski RJ. Adeno-associated Virus as a Mammalian DNA Vector. Microbiol Spectr. 2015;3(4):1–35.

112. Merten O-W, Gény-Fiamma C, Douar A. Current issues in adeno-associated viral vector production. Gene Ther. 2005;12:51–61.

113. Sonntag F, Schmidt K, Kleinschmidt JA. A viral assembly factor promotes AAV2 capsid formation in the nucleolus. PNAS. 2010;107(22):10220–5.

114. Sonntag F, Köther K, Schmidt K, Weghofer M, Raupp C, Nieto K, et al. The Assembly-Activating Protein Promotes Capsid Assembly of Different Adeno-Associated Virus Serotypes. J Virol. 2011;85(23):12686–97.

115. Srivastava A. In vivo tissue-tropism of adeno-associated viral vectors. Curr Opin Virol. 2016;21:75–80.

116. Lisowski L, Szun Tay S, Edward Alexander I, Edward I, by Andrew Baker EH, Thrasher AJ. Adeno-associated virus serotypes for gene therapeutics. Curr Opin Pharmacol. 2015;24:59–67.

117. Saraiva J, Nobre RJ, Pereira De Almeida L. Gene therapy for the CNS using AAVs: The impact of systemic delivery by AAV9. J Control Release. 2016;241:94–109.

118. Pillay S, Meyer NL, Puschnik AS, Davulcu O, Diep J, Jae LT, et al. An essential receptor for adeno-associated virus infection. Nature. 2016;530:108–14.

119. Kotin RM, Linden RM, Berns KI. Characterization of a preferred site on human chromosome 19q for integration of adeno-associated virus DNA by non-homologous recombination. EMBO J. 1992;11(13):5071–8.

120. Balagué C, Kalla M, Zhang W-W. Adeno-Associated Virus Rep78 Protein and Terminal Repeats Enhance Integration of DNA Sequences into the Cellular Genome. J Virol. 1997;71(4):3299–306.

121. Nault J-C, Datta S, Imbeaud S, Franconi A, Mallet M, Couchy G, et al. Recurrent AAV2-related insertional mutagenesis in human hepatocellular carcinomas. Nat Genet. 2015;47(10):1187–95.

122. Gil-Farina I, Fronza R, Kaeppel C, Lopez-Franco E, Ferreira V, D'Avola D, et al. Recombinant AAV Integration Is Not Associated With Hepatic Genotoxicity in Nonhuman Primates and Patients. Mol Ther. 2016;24(6):1100–5.

123. D'Avola D, López-franco E, Sangro B, Pañeda A, Grossios N, Gil-farina I, et al. Phase I open label liver-directed gene therapy clinical trial for acute intermittent porphyria. J Hepatol. 2016;65(4):776–83.

124. Manno CS, Pierce GF, Arruda VR, Glader B, Ragni M, Rasko JJE, et al. Successful transduction of liver in hemophilia by AAV-Factor IX and limitations imposed by the host immune response. Nat Med. 2006;12(3):342–8.

125. Fagiuoli S, Daina E, D'Antiga L, Colledan M, Remuzzi G. Monogenic diseases that can be cured by liver transplantation. J Hepatol. 2013;59(3):595–612.

126. Kattenhorn LM, Tipper CH, Stoica L, Geraghty DS, Wright TL, Clark KR, et al. Adeno-Associated Virus Gene Therapy for Liver Disease. Hum Gene Ther. 2016;27(12):947–61.

127. Loeb JE, Cordier WS, Harris ME, Weitzman MD, Hope TJ. Enhanced Expression of Transgenes from Adeno-Associated Virus Vectors with the Woodchuck Hepatitis Virus Posttranscriptional Regulatory Element: Implications for Gene Therapy. Hum Gene Ther. 1999;10:2295–305.

128. Nathwani AC, Reiss UM, Tuddenham EGD, Rosales C, Chowdary P, McIntosh J, et al. Long-Term Safety and Efficacy of Factor IX Gene Therapy in Hemophilia B. NEJM. 2014;371(21):1994–2004.

129. Samulski RJ, Srivastava A, Berns KI, Muzyczka N. Rescue of Adeno-Associated Virus from Recombinant Plasmids: Gene Correction within the Terminal Repeats of AAV. Cell. 1983;33:135–43.

130. Zhou Q, Tian W, Liu C, Lian Z, Dong X, Wu X. Deletion of the B-B' and C-C' regions of inverted terminal repeats reduces rAAV productivity but increases transgene expression. Sci Rep. 2017;7(1):1–13.

131. McCarty DM. Self-complementary AAV Vectors; Advances and Applications. Mol Ther. 2008;16(10):1648–56.

132. Bell P, Wang L, Chen S-J, Yu H, Zhu Y, Nayal M, et al. Effects of Self-Complementarity, Codon Optimization, Transgene, and Dose on Liver Transduction with AAV8. Hum Gene Ther. 2016;27(6):228–37.

133. Mauro VP, Chappell SA. A critical analysis of codon optimization in human therapeutics. Trends Mol Med. 2014;20(11):604–13.

134. Ronzitti G, Bortolussi G, van Dijk R, Collaud F, Charles S, Leborgne C, et al. A translationally optimized AAV-UGT1A1 vector drives safe and long-lasting correction of Crigler-Najjar syndrome. Mol Ther — Methods Clin Dev. 2016;3:1–10.

135. Grimm D, Büning H. Small but increasingly mighty - Latest advances in AAV vector research, design and evolution. Hum Gene Ther. 2017;28(11):1075–86.

136. Tarantal AF, Lee C, Martinez ML, Asokan A, Samulski RJ. Systemic and Persistent Muscle Gene Expression in Rhesus Monkeys with a Liver De-Targeted Adeno-Associated Virus

Vector. Hum Gene Ther. 2017;28(5):385–91.

137. Zinn E, Pacouret S, Khaychuk V, Turunen HT, Carvalho LS, Andres-Mateos E, et al. In Silico Reconstruction of the Viral Evolutionary Lineage Yields a Potent Gene Therapy Vector. Cell Rep. 2015;12:1056–68.

138. Crettaz J, Berraondo P, Mauleón I, Ochoa L, Shankar V, Barajas M, et al. Intrahepatic injection of adenovirus reduces inflammation and increases gene transfer and therapeutic effect in mice. Hepatology. 2006;44(3):623–32.

139. Mimuro J, Mizukami H, Hishikawa S, Ikemoto T, Ishiwata A, Sakata A, et al. Minimizing the inhibitory effect of neutralizing antibody for efficient gene expression in the liver with adeno-associated virus 8 vectors. Mol Ther. 2013;21(2):318–23.

140. Brunetti-Pierri N, Ng T, Iannitti DA, Palmer DJ, Beaudet AL, Finegold MJ, et al. Improved hepatic transduction, reduced systemic vector dissemination, and long-term transgene expression by delivering helper-dependent adenoviral vectors into the surgically isolated liver of nonhuman primates. Hum Gene Ther. 2006 Apr;17(4):391–404.

141. Brunetti-pierri N, Stapleton GE, Palmer DJ, Zuo Y, Mane VP, Finegold MJ, et al. Pseudo-hydrodynamic Delivery of Helper- dependent Adenoviral Vectors into Non-human Primates for Liver-directed Gene Therapy. Mol Ther. 2007;15(4):732–40.

142. Brunetti-pierri N, Stapleton GE, Law M, Breinholt J, Palmer DJ, Zuo Y, et al. Efficient , Long-term Hepatic Gene Transfer Using Clinically Relevant HDAd Doses by Balloon Occlusion Catheter Delivery in Nonhuman Primates. Mol Ther. 2009;17(2):327–33.

143. Brunetti-Pierri N, Ng T, Iannitti D, Cioffi W, Stapleton G, Law M, et al. Transgene expression up to 7 years in nonhuman primates following hepatic transduction with helper-dependent adenoviral vectors. Hum Gene Ther. 2013 Aug;24(8):761–5.

144. Brunetti-pierri N, Palmer DJ, Mane V, Finegold M, Beaudet AL, Ng P. Increased Hepatic Transduction with Reduced Systemic Dissemination and Proinflammatory Cytokines Following Hydrodynamic Injection of Helper-Dependent Adenoviral Vectors. Mol Ther. 2005;12(1):99–106.

145. Liu F, Song Y, Liu D. Hydrodynamics-based transfection in animals by systemic administration of plasmid DNA. Gene Ther. 1999;6:1258–66.

146. Oka K, Mullins CE, Kushwaha RS, Leen AM, Chan L. Gene therapy for rhesus monkeys heterozygous for LDL receptor de fi ciency by balloon catheter hepatic delivery of helper-dependent adenoviral vector. Gene Ther. 2014;22(1):87–95.

147. Greig J, Nordin J, Makaron L, Garnett M, Kattenhorn LM, Bell P, et al. Impact of intravenous infusion time on AAV8 vector pharmacokinetics, safety, and liver transduction in cynomolgus macaques. Mol Ther — Methods Clin Dev. 2016;3:1–7.

148. Gaj T, Gersbach CA, Barbas Iii CF. ZFN, TALEN and CRISPR/Cas-based methods for genome engineering. Trends Biotechnol. 2013;31(7):397–405.

149. Ran FA, Hsu PD, Wright J, Agarwala V, Scott DA, Zhang F. Genome engineering using the CRISPR-Cas9 system. Nat Protoc. 2013;8(11):2281–308.

150. Chatterjee N, Walker GC. Mechanisms of DNA damage, repair, and mutagenesis. Environ Mol Mutagen. 2017;58(5):235–63.

151. González-Marín C, Gosálvez J, Roy R. Types, causes, detection and repair of DNA fragmentation in animal and human sperm cells. Int J Mol Sci. 2012;13(11):14026–52.

152. Y Chang HH, Pannunzio NR, Adachi N, Lieber MR. Non-homologous DNA end joining and alternative pathways to double-strand break repair. Nat Rev Mol Cell Biol. 2017;18:495–506.

153. Mojica FJ, Juez G, Rodríguez-Valera F. Transcription at different salinities of Haloferax mediterranei sequences adjacent to partially modified PstI sites. Mol Microbiol. 1993;9(3):613–21.

154. Sorek R, Kunin V, Hugenholtz P. CRISPR — a widespread system that provides acquired resistance against phages in bacteria and archaea. Nat Rev Microbiol. 2008;6:181–6.

155. Duroux-Richard I, Giovannangeli C, Apparailly F. CRISPR-Cas9: A revolution in genome editing in rheumatic diseases. Jt Bone Spine. 2017;84:1–4.

156. Lander ES. The Heroes of CRISPR. Cell. 2016;164:18–28.

157. Ran FA, Cong L, Yan WX, Scott DA, Gootenberg JS, Kriz AJ, et al. In vivo genome editing using Staphylococcus aureus Cas9. Nature. 2015;520(7546):186–91.

158. Cheng R, Peng J, Yan Y, Cao P, Wang J, Qiu C, et al. Efficient gene editing in adult mouse

livers via adenoviral delivery of CRISPR/Cas9. FEBS Lett. 2014;588(21):3954–8.

159. Wang D, Mou H, Li S, Li Y, Hough S, Tran K, et al. Adenovirus-Mediated Somatic Genome Editing of Pten by CRISPR/Cas9 in Mouse Liver in Spite of Cas9-Specific Immune Responses. Hum Gene Ther. 2015;26(7):432–42.

160. Ding Q, Strong A, Patel KM, Ng SL, Gosis BS, Regan SN, et al. Permanent alteration of PCSK9 with in vivo CRISPR-Cas9 genome editing. Circ Res. 2014;115(5):488–92.

161. Pankowicz FP, Barzi M, Legras X, Hubert L, Mi T, Tomolonis JA, et al. Reprogramming metabolic pathways in vivo with CRISPR/Cas9 genome editing to treat hereditary tyrosinaemia. Nat Commun. 2016;7(110):1–6.

162. Overturf K, Al-Dhalimy M, Tanguay R, Brantly M, Ou C, Finegold M, et al. Hepatocytes corrected by gene therapy are selected in vivo in a model of hereditary tyrosinaemia type I. Nat Genet. 1996;12:266–73.

163. Yin H, Xue W, Chen S, Bogorad RL, Benedetti E, Grompe M, et al. Genome editing with Cas9 in adult mice corrects a disease mutation and phenotype. Nat Biotechnol. 2014;32(6):551–3.

164. Yin H, Song C-Q, Dorkin JR, Zhu LJ, Li Y, Wu Q, et al. Therapeutic genome editing by combined viral and non-viral delivery of CRISPR system components in vivo. Nat Biotechnol. 2016;34(3):328–33.

165. Yang Y, Wang L, Bell P, McMenamin D, He Z, White J, et al. A dual AAV system enables the Cas9-mediated correction of a metabolic liver disease in newborn mice. Nat Biotechnol. 2016;34(3):334–8.

166. Zischewski J, Fischer R, Bortesi L. Detection of on-target and off-target mutations generated by CRISPR/ Cas9 and other sequence-specific nucleases. Biotechnol Adv. 2017;35:95–104.

167. Lindsay H, Burger A, Biyong B, Felker A, Hess C, Zaugg J, et al. CrispRVariants charts the mutation spectrum of genome engineering experiments. Nat Biotechnol. 2016;34(7):701–2.

168. Vignaud C, Pietrancosta N, Williams EL, Rumsby G, Lederer F. Purification and characterization of recombinant human liver glycolate oxidase. Arch Biochem Biophys. 2007;465:410–6.

169. Ebeling M, Kung E, See A, Broger C, Steiner G, Berrera M, et al. Genome-based analysis of the nonhuman primate Macaca fascicularis as a model for drug safety assessment. Genome Res. 2011;21:1746–56.

170. Karaolanis G, Lionaki S, Moris D, Palla V-V, Vernadakis S. Secondary hyperoxaluria: a risk factor for kidney stone formation and renal failure in native kidneys and renal grafts. Transplant Rev. 2014;28:182–7.

171. Zabaleta N, Salas D, Paramo M, Hommel M, Sier-Ferreira V, Hernandez-Alcoceba R, et al. Improvement of Adeno-Associated Virus-Mediated Liver Transduction Efficacy by Regional Administration in Macaca fascicularis. Hum Gene Ther Clin Dev. 2017;28(2):68–73.

172. Plotkin JB, Kudla G. Synonymous but not the same: the causes and consequences of codon bias. Nat Rev Genet. 2011;12:32–42.

173. Rosano GL, Ceccarelli EA. Rare codon content affects the solubility of recombinant proteins in a codon bias-adjusted Escherichia coli strain. Microb Cell Fact. 2009;8(41):1–9.

174. Sauna ZE, Kimchi-Sarfaty C. Understanding the contribution of synonymous mutations to human disease. Nat Rev Genet. 2011;12:683–90.

175. Robert F, Barbeau M, Éthier S, Dostie J, Pelletier J. Pharmacological inhibition of DNA-PK stimulates Cas9-mediated genome editing. Genome Med. 2015;7(93):1–11.

176. Suzuki K, Tsunekawa Y, Hernandez-Benitez R, Wu J, Zhu J, Kim E, et al. In vivo genome editing via CRISPR/Cas9 mediated homology-independent targeted integration. Nature. 2016;540(7630):144–9.

177. Xue W, Chen S, Yin H, Tammela T, Papagiannakopoulos T, Joshi NS, et al. CRISPR-mediated direct mutation of cancer genes in the mouse liver. Nature. 2014;514(7522):380–4.

178. Schaefer K, Wu W-H, Colgan D, Tsang SH, Bassuk AG, Mahajan VB. Unexpected mutations after CRISPR– Cas9 editing in vivo. Nat Methods. 2017;14(6):547–8.

179. Kim S, Park J, Kim D, Kim K, Bae S, Schlesner M, et al. Questioning unexpected CRISPR off-target mutations in vivo. 2017;

180. Charlesworth C, Deshpande P, Dever D, Dejene B, Gomez-Ospina N, Mantri S, et al.

Identification of Pre-Existing Adaptive Immunity to Cas9 Proteins in Humans. bioRxiv. 2018;

181. Merienne N, Vachey G, De Longprez L, Perrier AL, Du Pasquier R, Dé Glon Correspondence N, et al. The Self-Inactivating KamiCas9 System for the Editing of CNS Disease Genes. Cell ReportsReports. 2017;20:2980–91.

182. Miller JB, Zhang S, Kos P, Xiong H, Zhou K, Perelman SS, et al. Non-Viral CRISPR/Cas Gene Editing In Vitro and In Vivo Enabled by Synthetic Nanoparticle Co-Delivery of Cas9 mRNA and sgRNA. Angew Chemie Int Ed. 2017;56(4):1059–63.

183. Yin H, Kauffman KJ, Anderson DG. Delivery technologies for genome editing. Nat Rev Drug Discov. 2017;16:387–99.

184. Chew W, Tabebordbar M, Cheng JKW, Mali P, Wu EY, Ng A, et al. A multifunctional AAV–CRISPR–cas9 and its host response. Nat Methods. 2016;13(10):868–74.

185. Han S-O, Ronzitti G, Arnson B, Leborgne C, Li S, Mingozzi F, et al. Low-Dose Liver-Targeted Gene Therapy for Pompe Disease Enhances Therapeutic Efficacy of ERT via Immune Tolerance Induction. Mol Ther Methods Clin Dev. 2017;4:126–36.

186. Sack BK, Herzog RW, Terhorst C, Markusic DM. Development of gene transfer for induction of antigen-specific tolerance. Mol Ther — Methods Clin Dev. 2014;1:1–9.

187. Doench JG, Hartenian E, Graham DB, Tothova Z, Hegde M, Smith I, et al. Rational design of highly active sgRNAs for CRISPR-Cas9 – mediated gene inactivation. Nat Biotechnol. 2014;32(12).

188. Hsu PD, Scott DA, Weinstein JA, Ran FA, Konermann S, Agarwala V, et al. DNA targeting specificity of RNA-guided nucleases. Nat Biotechnol. 2013;31(9):827–32.

8. PUBLICATION

Zabaleta N, Salas D, Paramo M, et al, Improvement of Adeno-Associated Virus-Mediated Liver Transduction Efficacy by Regional Administration in Macaca fascicularis. Hum Gene Ther Clin Dev; 2017, 28(2):68-73.
http://doi.org/10.1089/humc.2016.183